Technical University of Denmark

DTU

Thermoviscous Model Equations in Nonlinear Acoustics
Analytical and Numerical Studies of Shocks and Rarefaction Waves

Rasmussen, Anders Rønne; Bruus, Henrik; Sørensen, Mads Peter

Publication date:
2009

Document Version
Publisher's PDF, also known as Version of record

[Link back to DTU Orbit](#)

Citation (APA):
Rasmussen, A. R., Bruus, H., & Sørensen, M. P. (2009). Thermoviscous Model Equations in Nonlinear Acoustics: Analytical and Numerical Studies of Shocks and Rarefaction Waves. Kgs. Lyngby, Denmark: Technical University of Denmark (DTU).

DTU Library
Technical Information Center of Denmark

Thermoviscous Model Equations in Nonlinear Acoustics

Analytical and Numerical Studies of Shocks and Rarefaction Waves

PhD thesis, April 2009

Anders Rønne Rasmussen

Department of Mathematics

Technical University of Denmark

DTU Mathematics
Department of Mathematics

Abstract

Title: **Thermoviscous Model Equations in Nonlinear Acoustics. Analytical and Numerical Studies of Shocks and Rarefaction Waves**

Four nonlinear acoustical wave equations that apply to both perfect gasses and arbitrary fluids with a quadratic equation of state are studied. Shock and rarefaction wave solutions to the equations are studied. In order to assess the accuracy of the wave equations, their solutions are compared to solutions of the basic equations from which the wave equations are derived. A straightforward weakly nonlinear equation is the most accurate for shock modeling. A higher order wave equation is the most accurate for modeling of smooth disturbances. Investigations of the linear stability properties of solutions to the wave equations, reveal that the solutions may become unstable. Such instabilities are not found in the basic equations. Interacting shocks and standing shocks are investigated.

Resumé (in Danish)

Titel: **Termoviskose modelligninger i ikke-lineær akustik. Analytiske og numeriske undersøgelser af shock og fortyndingsbølger**

Fire ikke-lineære akustiske bølgeligninger, som kan anvendes på både ideal gasser og vilkårlige gasser og væsker med en kvadratisk tilstandsligning, undersøges. Shock- og fortyndningsbølgeløsninger til ligningerne undersøges. For at kunne vurdere nøjagtigheden af bølgeligningerne, er deres løsninger sammenlignet med løsninger til de grundlæggende ligninger, hvorfra bølgeligningerne er udledt. En direkte svagt ikke-lineær bølgeligning er den mest nøjagtige til at modellere shock. En højere ordens bølgeligning er den mest nøjagtige til at modellere glatte forstyrrelser. Undersøgelser af de lineære stabilitetsegenskaber af løsninger til bølgeligningerne afslører, at løsningerne kan blive ustabile. Sådanne instabiliteter optræder ikke i de grundlæggende ligninger. Vekselvirkende shock og stående shock undersøges.

Contents

Preface

The present thesis is submitted in partial fulfillment of the requirements for the PhD degree, at the Technical University of Denmark (DTU). The project was funded by DTU and the work was carried out at the Department of Mathematics from September 2005 to April 2009, including 7 months of parental leave. The project was supervised by Associate Professor Mads P. Sørensen.

First of all I would like to thank Mads P. Sørensen for dedicated effort as supervisor, and for allowing me great freedom to follow many different paths in my research. I would like also to thank Peter L. Christiansen from the Department of Physics, for his enthusiasm and commitment as co-supervisor. Mads and Peter first introduced me to the field of nonlinear science during my master's studies, and their captivating enthusiasm has kept me interested in the subject ever since. I would like also to express my gratitude to Yuri B. Gaididei from the Bogolyubov Institute for Theoretical Physics in Kiev, Ukraine, for sharing his thoughts on the project during his regular visits to the Department of Physics and the Department of Mathematics. Yuri contributed with many clever ideas that have been crucial in shaping the project. I would like to thank also Henrik Bruus from the Department of Micro- and Nanotechnology for inspiring discussions on acoustic resonances and acoustic streaming in microfluidic systems.

During two weeks of November 2008 I visited the Department of Mechanical Engineering at Blekinge Institute of Technology (BTH) in Karlkrona, Sweeden. I would like to thank Claes M. Hedberg and Oleg V. Rudenko for being very hospitable, and for sharing their extensive knowledge and long term experience within the field of nonlinear acoustics.

Finally, I would like to thank my family, my wife Charlotte and my son Johan, for always being understanding when work required much of my time, and for reminding me that there is life beyond work.

Kongens Lyngby, April 2009

Anders Rønne Rasmussen

List of Symbols

Symbol	Description	Unit
β	Viscous dissipation parameter	m^2/s
γ	Ratio of specific heats	1
ε	Mach number	1
ζ	Coefficient of bulk viscosity	$\mathrm{kg}/(\mathrm{m\ s})$
η	Time derivative of ψ	$(\mathrm{m/s})^2$
κ	Thermal conductivity	$\mathrm{kg\ m}/(\mathrm{K\ s}^3)$
μ	Coefficient shear viscosity	$\mathrm{kg}/(\mathrm{m\ s})$
$\rho,\ \rho_0$	Mass density, ambient value	$\mathrm{kg/m}^3$
ψ	Velocity potential	m^2/s
B/A	Fluid nonlinearity parameter	1
b	Thermoviscous dissipation parameter	m^2/s
$c,\ c_0$	Sound velocity, small-signal sound velocity	$\mathrm{m/s}$
c_p	Specific heat capacity at constant pressure	$\mathrm{m}^2/(\mathrm{K\ s}^2)$
c_v	Specific heat capacity at constant volume	$\mathrm{m}^2/(\mathrm{K\ s}^2)$
h	Specific enthalpy	$\mathrm{m}^2/\mathrm{s}^2$
$p,\ p_0$	Thermodynamic pressure, ambient value	$\mathrm{kg}/(\mathrm{m\ s}^2)$
$s,\ s_0$	Specific entropy, ambient value	$\mathrm{m}^2/(\mathrm{K\ s}^2)$
$T,\ T_0$	Absolute temperature, ambient value	K
t	Time	s
u	Fluid particle velocity	$\mathrm{m/s}$
v	Traveling wave propagation velocity	$\mathrm{m/s}$
x	One-dimensional spatial coordinate	m
$\Box_x$	Partial differentiation with respect to x	
$\Box_t$	Partial differentiation with respect to t	
$\hat{\Box}$	Dummy integration variables	
$\tilde{\Box}$	Dimensionless variables	

Chapter 1

Introduction

In a great deal of problems in acoustics the wave behavior of sound, for example, propagation, reflection, transmission, and diffraction, is described in terms of the linear wave equation. If the wave amplitude becomes high enough, nonlinear effects occur and the linear wave equation becomes inadequate. In nonlinear acoustics, novel phenomena unknown in linear acoustics are observed, for example, waveform distortion, formation of shocks, and nonlinear interaction (as opposed to superposition) when two waves are mixed.

The main emphasis in this thesis is on a number of model equations of acoustics that take into account the nonlinear effects. In our studies of these model equations we shall see examples of the nonlinear phenomena mentioned above. Our studies began with an investigation of the Kuznetsov equation (Kuznetsov, 1971), which is a nonlinear wave equation and is frequently used within acoustics. By applying traveling wave analysis to the Kuznetsov equation we derived an exact thermoviscous shock solution. This solution was reported recently by Jordan (2004). During our investigations of the Kuznetsov equation, we found that the equation does not conserve the Hamiltonian structure of the basic equations from which it is derived. In order to remedy the lack of Hamiltonian structure we proposed a new wave equation, which is similar to the Kuznetsov equation, but conserves the Hamiltonian structure. Later on in the project we became aware of a higher order acoustic wave equation (Söderholm, 2001), which was also included in our studies. In order to assess the accuracy of the various nonlinear wave equations, we investigated also the basic equations from which the nonlinear acoustic wave equations are derived, that is the compressible Navier-Stokes and Euler equations.

The thesis is structured as follows. Appendix A includes a manuscript that is intended for submission to the journal 'Physics Letters A'. The manuscript is concerned with an investigation of thermoviscous shocks based on our Hamiltonian model equation. Appendix B includes a manuscript that is submitted to the proceedings of the The European Consortium for Mathematics in Industry (ECMI) 2008 conference. The manuscript is based on the material in Appendix A. Appendix C includes a manuscript that is intended for submission to the 'Journal of the Acoustical Society of America'. The manuscript is

concerned with an investigation of thermoviscous shocks and rarefaction waves
based on the higher order wave equation proposed by Söderholm (2001). In
Chapter 2 we introduce various nonlinear acoustic wave equations and the basic
equations from which they are derived. In Chapter 3 we study and compare
shock solutions to the basic equations and the various nonlinear acoustic wave
equations. We study both the lossless and dissipative cases. In Chapter 4 we
demonstrate that instabilities may occur in the solutions of the nonlinear wave
equations. In Chapter 5 we study the process of shock formation. In particular
we elaborate on a work recently reported by Christov et al. (2007). In Chapter 6
we investigate problems with compound waves. In particular we study problems
with shock collisions, and we study solutions to the Riemann problem. In Chap-
ter 7 we study nonlinear standing waves in closed tubes, and we derive exact
solutions that resemble the waves observed in a nonlinear resonator. Chapter 8
contains our conclusions.

Chapter 2

Equations of Nonlinear Acoustics

In this chapter we give the basic equations of continuum mechanics, that describe the motion of a viscous and heatconducting compressible Newtonian fluid. From these equations we derive a higher order acoustic wave equation in one single dependent variable. The equation takes into account the nonlinear terms exactly and the dissipative terms to lowest order, neglecting nonlinearities in the latter. In the lossless case, we demonstrate that the higher order acoustic wave equation and the basic equations have the same Hamiltonian structure. Finally, we discuss various approaches to obtain weakly nonlinear acoustic wave equations that take into account the nonlinear terms up to quadratic order only.

2.1   Basic Equations

Four equations are required to describe the general motion of a viscous and heatconducting (thermoviscous) fluid: (i) mass conservation, (ii) momentum conservation, (iii) entropy balance, and (iv) thermodynamic state. The presentation of these equations given below draws to some extent on Section 2 in Hamilton and Morfey (1998), which introduces the equations in the context of nonlinear acoustics. We assume that the fluid is homogeneous in composition, that its unperturbed density and pressure are uniform, and that the dependence of viscosity and heatconduction coefficients on the disturbance due to the sound wave may be neglected. A detailed derivation and discussion of the equations which follow can be found in the book by Landau and Lifshitz (1987). Below we give the equations in the case of one spatial dimension.[1] These describe the case of one-dimensional plane fields, in which surfaces of constant phase are infinite parallel planes normal to the direction of propagation. The analysis in all subsequent chapters is concerned with the one-dimensional case.

The mass conservation, or continuity, equation is

$$\rho_t + (\rho u)_x = 0, \tag{2.1}$$

---

[1]The corresponding full three-dimensional equations are given in the manuscript in Appendix A.

where ρ is the mass density, u is the fluid particle velocity, and subscripts denote partial differentiation, e.g. $\rho_t = \partial\rho/\partial t$.[2] The momentum equation, or equation of motion, may be written as

$$\rho(u_t + uu_x) + p_x = \left(\frac{4}{3}\mu + \zeta\right)u_{xx}, \tag{2.2}$$

where p is the thermodynamic pressure appearing in Eq. (2.4) below, and μ and ζ are the coefficients of shear and bulk viscosity. The entropy, or heat transfer, equation is

$$\rho T\left(s_t + us_x\right) = \left(\frac{\mu}{2} + \zeta\right)(u_x)^2 + \kappa T_{xx}, \tag{2.3}$$

where s is the specific entropy, T is the absolute temperature, and κ is the thermal conductivity. Finally, we introduce the equation of thermodynamic state

$$p = p(\rho, s). \tag{2.4}$$

Two specific examples of the equation of state for various media will be introduced in Sections 2.2.3 and 2.2.4.

2.2   A Higher Order Acoustic Wave Equation

In the following we go through the derivation of a higher order acoustic wave equation governing the velocity potential. In the derivation nonlinear contributions to dissipation are neglected. However, the lossless part of the equation is exact in the sense that all nonlinear contributions are retained. Our derivation basically follows Söderholm (2001), who carefully derives the equation in his paper with the title, 'A Higher Order Acoustic Equation for the Slightly Viscous Case'. Furthermore, detailed and helpful derivations of an exact lossless nonlinear wave equation governing the velocity potential are given by Hamilton and Morfey (1998) and Christov et al. (2007). The lossless equation obtained by these authors is identical to Söderholm's equation when the dissipative term is neglected in the latter. Helpful are also the review papers by Makarov and Ochmann (1996a,b) and the book by Enflo and Hedberg (2002), which discuss, within the context of the Kuznetsov equation (Kuznetsov, 1971), the lowest order approximation in the dissipative terms. The Kuznetsov equation, which is considered to be the "classical" equation of nonlinear acoustics (Aanonsen et al., 1984; Jordan, 2004), is a model equation in the velocity potential that takes into account nonlinear terms up to second order, and the dissipative terms to lowest order. In Section 2.4 we shall demonstrate that the higher order acoustic wave equation reduces to Kuznetsov's equation if a particular approximation scheme is applied. Our main objective in this section is to outline the necessary steps in the derivation of the higher order acoustic wave equation. For detailed discussions and justifications of the individual steps we refer to the references given in the text.

---

[2]A list of symbols can be found on page viii.

2.2.1 Lowest Order Thermoviscous Approximation

In the approximation considered, we take into account nonlinearities to all orders, dissipation to lowest order, and neglect the cross terms of nonlinearity and dissipation. Then, by arguments given by Söderholm (2001), the equation of state (2.4) can be written as

$$p(\rho, s) = p(\rho, s_0) + a(s - s_0), \qquad (2.5)$$

where

$$a = \left. \frac{\partial p}{\partial s} \right|_{\rho=\rho_0, s=s_0} \qquad (2.6)$$

is a constant and s_0 is the ambient value of the entropy. In order to eliminate s from Eq. (2.5) we use the entropy equation (2.3). The approximation considered here takes into account dissipation to lowest order only, neglecting nonlinear corrections to those terms. As a result Eq. (2.3) reduces to

$$\rho_0 T_0 s_t = \kappa T_{xx}, \qquad (2.7)$$

where ρ_0 and T_0 are ambient values. Using Eq. (2.7) and basic thermodynamic identities, and neglecting nonlinear contributions in the dissipative terms, one finds that Eq. (2.5) becomes

$$p = p(\rho, s_0) - \kappa \left(\frac{1}{c_v} - \frac{1}{c_p} \right) u_x, \qquad (2.8)$$

where c_v and c_p are the heat capacities at constant volume and pressure, respectively. For full details on how to obtain Eq. (2.8) see e.g. Rudenko and Soluyan (1977), or Makarov and Ochmann (1996a). When using Eq. (2.8) there is no need for the entropy equation anymore and it is therefore adequate to concentrate upon the mass conservation and momentum equations (Makarov and Ochmann, 1996b).

Inserting Eq. (2.8) into the momentum equation (2.2), and dividing by ρ, we obtain

$$u_t + u u_x + \frac{p_x}{\rho} = b u_{xx}, \qquad (2.9)$$

where $p = p(\rho, s_0)$ and the thermoviscous dissipation parameter b is given by

$$b \equiv \frac{1}{\rho_0} \left\{ \frac{4}{3}\mu + \zeta + \kappa \left(\frac{1}{c_v} - \frac{1}{c_p} \right) \right\}. \qquad (2.10)$$

Sometimes b is called the diffusivity of sound (Lighthill, 1956; Hamilton and Morfey, 1998). Note that in Eq. (2.9) we have neglected nonlinear contributions in the dissipative term (the term on the right-hand side) by using $\rho \approx \rho_0$.

2.2.2 The Acoustic Wave Equation

In order to derive the acoustic equation it turns out to be convenient to introduce the function

$$h(\rho) = \int_{\rho_0}^{\rho} \frac{1}{\hat{\rho}} \left. \frac{\partial p}{\partial \rho} \right|_{\rho=\hat{\rho}, s=s_0} d\hat{\rho}, \qquad (2.11)$$

where $\hat{\rho}$ is a dummy integration variable. The quantity h is the enthalpy at constant entropy (Söderholm, 2001). Using Eq. (2.11) we can now rewrite the third term on the left-hand side in Eq. (2.9) as

$$\frac{p_x}{\rho} = \frac{1}{\rho}\frac{\partial p}{\partial \rho}\bigg|_{s=s_0}\rho_x = \frac{dh}{d\rho}\rho_x = h_x. \tag{2.12}$$

Moreover, the mass conservation equation (2.1) can be recast in the form

$$h_t + uh_x = -c^2 u_x, \tag{2.13}$$

where

$$c^2 = \frac{\partial p}{\partial \rho}\bigg|_{s=s_0} = \rho\frac{dh}{d\rho} \tag{2.14}$$

is the local speed of sound.

Upon inserting Eq. (2.12) into Eq. (2.9), introducing the velocity potential ψ, which is defined by

$$u = -\psi_x, \tag{2.15}$$

and integrating with respect to x, we obtain the following relation

$$h = \psi_t - \frac{(\psi_x)^2}{2} - b\psi_{xx}. \tag{2.16}$$

Similarly, in terms of the velocity potential, Eq. (2.13) becomes

$$h_t - \psi_x h_x = c^2 \psi_{xx}. \tag{2.17}$$

Finally, inserting Eq. (2.16) into Eq. (2.17) and neglecting nonlinear dissipative terms we obtain

$$\psi_{tt} - 2\psi_{xt}\psi_x + (\psi_x)^2\psi_{xx} - b\psi_{xxt} = c^2\psi_{xx}. \tag{2.18}$$

This is the higher order acoustic wave equation in terms of the velocity potential, which takes all orders of nonlinearity into account and the dissipative terms to lowest order. To the best of our knowledge this equation was first proposed by Söderholm (2001). Note that Eq. (2.18) applies to any equation of state. Hence, c is an unknown function to be determined from a given equation of state. Below we discuss two specific examples of explicit equations of state. Each of these state equations make it possible to express c in terms of ψ, so that we can obtain closed-form equations for the velocity potential.

2.2.3 Case of a Perfect Gas

A commonly used explicit form of the equation of state (2.4) is that for a perfect gas, that is, a gas for which both $p/\rho T$ and the specific-heat ratio are constants

$$\frac{p}{p_0} = \left(\frac{\rho}{\rho_0}\right)^\gamma \exp\left(\frac{s - s_0}{c_v}\right). \tag{2.19}$$

Here $\gamma = c_p/c_v$ is the ratio of specific heats, which in air at 20℃ takes the value of $\gamma = 1.4$. In the case of isentropic flow with $s = s_0$, Eq. (2.19) reduces to

$$\frac{p}{p_0} = \left(\frac{\rho}{\rho_0}\right)^\gamma.$$

(2.20)

The derivation of the higher order acoustic wave equation, and the derivations of the weakly nonlinear equations to be introduced later on, rely on the above isentropic assumption. However, the isentropic (actually homentropic) assumption $s = s_0$ is not valid, strictly speaking, if viscosity is present, see e.g. Ockendon and Ockendon (2004) pp. 12–13. For a gas described by (2.20) we find from (2.14) that

$$c^2 = \left.\frac{\partial p}{\partial \rho}\right|_{s=s_0} = c_0^2 \left(\frac{\rho}{\rho_0}\right)^{\gamma-1},$$

(2.21)

where $c_0^2 = \gamma p_0/\rho_0$ is the small signal sound velocity. Furthermore, by substituting Eq. (2.21) into Eq. (2.11) and carrying out the integration we obtain

$$h = \frac{1}{\gamma - 1}\left[c_0^2 \left(\frac{\rho}{\rho_0}\right)^{\gamma-1} - c_0^2\right] = \frac{c^2 - c_0^2}{\gamma - 1}.$$

(2.22)

Solving for c and using Eq. (2.16) to eliminate h yields

$$c^2 = c_0^2 + (\gamma - 1)\left(\psi_t - \frac{(\psi_x)^2}{2} - b\psi_{xx}\right),$$

(2.23)

Substituting Eq. (2.23) into Eq. (2.18) and neglecting nonlinear dissipative terms yields the following closed-form equation for the velocity potential

$$\psi_{tt} - c_0^2\psi_{xx} = (\gamma - 1)\psi_{xx}\psi_t + 2\psi_{xt}\psi_x - \frac{\gamma + 1}{2}(\psi_x)^2\psi_{xx} + b\psi_{xxt},$$

(2.24)

which is also given in Söderholm (2001). Finally, by equating Eqs. (2.21) and (2.23) and solving for ρ we obtain

$$\rho = \rho_0\left[1 + \frac{\gamma - 1}{c_0^2}\left(\psi_t - \frac{(\psi_x)^2}{2} - b\psi_{xx}\right)\right]^{\frac{1}{\gamma-1}},$$

(2.25)

which is the relationship between ρ and ψ. In later chapters we shall make use of this relationship in order to compare solutions of Eq. (2.24) to solutions of the basic equations introduced in Section 2.1. The relationship between p and ψ is obtained by inserting Eq. (2.25) into Eq. (2.20).

2.2.4 Case of a Fluid with a Quadratic Equation of State

In many cases the above assumption of perfect-gas behavior is unnecessarily restrictive. In order to obtain a model equation that is valid in arbitrary fluids, gases as well as liquids, we shall alternatively expand the equation of state (2.4) in a Taylor series about $(\rho, s) = (\rho_0, s_0)$. Within the field of nonlinear acoustics

it has become customary (Makarov and Ochmann, 1996a) to retain only the
following terms in the Taylor series

$$p - p_0 = c_0^2(\rho - \rho_0) + \frac{c_0^2}{\rho_0} \frac{B/A}{2}(\rho - \rho_0)^2 + \frac{\partial p}{\partial s}\Big|_{\rho=\rho_0, s=s_0} (s - s_0), \qquad (2.26)$$

where

$$c_0^2 = \frac{\partial p}{\partial \rho}\Big|_{\rho=\rho_0, s=s_0} \qquad (2.27)$$

is the small signal sound velocity, and

$$B/A = \frac{\rho_0}{c_0^2} \frac{\partial^2 p}{\partial \rho^2}\Big|_{\rho=\rho_0, s=s_0} \qquad (2.28)$$

is the non-dimensional fluid nonlinearity parameter (Beyer, 1974). The expansion (2.26) contains terms up to second order in $\rho - \rho_0$, but contains only terms
up to first order in $s - s_0$ since we neglect nonlinear contributions in the dissipative terms. Note that the same line of thought is utilized in Eq. (2.5).

A detailed study of the case of an arbitrary fluid, described by the quadratic
equation of state (2.26), is given in Christov et al. (2007). These authors
show that in this case the function c in Eq. (2.18) involves the Lambert W-function (Corless et al., 1996). Thus, their analysis leads to a wave equation,
which (according to the authors themselves) is quite complicated and likely intractable. However, by assuming that the Mach number $\varepsilon = u_{\max}/c_0$, where
$u_{\max} = \max |u|$, is small, they show that their complicated equation may be
approximated by Eq. (2.24) with $\gamma - 1$ replaced by B/A.[3]

Alternatively, a connection between the equations of state (2.20) and (2.26)
is established by inserting the perfect gas law (2.20) into (2.28) to obtain

$$B/A = \gamma - 1. \qquad (2.29)$$

Hence, there is a direct connection between the ratio of specific heats and the
parameter of nonlinearity. In arbitrary fluids described by Eq. (2.26) the parameters c_0 and B/A are typically determined by experimental methods and
values for a wide range of media can be looked up in tables. A few examples are
given in Table 2.1. The parameter values for soft tissue are included in the table
due to the fact that nonlinear acoustics is of great importance within the field
of biomedical ultrasound, see e.g. Yang and Cleveland (2005) and references
therein.

2.2.5 Some Remarks on the Higher Order Acoustic Wave Equation

In the derivation of the higher order acoustic wave equation (2.24) we took
into account the dissipative terms to lowest order only, neglecting nonlinearities
in those terms. Accordingly, Eq. (2.24) is an *approximation* to the four basic

---

[3]The study conducted by Christov and coworkers is carried out for the lossless case, however, their analysis and results readily generalizes to take into account the linear thermoviscous
effects discussed above.

Table 2.1. Values of c_0 and B/A for three different substances.

Substance	c_0 (m/s)	B/A
Water	1483 (20℃)[a]	5.0 (20℃)[b]
Air	343 (20℃)[a]	0.4 (20℃)[b]
Soft tissue	1540[c]	9.6 (37℃)[b]

[a] Lide (2007)
[b] Beyer (1998)
[c] Gent (1997)

equations (2.1)–(2.4). On the other hand, from the derivation (see Section 2.2.1) it follows that, if the entropy equation (2.3) is not taken into account, the result would still be Eq. (2.24), but with b replaced by the following

$$\beta = \frac{1}{\rho_0} \left(\frac{4}{3}\mu + \zeta \right), \tag{2.30}$$

where β is obtained by setting $\kappa = 0$ in Eq. (2.10). From this observation we draw two conclusions, (i) Eq. (2.24) with b replaced by β is an approximation to just *three* of the basic equations, namely Eqs. (2.1), (2.2) and (2.4), (ii) taking into account the entropy equation (2.3) in the derivation of Eq. (2.24) has no effect on the lossless part of the equation. Thus, for a given problem, it is consistent and relevant to compare the solution of the higher order acoustic wave equation Eq. (2.24) with b replaced by β, to the solution of the three basic equations (2.1), (2.2) and (2.4), omitting Eq. (2.3). In later chapters we are going to perform such comparisons in order to investigate the accuracy of the higher order acoustic wave equation.

2.2.6 Lossless Fluids

In order to study lossless fluids, one should set μ, ζ, and κ to zero. The entropy equation (2.3) leads to the trivial conclusion $s = s_0$ (because the fluid is initially uniform with $s = s_0$ everywhere), and the equation of state (2.4) reduces to $p = p(\rho)$. The mass conservation and momentum equations (2.1) and (2.2) reduce to

$$\rho_t + (\rho u)_x = 0, \tag{2.31}$$

$$\rho(u_t + u u_x) + p_x = 0, \tag{2.32}$$

which are Euler's equations. It follows from the derivation of the higher order acoustic wave equation (2.24) that the lossless part of the equation, that is

$$\psi_{tt} - c_0^2 \psi_{xx} = (\gamma - 1)\psi_{xx}\psi_t + 2\psi_{xt}\psi_x - \frac{\gamma + 1}{2} (\psi_x)^2 \psi_{xx}, \tag{2.33}$$

is exact for a lossless perfect gas described by Eq. (2.20), which we repeat here

$$\frac{p}{p_0} = \left(\frac{\rho}{\rho_0} \right)^\gamma. \tag{2.34}$$

Here the term 'exact' signifies that all nonlinearities in Eqs. (2.31), (2.32) and (2.34) are retained in Eq. (2.33). Similar conclusions are made in Hamilton and Morfey (1998) and Christov et al. (2007), who give detailed derivations of the lossless equation. Furthermore, in order to emphasize the exactness of Eq. (2.33), Christov and coworkers termed it the potential Euler equation.

Setting $b = 0$ in Eq. (2.25) yields

$$\rho = \rho_0 \left[1 + \frac{\gamma - 1}{c_0^2} \left(\psi_t - \frac{(\psi_x)^2}{2} \right) \right]^{\frac{1}{\gamma - 1}}, \tag{2.35}$$

which is the exact relationship between ρ and ψ in the lossless case. Furthermore, we recall that from Eq. (2.15) we have $u = -\psi_x$, which is also exact. Hence, upon using the two relationships (2.15) and (2.35), we expect that Eq. (2.33) is equivalent to the system (2.31), (2.32) and (2.34). However, in Chapter 3 we shall see that the equations are not equivalent if the shocks (or jump discontinuities) are present in the solution.

2.3   Hamiltonian Structure

The introduction of a Hamiltonian structure for conservative, or lossless, non-linear continuous media is essentially the generalization of the Hamiltonian formalism for systems with a finite number of degrees of freedom to systems with an infinite number of degrees of freedom. An introduction to the Hamiltonian formalism for nonlinear waves can be found in the review paper by Zakharov and Kuznetsov (1997) or in the book by Goldstein et al. (2001). In the following we introduce Lagrangian densities associated with Euler's equations and the lossless nonlinear wave equation. From the Lagrangian density we derive the corresponding Hamiltonian density using the Legendre transformation.

Upon introducing the velocity potential (2.15) into the mass conservation equation (2.1), and setting $b = 0$ in Eq. (2.16), we obtain Euler's equations in the following form

$$\rho_t - (\rho \psi_x)_x = 0, \tag{2.36}$$

$$\psi_t - \frac{(\psi_x)^2}{2} - h = 0, \tag{2.37}$$

where $h = h(\rho)$ is defined in Eq. (2.11). Basic to the Lagrangian approach is the assumption that the action integral

$$L = \int_{t_1}^{t_2} \int_{x_1}^{x_2} \mathcal{L}(x, t, y, y_x, y_t) \, dx \, dt \tag{2.38}$$

takes a maximum or a minimum along the true solution $y = y(x, t)$. This is the case if the Euler-Lagrange variational equation

$$\frac{\partial \mathcal{L}}{\partial y} - \frac{\partial}{\partial x} \left(\frac{\partial \mathcal{L}}{\partial y_x} \right) - \frac{\partial}{\partial t} \left(\frac{\partial \mathcal{L}}{\partial y_t} \right) = 0 \tag{2.39}$$

is satisfied, see e.g. Arfken and Weber (2001). It follows that Euler's equations (2.36) and (2.37) may be obtained from a Lagrangian density $\mathcal{L}$ of the following form

$$\mathcal{L} = \rho \left(\psi_t - \frac{(\psi_x)^2}{2} \right) - H, \tag{2.40}$$

where the function $H = H(\rho)$ is defined by

$$H = \int_{\rho_0}^{\rho} h(\hat{\rho}) \, d\hat{\rho}. \tag{2.41}$$

In order to verify this, take $y = (\psi, \rho)$ and insert Eq. (2.40) into Eq. (2.39), which immediately yields Eqs. (2.36) and (2.37).

Using Eq. (2.11) we find that H may be rewritten as

$$H = \rho \, h(\rho) - p(\rho). \tag{2.42}$$

Then, by taking into account that from Eq. (2.37) we have

$$h = \psi_t - \frac{(\psi_x)^2}{2}, \tag{2.43}$$

we obtain by inserting into Eq. (2.40) that the Lagrangian density takes the form

$$\mathcal{L} = p\left(\rho(h) \right) \tag{2.44}$$

with h given by Eq. (2.43). In the case of a lossless perfect gas we obtain, by inserting Eq. (2.35) into Eq. (2.34) and inserting the result into Eq. (2.44), the following Lagrangian density

$$\mathcal{L} = p_0 \left[1 + \frac{\gamma - 1}{c_0^2} \left(\psi_t - \frac{(\psi_x)^2}{2} \right) \right]^{\frac{\gamma}{\gamma - 1}}. \tag{2.45}$$

Taking $y = \psi$ and inserting Eq. (2.45) into Eq. (2.39) yields, after some calculations, the lossless higher order acoustic wave equation (2.33) as expected. This achievement confirms that Eq. (2.45) is the Lagrangian density associated with Eq. (2.33).

The Hamiltonian density can be obtained using the Legendre transformation (Goldstein et al., 2001), which takes the form

$$\mathcal{H} = \frac{\partial \mathcal{L}}{\partial \psi_t} \psi_t - \mathcal{L}. \tag{2.46}$$

Inserting Eq. (2.45) into Eq. (2.46) yields the following Hamiltonian density

$$\mathcal{H} = p_0 \left[1 + \frac{\gamma - 1}{c_0^2} \left(\psi_t - \frac{(\psi_x)^2}{2} \right) \right]^{\frac{\gamma}{\gamma - 1}}$$
$$\times \left\{ 1 - \frac{\gamma}{c_0^2} \left[1 + \frac{\gamma - 1}{c_0^2} \left(\psi_t - \frac{(\psi_x)^2}{2} \right) \right]^{-1} \right\}. \tag{2.47}$$

The Hamiltonian density is the sum of the kinetic and potential energy density in the system.

2.4 Weakly Nonlinear Wave Equations

The higher order acoustic wave equation (2.24) derived above retains all non-linear contributions in the lossless terms. However, under some circumstances analytical treatment of such equations become unwieldy, or even unfeasible. In order to obtain equations that are more amenable to analysis it is common in the theory of nonlinear acoustics to consider equations, which take only quadratic nonlinear terms into account. In the following we present four such weakly nonlinear equations, that are derived from the the higher order acoustic wave equation using various approximation schemes.

2.4.1 Straightforward Weakly Nonlinear Equation

Upon neglecting the cubic nonlinear term in Eq. (2.24) we obtain

$$\psi_{tt} - c_0^2 \psi_{xx} = (\gamma - 1)\psi_{xx}\psi_t + 2\psi_{xt}\psi_x + b\psi_{xxt}. \qquad (2.48)$$

This equation appears in a review paper by Crighton (1979), but has not received much attention since. However, recently Christov et al. (2007) advocated the lossless form of this equation, saying that it is the most consistent and most obvious weakly nonlinear approximation. To emphasize this, those authors denoted the lossless form of Eq. (2.48) the straightforward weakly nonlinear equation.

2.4.2 The Kuznetsov Equation

A slightly different weakly nonlinear model is the Kuznetsov equation (Kuznetsov, 1971), which takes the form

$$\psi_{tt} - c_0^2 \psi_{xx} = \frac{\gamma - 1}{c_0^2}\psi_{tt}\psi_t + 2\psi_{xt}\psi_x + b\psi_{xxt}. \qquad (2.49)$$

This equation is immediately obtained by invoking the first order approximation $\psi_{tt} = c_0^2 \psi_{xx}$ in the first term on the right hand side of Eq. (2.48).

Traditionally, the Kuznetsov equation is the most widespread model equation and some authors (Aanonsen et al., 1984; Jordan, 2004) literally denote it the "classical" equation of nonlinear acoustics. Both Eq. (2.49) and its paraxial approximation, the KZK equation (Zabolotskaya and Khokhlov, 1969; Kuznetsov, 1971), are frequently encountered within studies related to nonlinear wave propagation.

2.4.3 Hamiltonian Weakly Nonlinear Equation

In the following we describe a novel approach based on the Lagrangian and Hamiltonian structure to obtain a weakly nonlinear approximation. In Section 2.3 we demonstrated that Euler's equations and the lossless version of the higher order acoustic wave equation are of Hamiltonian structure. However, this fundamental property is *not* retained in the lossless versions of the straightforward weakly nonlinear equation and the Kuznetsov equation introduced above. Hence, these equations cannot be associated with Lagrangian and Hamiltonian

densities. In order to obtain a weakly nonlinear model with a Hamiltonian and Lagrangian structure, we shall make the weakly nonlinear approximation based on the Lagrangian density.

Making a series expansion of the Lagrangian density (2.45) around $(\psi_t, \psi_x) = (0, 0)$ and keeping only nonlinear terms up to third order we obtain, after several calculations, the following result

$$\mathcal{L} = \frac{(\psi_t)^2}{2} - c_0^2 \frac{(\psi_x)^2}{2} - \frac{\gamma - 1}{6c_0^2}(\psi_t)^3 - \frac{\psi_t(\psi_x)^2}{2}. \tag{2.50}$$

Inserting this Lagrangian density into the Euler-Lagrange equation (2.39), taking $y = \psi$, yields

$$\psi_{tt} - c_0^2 \psi_{xx} = \psi_t \psi_{xx} + \frac{\gamma - 2}{c_0^2} \psi_{tt} \psi_t + 2\psi_{xt} \psi_x, \tag{2.51}$$

which is our Hamiltonian weakly nonlinear equation. In order to take into account thermoviscous effects to lowest order, Eq. (2.51) should be augmented in the following way

$$\psi_{tt} - c_0^2 \psi_{xx} = \psi_t \psi_{xx} + \frac{\gamma - 2}{c_0^2} \psi_{tt} \psi_t + 2\psi_{xt} \psi_x + b\psi_{xxt}. \tag{2.52}$$

This equation forms the basis for the analysis in our paper in Appendix A. To the best of our knowledge Eq. (2.52) has not been previously reported in the literature. Without fear of confusion, we are going to refer to Eq. (2.52) as the Hamiltonian weakly nonlinear equation, even though the Hamiltonian property concerns only the lossless part of the equation.

Similarly to the Kuznetsov equation, our Hamiltonian weakly nonlinear equation can be obtained from the straightforward weakly nonlinear equation (2.48) by performing simple manipulations. To see this we rewrite the first term on the right hand side of Eq. (2.48) in the following way

$$(\gamma - 1)\psi_{xx}\psi_t = (1 + \gamma - 2)\psi_{xx}\psi_t = \psi_{xx}\psi_t + \frac{\gamma - 2}{c_0^2}\psi_{tt}\psi_t, \tag{2.53}$$

where the first order approximation $\psi_{tt} = c_0^2 \psi_{xx}$ is used in the last step. Inserting Eq. (2.53) into Eq. (2.48) immediately yields Eq. (2.52).

Inserting Eq. (2.50) into Eq. (2.46) yields the corresponding Hamiltonian density

$$\mathcal{H} = c_0^2 \frac{(\psi_x)^2}{2} + \frac{(\psi_t)^2}{2} - \frac{\gamma - 2}{3c_0^2}(\psi_t)^3, \tag{2.54}$$

which is given here for the sake of completeness.

2.4.4 The Burgers Equation

Finally, we mention the Burgers equation, which have played a central role in the development of the understanding of nonlinear wave phenomena in acoustics. Burgers' equation takes the form

$$u_x - \frac{\gamma + 1}{2c_0^2} u u_\tau = \frac{b}{2c_0^3} u_{\tau\tau}, \tag{2.55}$$

where $\tau = t - x/c_0$ is the retarded time. The equation can be obtained from the above acoustic wave equations by application of a certain approximation scheme, see e.g. Jordan (2004).

Chapter 3

Lossless, Viscous and Thermoviscous Shocks

A shock is a type of propagating disturbance. Like an ordinary wave, it carries energy and can propagate through a medium (solid, liquid or gas). Shocks are characterized by an abrupt, nearly discontinuous change in the in pressure, temperature and density of the flow and arise in various situations. A shock can form due to steepening of ordinary waves. Probably, the best-known example of this phenomenon is ocean waves that form breakers on the shore. In Chapter 5 we shall investigate a problem, which is related to the formation of a shock due to the steepening of an acoustic wave generated by a vibrating piston in a tube. Shocks also arise in shock tubes. A simple shock tube is a metal tube in which a gas at low pressure and a gas at high pressure are separated using a diaphragm. This diaphragm suddenly bursts open to produce a shock that travels down the tube. In Chapter 6 we shall study a problem which is related to a shock tube. Other situations in which shocks are caused by a sudden, violent disturbance of a fluid, are those created by a powerful explosion or by the supersonic flow of the fluid over a solid object. The latter one arises e.g. in supersonic flight.

In this chapter we shall investigate how the phenomenon of a shock can be described by the equations of nonlinear acoustics. In this context we consider the basic equations as well as the higher order acoustic wave equation and the weakly nonlinear wave equations introduced in the previous chapter. We study both the lossless case and the dissipative case.

3.1 Hyperbolic Systems of Conservation Laws

Traditionally, much of the mathematical analysis of lossless shocks is based on the theory for hyperbolic systems of conservation laws, which are systems of linear or nonlinear partial differential equations. It shall prove useful to start by introducing the notion of such systems. Much af the basic theory for hyperbolic equations is due to Lax (1957). A helpful introduction is given in the book by LeVeque (2002), which also discusses the application of finite volume methods

15

to obtain numerical solutions to conservation laws.

With an eye to the analysis of the following sections, it shall prove sufficient to consider systems of two conservation laws in one spatial dimension. Generally, such systems are written in the form

$$
\left[\begin{array}{c} q_1(x,t) \\ q_2(x,t) \end{array}\right]_t + \left[\begin{array}{c} f_1\big(q_1(x,t), q_2(x,t)\big) \\ f_2\big(q_1(x,t), q_2(x,t)\big) \end{array}\right]_x = q_t + f(q)_x = 0, \qquad (3.1)
$$

where $q = q(x,t)$ is a vector with two components representing the unknown functions, e.g. density and particle velocity, we wish to determine, and $f(q)$ is the flux function. We let

$$
\lambda_1 = \lambda_1(q) \leq \lambda_2 = \lambda_2(q) \qquad (3.2)
$$

be the eigenvalues of the Jacobian matrix

$$
f'(q) = \left[\begin{array}{cc} \dfrac{\partial f_1}{\partial q_1} & \dfrac{\partial f_1}{\partial q_2} \\ \dfrac{\partial f_2}{\partial q_1} & \dfrac{\partial f_2}{\partial q_2} \end{array}\right], \qquad (3.3)
$$

while

$$
e_1(q), e_2(q) \qquad (3.4)
$$

are the corresponding eigenvectors. The eigenvectors $e_p(q)$ are the normal modes for the propagation of small amplitude signals, linearized about the state q, while $\lambda_p(q)$ are the corresponding wave speeds. The system (3.1) is *hyperbolic* if the λ_p are real. If the λ_p are real and distinct the system is called *strictly hyperbolic*.

To have a shock solution[1] of Eq. (3.1), separating two constant states and propagating at the velocity v, the Rankine-Hugoniot jump condition

$$
v\,(q_r - q_l) = f(q_r) - f(q_l) \qquad (3.5)
$$

must hold. Here q_r and q_l denote the constant states to the right and left of the shock. Alternatively, using square brackets with sub- and superscripts to denote the change in value of any quantity across a shock, e.g.

$$
[\rho]_l^r = \rho_r - \rho_l, \qquad (3.6)
$$

we may write Eq. (3.5) in the following way

$$
[f(q) - vq]_l^r = 0. \qquad (3.7)
$$

This notation will be used throughout the text. Note that the shock propagation velocity v is measured in a fixed coordinate system. Hence, v does not change across a shock.

It is well-known that the Rankine-Hugoniot jump condition (3.7) admits many non-physical solutions to Eq. (3.1) (Schecter et al., 1996; LeVeque, 2002;

---

[1]In the context of the lossless equations considered here, a shock takes the form of a jump discontinuity.

Li, 2004). In order to illustrate this we note that, if $q_r = q_2$ and $q_l = q_1$ satisfy the jump condition (3.7), then $q_r = q_1$ and $q_l = q_2$ also satisfy the condition if v remains unchanged. Two such solutions are shown in Fig. 3.1, only one of these solutions is in fact the physically correct shock solution. The Lax entropy condition (Lax, 1957) states that, for the correct solution there is an index p such that

$$\lambda_p(q_l) > v > \lambda_p(q_r). \qquad (3.8)$$

In the case of a system of two conservation laws, p is either 1 or 2. Recall that $\lambda_p(q)$ are the wave speeds for the propagation of small amplitude signals, linearized about the state q. That is, $\lambda_p(q)$ is equivalent to the local speed of sound. Hence, the Lax entropy condition states that the shock propagation velocity is supersonic with respect to the fluid ahead of the shock, and subsonic with respect to the fluid behind it (Smoller, 1994).
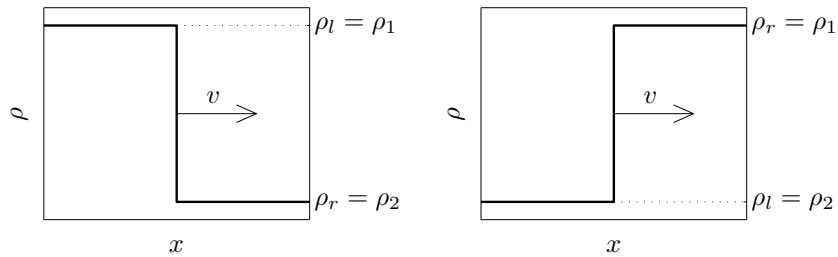

Fig. 3.1. Lossless shocks that satisfy the Rankine-Hugoniot jump condition (3.7). In this example we have taken $q_1 = \rho$. If, let us say, $q_2 = u$, then the corresponding plots for u are obtained by replacing ρ by u everywhere in the figure.

3.2   The Basic Equations for a Perfect Gas

In the following we study shock solutions derived from the basic equations introduced in the previous chapter. In particular, we shall demonstrate that caution is required if the equations are subjected to simple manipulations, or if small nonlinear correction terms are neglected in the dissipative terms. Such manipulations or approximations may have unexpected influence on the shock solutions of the new equations obtained. Based on comparisons of shock solutions derived from various manipulated forms of the basic equations, and from equations that retain only the lowest order dissipative terms, we shall illustrate the problems that arise. Recall that the acoustic wave equations introduced in Chapter 2 are obtained by manipulating the basic equations and neglecting nonlinear dissipative terms. Thus, the results of this section is of relevance to those equations also.

3.2.1   Manipulations of the Equations

We consider the mass conservation equation (2.1), the momentum equation (2.2), and the equation of state for a perfect gas (2.20), which we repeat here

for convenience

$$\rho_t + (\rho u)_x = 0, \tag{3.9}$$

$$\rho(u_t + u u_x) + p_x = \left(\frac{4}{3}\mu + \zeta\right) u_{xx}, \tag{3.10}$$

$$\frac{p}{p_0} = \left(\frac{\rho}{\rho_0}\right)^\gamma. \tag{3.11}$$

These equations are of particular interest since, according to Section 2.2.5, the higher order acoustic wave equation (2.24) is an approximation to Eqs. (3.9), (3.10) and (3.11). Furthermore, given that the weakly nonlinear wave equations introduced in Section 2.4 are approximations to the higher order wave equation, it follows that these equations are also approximations to the above three equations.

In order to obtain a system of conservation laws we insert Eq. (3.11) into Eq. (3.10) and use $c_0^2 = \gamma p_0/\rho_0$ to achieve

$$\rho(u_t + u u_x) + \frac{c_0^2 \rho_0}{\gamma} \left[\left(\frac{\rho}{\rho_0}\right)^\gamma\right]_x = \rho_0 \beta u_{xx}. \tag{3.12}$$

Here β is the viscous dissipation parameter defined in Eq. (2.30). Dividing by ρ in all terms in Eq. (3.12) and combining with Eq. (3.9) we find the following closed form system of equations

$$\left[\begin{array}{c} \rho \\ u \end{array}\right]_t + \left[\begin{array}{c} \rho u \\ \frac{u^2}{2} + \frac{c_0^2}{\gamma - 1}\left(\frac{\rho}{\rho_0}\right)^{\gamma-1} \end{array}\right]_x = \left[\begin{array}{c} 0 \\ \frac{\rho_0 \beta u_{xx}}{\rho} \end{array}\right]. \tag{3.13}$$

A slightly different system of equations is obtained by adding Eq. (3.9) multiplied by u to Eq. (3.12)

$$\left[\begin{array}{c} \rho \\ \rho u \end{array}\right]_t + \left[\begin{array}{c} \rho u \\ \rho u^2 + \frac{c_0^2 \rho_0}{\gamma}\left(\frac{\rho}{\rho_0}\right)^\gamma \end{array}\right]_x = \left[\begin{array}{c} 0 \\ \rho_0 \beta u_{xx} \end{array}\right]. \tag{3.14}$$

If we set $\beta = 0$ in Eqs. (3.13) and (3.14) each system reduces to a system of conservation laws of the form (3.1). These, two systems will be treated in detail in the next subsection.

The set of equations (3.14) is equivalent to the previous set (3.13) for smooth solutions, but it is important to note that the manipulations performed above depend on smoothness. In the *lossless case*, which is obtained by setting $\beta = 0$, shocks take the form of jump discontinuities. Hence, in the lossless case, the two sets of conservation laws *are not equivalent* if shocks occur in the solution. Generally, as pointed out in the book by LeVeque (2002), such troubles arise whenever systems of conservation laws are subjected to manipulations that depend on smoothness. In the *dissipative case*, i.e. when $\beta \neq 0$, shocks take the form of smooth steps (viscous shocks). Thus, in the dissipative case, the two sets of equations (3.13) and (3.14) are equivalent, even for problems with

viscous shocks. In the following two subsections we shall verify these observations by calculating the Rankine-Hugoniot jump conditions in the lossless cases, and studying the viscous shock solutions in the dissipative cases by means of traveling wave analysis.

3.2.2 Rankine-Hugoniot Jump Conditions for the Lossless Equations

The system of conservation laws obtained by setting $\beta = 0$ in Eq. (3.13) is the following

$$\begin{bmatrix} \rho \\ u \end{bmatrix}_t + \begin{bmatrix} \rho u \\ \dfrac{u^2}{2} + \dfrac{c_0^2}{\gamma - 1}\left(\dfrac{\rho}{\rho_0}\right)^{\gamma-1} \end{bmatrix}_x = 0. \tag{3.15}$$

Comparing with Eq. (3.1) we find that

$$q = \begin{bmatrix} \rho \\ u \end{bmatrix} = \begin{bmatrix} q_1 \\ q_2 \end{bmatrix}, \tag{3.16}$$

$$f = \begin{bmatrix} \rho u \\ \dfrac{u^2}{2} + \dfrac{c_0^2}{\gamma - 1}\left(\dfrac{\rho}{\rho_0}\right)^{\gamma-1} \end{bmatrix} = \begin{bmatrix} q_1 q_2 \\ \dfrac{q_2^2}{2} + \dfrac{c_0^2}{\gamma - 1}\left(\dfrac{q_1}{\rho_0}\right)^{\gamma-1} \end{bmatrix}. \tag{3.17}$$

The eigenvalues of the Jacobian matrix $f'(q)$ are

$$\lambda_{1,2} = u \mp c_0 \sqrt{\left(\frac{\rho}{\rho_0}\right)^{\gamma-1}}. \tag{3.18}$$

Since $\rho > 0$ and $\rho_0 > 0$, the eigenvalues are always real and distinct. Hence, we conclude that the system (3.15) is always strictly hyperbolic. Note that, upon inserting the perfect gas state equation Eq. (3.11) into Eq. (2.14), and using $c_0^2 = \gamma p_0 / \rho_0$, yields the following local sound velocities

$$c = \mp c_0 \sqrt{\left(\frac{\rho}{\rho_0}\right)^{\gamma-1}}. \tag{3.19}$$

Thus, by comparing Eqs. (3.18) and (3.19), we see that λ and c are the sound velocities measured in a fixed coordinate system, and a coordinate system that moves with the velocity u, receptively.

For the system (3.15), the Rankine-Hugoniot jump condition (3.7) gives the following system of two equations that must be satisfied simultaneously

$$[\rho(u - v)]_l^r = 0, \tag{3.20a}$$

$$\left[\frac{c_0^2}{\gamma - 1}\left(\frac{\rho}{\rho_0}\right)^{\gamma-1} + \frac{u^2}{2} - vu \right]_l^r = 0. \tag{3.20b}$$

Thus, there exists a shock solution of the system (3.15). The constant values of ρ and u to the right and left of the shock, and the shock propagation velocity v, must satisfy the jump condition (3.20). We thus have a system of two equations

for the five variables ρ_r, ρ_l, u_r, u_l and v. Hence, if we fix three of these variables the shock solution is completely determined.

Returning now to Eq. (3.14), we obtain by setting $\beta = 0$ the following

$$\begin{bmatrix} \rho \\ \rho u \end{bmatrix}_t + \begin{bmatrix} \rho u \\ \rho u^2 + \dfrac{c_0^2 \rho_0}{\gamma} \left(\dfrac{\rho}{\rho_0} \right)^\gamma \end{bmatrix}_x = 0, \qquad (3.21)$$

which is a system of conservation laws with

$$q = \begin{bmatrix} \rho \\ \rho u \end{bmatrix} = \begin{bmatrix} q_1 \\ q_2 \end{bmatrix}, \qquad (3.22)$$

$$f = \begin{bmatrix} \rho u \\ \rho u^2 + \dfrac{c_0^2 \rho_0}{\gamma} \left(\dfrac{\rho}{\rho_0} \right)^\gamma \end{bmatrix} = \begin{bmatrix} q_2 \\ \dfrac{q_2^2}{q_1} + \dfrac{c_0^2 \rho_0}{\gamma} \left(\dfrac{q_1}{\rho_0} \right)^\gamma \end{bmatrix}. \qquad (3.23)$$

The eigenvalues of the Jacobian matrix $f'(q)$ are *identical* to those derived from Eq. (3.15) above. This is not surprising, since the systems (3.15) and (3.21) are equivalent for smooth solutions, as noted in the previous subsection. For the system (3.21) the Rankine-Hugoniot jump condition (3.7) gives

$$[\rho(u - v)]_l^r = 0, \qquad (3.24a)$$

$$\left[\dfrac{c_0^2 \rho_0}{\gamma} \left(\dfrac{\rho}{\rho_0} \right)^\gamma + \rho u^2 - v \rho u \right]_l^r = 0. \qquad (3.24b)$$

Thus, the system (3.21) has a shock solution, which satisfies the jump condition (3.24).

By comparing the jump condition (3.20), which corresponds to the system (3.15), to the jump condition (3.24), which corresponds to the system (3.21), we observe that the two are *not* equivalent. This observation is also clearly seen in Fig. 3.2. The two curves in this figure are obtained by eliminating ρ_l from each of the systems (3.20) and (3.24), setting $\rho_r = \rho_0$ and $u_r = 0$, and plotting u_l versus v. The specific case of $\rho_r = \rho_0$ and $u_r = 0$ corresponds to the fluid on the right side of the shock being the quiescent state. Which one of the two jump conditions gives the correct physical behavior is not clear at the moment, but will be clarified as we come to the study of the dissipative case in the next subsection. The two jump conditions not being equivalent is not surprising, since in the previous subsection we made the conclusion that the two systems (3.15) and (3.21) are not equivalent for problems with shocks. Equations (3.15) and (3.21) are the results of simple manipulations of the same equations. These manipulations, however, depend on smoothness and the results of this subsection illustrates that, indeed, caution must be taken when the governing equations are subjected to such manipulations. From Fig. 3.2 we see that in the case of infinitely weak shocks, that is $u_l \to 0$, the shock propagation velocities v approach the small signal sound speed c_0. This behavior agrees with linear acoustics. In the vicinity of the point $(v, u_l) = (c_0, 0)$, there is a fine agreement between the Rankine-Hugoniot jump conditions corresponding to the two conservation laws. Another observation that relates to Fig. 3.2 is the following. In the case of the

specific choice of parameters in the figure, the sound speed to the right of the shock is c_0, cf. Eqs. (3.18) and (3.19). Thus, when $v > c_0$ the shock propagation velocity is supersonic with respect to the fluid ahead of the shock[2] and the Lax entropy condition (3.8) is satisfied. On the other hand, shocks with $0 < v < c_0$, i.e. the lower left rectangle indicated by dotted line, are subsonic with respect to the fluid ahead of the shock, and thus violate the entropy condition. These shocks are physically unrealistic.
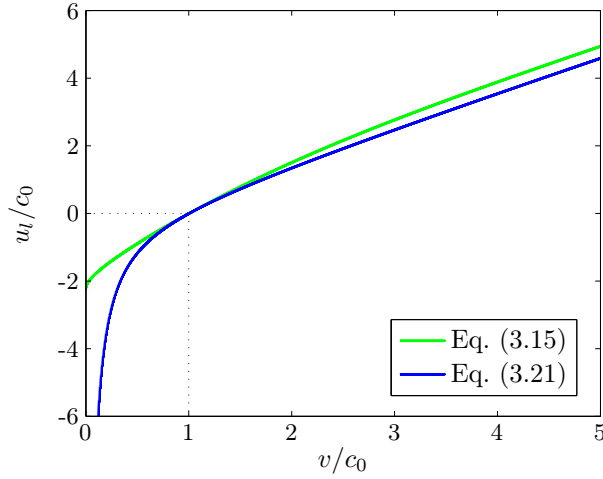

Fig. 3.2. Comparison of the Rankine-Hugoniot jump conditions (3.20) and (3.24) corresponding to the system of conservation laws (3.15) and (3.21), respectively. The following parameters are used: $\rho_r = \rho_0$, $u_r = 0$ and $\gamma = 1.4$.

3.2.3 Traveling Wave Analysis of the Dissipative Equations

In order to study the viscous shock solutions to the dissipative equations (3.13) and (3.14) we search for a traveling wave solutions of the form

$$\rho(x,t) = P(\xi), \qquad u(x,t) = U(\xi), \tag{3.25}$$

where $\xi = x - vt$ is a wave variable, and v is the propagation velocity of the traveling wave. Inserting Eqs. (3.25) into Eq. (3.13) yields

$$-vP' + (PU)' = 0, \tag{3.26}$$

$$-vU' + \left[\frac{U^2}{2} + \frac{c_0^2}{\gamma - 1}\left(\frac{P}{\rho_0}\right)^{\gamma - 1}\right]' = \frac{\rho_0 \beta U''}{P}, \tag{3.27}$$

where prime denotes differentiation with respect to ξ. Integration of Eq. (3.26) gives

$$P(U - v) = -C_1 \Leftrightarrow P = \frac{C_1}{v - U}, \tag{3.28}$$

---

[2]It can be shown that when $v > c_0$ the shock propagation velocity is subsonic with respect to the fluid behind the shock.

where C_1 is an integration constant. Using Eq. (3.28) to eliminate P from Eq. (3.27), rewriting the result and integrating once yields the following first order ordinary differential equation (ODE) for $U(\xi)$

$$\frac{c_0^2 \rho_0}{\gamma \rho_0^{\gamma}} \left(\frac{C_1}{v - U}\right)^{\gamma} - C_1 U = \rho_0 \beta U' + C_2, \qquad (3.29)$$

where C_2 is yet another integration constant. By separation of variables we obtain

$$\xi - x_0 = \rho_0 \beta \int^{U} \left\{ \frac{c_0^2 \rho_0}{\gamma \rho_0^{\gamma}} \left(\frac{C_1}{v - \hat{U}}\right)^{\gamma} - C_1 \hat{U} - C_2 \right\}^{-1} d\hat{U}, \qquad (3.30)$$

where x_0 is an integration constant. Equation (3.30) represents the structure of the exact viscous shock solution to Eq. (3.13). The integral in Eq. (3.30) cannot be readily solved by analytical methods, however, a solution can be obtained by means of numerical methods. The viscous shock profiles shown in Fig. 3.3 are obtained by solving Eq. (3.30) using an implementation of the trapezoidal method, which is available in the software package MATLAB®.[3] Once U is computed, P follows directly by inserting U into Eq. (3.28). From Fig. 3.3 we see that the structure of weak shocks propagating at velocities near the small signal sound velocity c_0, resemble the structure of the hyperbolic tangent. For stronger shocks propagating at higher speeds the shock structure becomes more smooth on the front of the shock and less smooth on the back of the shock. Furthermore, we observe that the shock thickness is proportional to the viscous dissipation β. In the lossless limit of $\beta \to 0$, the thickness of the shock approaches zero. That is the viscous shock approaches a jump discontinuity.
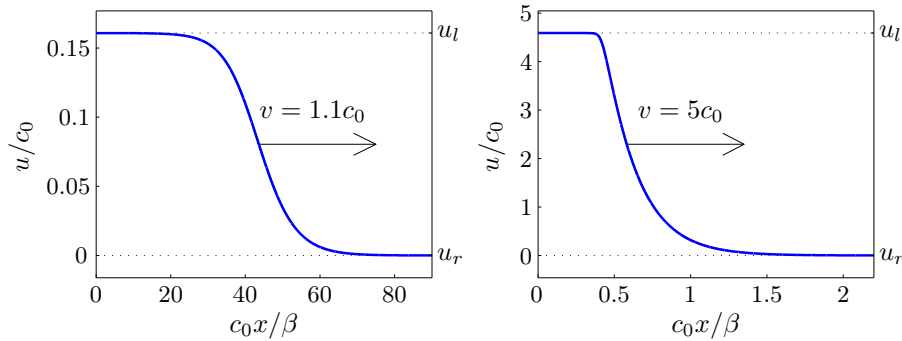

Fig. 3.3. Viscous shock profile given by Eq (3.30) with $C_1 = v\rho_0$, $C_2 = c_0^2 \rho_0/\gamma$ and $\gamma = 1.4$. The integration constants C_1 and C_2 are determined in such a way that $u_r = 0$ and $\rho_r = \rho_0$, where u_r and ρ_r are the right asymptotic boundary values of U and P, respectively. Left figure: weak shock propagating at lower speed. Right figure: strong shock propagating at higher speed.

In order to study the asymptotic boundary conditions of the viscous shock solution (3.30), it turns out to be convenient to invoke Eq. (3.28) in Eq. (3.29)

---

[3] http://www.mathworks.com

to obtain

$$\frac{c_0^2 \rho_0}{\gamma} \left(\frac{P}{\rho_0} \right)^{\gamma} + PU^2 - vPU = \rho_0 \beta U' + C_2. \tag{3.31}$$

Furthermore, we note that the viscous shock solution satisfies $U' \to 0$ and $P' \to 0$ as $\xi \to \pm\infty$, and we introduce the following notation for its asymptotic boundary conditions

$$P \to \begin{cases} \rho_r, & \xi \to +\infty \\ \rho_l, & \xi \to -\infty \end{cases} \quad \text{and} \quad U \to \begin{cases} u_r, & \xi \to +\infty \\ u_l, & \xi \to -\infty \end{cases}. \tag{3.32}$$

Then, introducing Eqs. (3.32) into Eq. (3.31) yields

$$\xi \to +\infty: \qquad v\rho_r u_r = \rho_r u_r^2 + \frac{c_0^2 \rho_0}{\gamma} \left(\frac{\rho_r}{\rho_0} \right)^{\gamma} - C_2, \tag{3.33a}$$

$$\xi \to -\infty: \qquad v\rho_l u_l = \rho_l u_l^2 + \frac{c_0^2 \rho_0}{\gamma} \left(\frac{\rho_l}{\rho_0} \right)^{\gamma} - C_2, \tag{3.33b}$$

and introducing Eqs. (3.32) into Eq. (3.28) yields

$$\xi \to +\infty: \qquad \rho_r(u_r - v) = C_1, \tag{3.34a}$$

$$\xi \to -\infty: \qquad \rho_l(u_l - v) = C_1. \tag{3.34b}$$

Finally, subtracting Eq. (3.33b) from Eq. (3.33a), and Eq. (3.34b) from Eq. (3.34a), yields two equations for the four asymptotic boundary conditions ρ_r, ρ_l, u_r, u_l, and the propagation velocity v. It is immediately seen that these two equations are *identical* to the Rankine-Hugoniot jump condition (3.24), which correspond to the lossless equations (3.21). Thus, the asymptotic boundary conditions and the propagation velocity of the viscous shock solution to Eq. (3.13) satisfy the jump condition for the lossless shock solution of Eq. (3.21). Note also that this result implies, that the equations for the asymptotic boundary conditions and the propagation velocity obtained in the dissipative case do not depend on the dissipation parameter β.

In a similar way, we can obtain the viscous shock solution to Eq. (3.14) by inserting the solution ansatz (3.25) into Eq. (3.14) and repeating the above procedure. Following these steps, it turns out that the viscous shock solution to Eq. (3.14) is, in every sense, *identical* to the viscous shock solution of Eq. (3.13) derived above. This is not surprising, since in Section 3.2.1 we made the conclusion that the dissipative equations (3.13) and (3.14) are equivalent.

3.2.4 Approximations in the Dissipative Terms

In Section 3.2.2 we showed that the jump condition of a lossless shock solution is altered if the governing equations are subjected to small manipulations that depend on smoothness. On the other hand, in Section 3.2.3 we demonstrated that the viscous shock solutions of the dissipative equations are not influenced by such manipulations. In the following we shall investigate whether the equations for the asymptotic boundary conditions and the propagation velocity of a viscous

shock solution to a system of dissipative equations alters, if we neglect nonlinear contributions in the dissipative terms. Recall that this particular approximation scheme was used extensively in the derivation of the higher order and weakly nonlinear thermoviscous wave equations in the previous chapter. Hence, the following investigation is of relevance to those equations also.

Equations (3.13) include a nonlinear dissipative term (the term on the right hand side in the second equation). Expanding $1/\rho$ in a Taylor series about $\rho = \rho_0$ yields

$$\frac{1}{\rho} = \frac{1}{\rho_0} - \frac{\rho - \rho_0}{\rho_0^2} + \frac{(\rho - \rho_0)^2}{\rho_0^3} + \dots . \tag{3.35}$$

Upon substituting Eq. (3.35) into the dissipative term and neglecting nonlinear contributions,[4] Eq. (3.13) reduces to

$$\begin{bmatrix} \rho \\ u \end{bmatrix}_t + \begin{bmatrix} \rho u \\ \dfrac{u^2}{2} + \dfrac{c_0^2}{\gamma - 1}\left(\dfrac{\rho}{\rho_0}\right)^{\gamma-1} \end{bmatrix}_x = \begin{bmatrix} 0 \\ \beta u_{xx} \end{bmatrix}. \tag{3.36}$$

Inserting the traveling wave assumption (3.25) into this equation and integrating once yields

$$P(U - v) = C_1, \tag{3.37}$$

$$vU = \frac{U^2}{2} + \frac{c_0^2}{\gamma - 1}\left(\frac{P}{\rho_0}\right)^{\gamma-1} - \beta U' + C_2, \tag{3.38}$$

where C_1 and C_2 are integration constants. In order to obtain the equations for the asymptotic boundary conditions of the corresponding viscous shock solution we note, again, that the solution satisfy $U' \to 0$ and $P' \to 0$ as $\xi \to \pm\infty$, and then repeat the steps (3.32) to (3.34) for Eqs. (3.37) and (3.38). Following this procedure, we find that the resulting equations for the asymptotic boundary conditions and the propagation velocity are *identical* to Eqs. (3.20). That is, the asymptotic boundary conditions of the viscous shock solution of Eq. (3.36) satisfy the jump condition for the lossless shock solution of Eq. (3.15). Thus, upon neglecting nonlinear contributions in the dissipative terms in Eq. (3.13), the corresponding jump condition changed from (3.24) to (3.20). Note that this result is obtained, despite the fact that the jump conditions do not depend on β.

3.2.5   Some Remarks on the Jump Conditions

We have now studied the shock solutions to five different versions of the basic equations for a perfect gas. In each case the Rankine-Hugoniot jump condition for the lossless shocks, or the equations for the asymptotic boundary conditions and the propagation velocity of the viscous shocks, are given either by Eqs. (3.20) or Eqs. (3.24). The specific findings are summarized in Table 3.1. The results signify that, of the two lossless systems of equations (3.15) and (3.21), the latter

---

[4]A parallel approximation was introduced in Eq. (2.9).

one gives the correct physical behavior, since the corresponding jump condition agrees with that of the dissipative equations (3.13) and (3.14). Equations (3.15) and (3.36) lead to the same jump condition. This jump condition differs from the correct physical one, as can be seen in Fig. 3.2. Hence, we have demonstrated that caution is required if either the lossless equations are subjected to manipulations that depend on smoothness, or if nonlinear dissipative terms are neglected in the dissipative equations. Finally, we note that the jump conditions of the dissipative equations (3.14) and (3.36) are *identical* to the jump conditions of the corresponding lossless equations (3.21) and (3.15), respectively. In these two cases the dissipative terms are linear. On the other hand, the jump condition of the dissipative equation (3.13) is *not identical* to the corresponding lossless equation (3.15). In this case the dissipative term is nonlinear.

3.3 The Basic Equations for Arbitrary Fluids

In the following we briefly discuss shock solutions in the case of an arbitrary fluid described by the state equation (2.26). If in Section 3.2.1 we replace Eq. (3.11) by Eq. (2.26), we find that Eq. (3.14) becomes

$$\left[\begin{array}{c} \rho \\ \rho u \end{array} \right]_t + \left[\begin{array}{c} \rho u \\ \rho u^2 + c_0^2(1 - B/A)\rho + \dfrac{c_0^2}{\rho_0}\dfrac{B/A}{2}\rho^2 \end{array} \right]_x = \left[\begin{array}{c} 0 \\ \rho_0 \beta u_{xx} \end{array} \right]. \qquad (3.39)$$

Setting $\beta = 0$ in Eqs. (3.39) yields a system of conservation laws, for which the Rankine-Hugoniot jump condition (3.7) gives

$$[\rho(u - v)]_l^r = 0, \qquad (3.40a)$$

$$\left[c_0^2(1 - B/A)\rho + \dfrac{c_0^2}{\rho_0}\dfrac{B/A}{2}\rho^2 + \rho u^2 - v\rho u \right]_l^r = 0. \qquad (3.40b)$$

Recall that if $\gamma - 1$ is replaced by B/A in the acoustic wave equations introduced in Chapter 2, i.e. the higher order and the weakly nonlinear equations, these equations model arbitrary fluids described by the state equation (2.26), cf. Section 2.2.4. Equation (3.40) is the reference (or exact) jump condition for this case derived from the basic equations. Accordingly, we are going to compare the jump conditions derived from the wave equations with the jump condition (3.40), in later sections of this chapter.

The structure of the viscous shock solution of Eqs. (3.39) can be derived by invoking Eqs. (3.25). Omitting the details of the derivation, we obtain the following result

$$\frac{\xi - x_0}{\beta} = A_0 \ln(|U|) + A_1 \ln(|U - u_1|) + A_2 \ln(|U - u_2|), \qquad (3.41)$$

where A_0, A_1, A_2, u_1 and u_2 can be expressed in terms of c_0, B/A, v, u_r and ρ_r. Equation (3.41) gives an implicit closed form expression for the solution $\xi(U)$. However, from Eq. (3.41) we cannot, in general, obtain an explicit closed form expression for $U(\xi)$. Nevertheless, one can easily compute $\xi(U)$ and plot U versus ξ. The structure of the solution is similar to that for the case of a perfect gas presented in Fig. 3.3.

Table 3.1. The table summarizes the lossless and dissipative equations and their shock solutions. The equations for the asymptotic boundary conditions (BCs) for the viscous shocks (left column), and the jump conditions for the lossless shocks (right column), are defined either by Eqs. (i) and (ii), or by Eqs. (i) and (iii),[a] in accordance with Eqs. (3.20) and (3.24). Equation (3.36) is obtained by linearizing the dissipative term in Eq. (3.13).

Dissipative cases $(\beta \neq 0)$		Lossless cases $(\beta = 0)$	
Equation	Asymptotic BCs	Equation	Jump condition
$(3.13)\colon \begin{bmatrix} \rho \\ u \end{bmatrix}_t + \begin{bmatrix} \rho u \\ \dfrac{u^2}{2} + \dfrac{c_0^2}{\gamma-1}\left(\dfrac{\rho}{\rho_0}\right)^{\gamma-1} \end{bmatrix}_x = \begin{bmatrix} 0 \\ \dfrac{\rho_0 \beta u_{xx}}{\rho} \end{bmatrix}$	(i), (iii)	$(3.15)\colon \begin{bmatrix} \rho \\ u \end{bmatrix}_t + \begin{bmatrix} \rho u \\ \dfrac{u^2}{2} + \dfrac{c_0^2}{\gamma-1}\left(\dfrac{\rho}{\rho_0}\right)^{\gamma-1} \end{bmatrix}_x = 0$	(i), (ii)
$(3.14)\colon \begin{bmatrix} \rho \\ \rho u \end{bmatrix}_t + \begin{bmatrix} \rho u \\ \rho u^2 + \dfrac{c_0^2 \rho_0}{\gamma}\left(\dfrac{\rho}{\rho_0}\right)^{\gamma} \end{bmatrix}_x = \begin{bmatrix} 0 \\ \rho_0 \beta u_{xx} \end{bmatrix}$	(i), (iii)	$(3.21)\colon \begin{bmatrix} \rho \\ \rho u \end{bmatrix}_t + \begin{bmatrix} \rho u \\ \rho u^2 + \dfrac{c_0^2 \rho_0}{\gamma}\left(\dfrac{\rho}{\rho_0}\right)^{\gamma} \end{bmatrix}_x = 0$	(i), (iii)
$(3.36)\colon \begin{bmatrix} \rho \\ u \end{bmatrix}_t + \begin{bmatrix} \rho u \\ \dfrac{u^2}{2} + \dfrac{c_0^2}{\gamma-1}\left(\dfrac{\rho}{\rho_0}\right)^{\gamma-1} \end{bmatrix}_x = \begin{bmatrix} 0 \\ \beta u_{xx} \end{bmatrix}$	(i), (ii)		

[a] Jump conditions

$$[\rho(u-v)]_l^r = 0 \quad \text{(i)}, \qquad \left[\frac{c_0^2}{\gamma-1}\left(\frac{\rho}{\rho_0}\right)^{\gamma-1} + \frac{u^2}{2} - vu\right]_l^r = 0 \quad \text{(ii)}, \qquad \left[\frac{c_0^2 \rho_0}{\gamma}\left(\frac{\rho}{\rho_0}\right)^{\gamma} + \rho u^2 - v\rho u\right]_l^r = 0 \quad \text{(iii)}.$$

3.4 The classical Rankine-Hugoniot relations

For the sake of completeness, we include here the following classical result. Within fluid dynamics the Rankine-Hugoniot shock relations, connect the physical quantities of the flow on each side of a shock. These relations are conservation equations for mass, momentum and energy. For further details see e.g. the textbooks by Landau and Lifshitz (1987) and Chapman (2000).

Using the notation introduced in Eq. (3.6) the Rankine-Hugoniot relations may be written as

$$\text{mass}: \qquad [\rho\,(u-v)]_l^r = 0, \qquad\qquad (3.42)$$

$$\text{momentum}: \qquad \left[p + \rho\,(u-v)^2\right]_l^r = 0, \qquad\qquad (3.43)$$

$$\text{energy}: \qquad \left[h + (u-v)^2/2\right]_l^r = 0, \qquad\qquad (3.44)$$

where v is the shock propagation velocity and h is the enthalpy. All the model equations discussed in this chapter employ the isentropic approximation. In this case the conservation-of-energy equation (3.44) drops out (LeVeque, 2002). It is immediately seen that Eq. (3.42) is *identical* to Eq. (3.24a). Furthermore, using Eq. (3.11) to eliminate p from Eq. (3.43) yields

$$\left[\frac{c_0^2 \rho_0}{\gamma}\left(\frac{\rho}{\rho_0}\right)^\gamma + \rho u^2 + v(v\rho) - 2v\rho u\right]_l^r = 0. \qquad\qquad (3.45)$$

Then, rewriting Eq. (3.42) as $[v\rho]_l^r = [\rho u]_l^r$ and inserting this into (3.45) we obtain a jump condition which is *identical* to Eq. (3.24b). Thus, the jump condition derived from the Euler equations (3.21), agrees with the classical fluid dynamical Rankine-Hugoniot relations.

3.5 The Higher Order Acoustic Wave Equation

In the following we study shock solutions of the higher order acoustic wave equation (2.24), which we repeat here for convenience

$$\psi_{tt} - c_0^2 \psi_{xx} = (\gamma-1)\psi_{xx}\psi_t + 2\psi_{xt}\psi_x - \frac{\gamma+1}{2}\left(\psi_x\right)^2\psi_{xx} + b\psi_{xxt}. \qquad (3.46)$$

In order to investigate lossless shock solutions, we are going to reformulate Eq. (3.46) as a system of conservation laws. Furthermore, we find the structure of the thermoviscous shock solution by means of traveling wave analysis. Recall that, according to Section 2.2.5, Eq. (3.46) is an approximation to the system of the three basic equations (2.1), (2.2) and (2.4). The equation of state (2.4) takes the form of either the perfect gas state equation (2.19), or the quadratic equation state (2.26). Hence, it is relevant to compare the shock solutions derived from Eq. (3.46) to those derived from the basic equations in the previous sections.

3.5.1 Lossless Case

In order to reformulate Eq. (3.46) as a system of conservation laws we introduce

$$\eta = \psi_t, \tag{3.47}$$

use Eq. (2.15), that is $u = -\psi_x$, in order to obtain the following system of equations

$$\left[\begin{array}{c} \eta - \left(1 - \dfrac{\gamma - 1}{2}\right) u^2 \\ u \end{array} \right]_t + \left[\begin{array}{c} \left[c_0^2 + (\gamma - 1)\eta\right] u - \dfrac{\gamma + 1}{6} u^3 \\ \eta \end{array} \right]_x$$

$$= \left[\begin{array}{c} b u_{xt} \\ 0 \end{array} \right]. \tag{3.48}$$

Now, we introduce the variable transformation

$$\vartheta = \eta - \left(1 - \dfrac{\gamma - 1}{2}\right) u^2, \tag{3.49}$$

which, upon substitution into Eq. (3.48), yields

$$\left[\begin{array}{c} \vartheta \\ u \end{array} \right]_t + \left[\begin{array}{c} \left\{c_0^2 + (\gamma - 1)\left[\vartheta + \left(1 - \dfrac{\gamma - 1}{2}\right) u^2\right]\right\} u - \dfrac{\gamma + 1}{6} u^3 \\ \vartheta + \left(1 - \dfrac{\gamma - 1}{2}\right) u^2 \end{array} \right]_x$$

$$= \left[\begin{array}{c} -b u_{xt} \\ 0 \end{array} \right]. \tag{3.50}$$

Upon neglecting the linear dissipative term on the right hand side Eqs. (3.50) reduce to a system of conservation laws. Comparing with Eq. (3.1) we find that

$$q = \left[\begin{array}{c} \vartheta \\ u \end{array} \right], \tag{3.51}$$

$$f = \left[\begin{array}{c} \left\{c_0^2 + (\gamma - 1)\left[\vartheta + \left(1 - \dfrac{\gamma - 1}{2}\right) u^2\right]\right\} u - \dfrac{\gamma + 1}{6} u^3 \\ \vartheta + \left(1 - \dfrac{\gamma - 1}{2}\right) u^2 \end{array} \right]. \tag{3.52}$$

The eigenvalues of the Jacobian matrix $f'(q)$ are

$$\lambda_{1,2} = u \mp \sqrt{c_0^2 + (\gamma - 1)\left(\dfrac{2 - \gamma}{2} u^2 + \vartheta\right)}. \tag{3.53}$$

Upon inserting Eq. (3.49) into Eq. (3.53) the eigenvalues can be written in terms of η and u as

$$\lambda_{1,2} = u \mp \sqrt{c_0^2 + (\gamma - 1)\left(\eta - \dfrac{u^2}{2}\right)}. \tag{3.54}$$

Furthermore, by substituting Eq. (2.35) into Eq. (3.54) we may write the eigenvalues in terms of ρ and u as

$$\lambda_{1,2} = u \mp c_0 \sqrt{\left(\frac{\rho}{\rho_0}\right)^{\gamma-1}}. \qquad (3.55)$$

These eigenvalues are *identical* to those given in Eq. (3.18). Thus, the eigenvalues of the lossless higher order acoustic wave equation are identical to those of the Euler equations for a perfect gas. This is not surprising since the lossless higher order equation is exact, i.e. it retains all nonlinear contributions from the Euler equations, cf. Section 2.2.6.

For the conservation law given by Eqs. (3.50) with $b = 0$, the Rankine-Hugoniot jump condition (3.7) gives

$$\left[c_0^2 u + (\gamma - 1)\vartheta u - \frac{3\gamma^2 - 11\gamma + 10}{6}u^3 - v\vartheta\right]_l^r = 0. \qquad (3.56a)$$

$$\left[\vartheta + \frac{3 - \gamma}{2}u^2 - vu\right]_l^r = 0. \qquad (3.56b)$$

This jump condition can be expressed in terms of η and u by invoking (3.49). Furthermore, upon solving Eq. (2.35) for $\eta = \psi_t$ yields

$$\eta = \frac{c_0^2}{\gamma - 1}\left[\left(\frac{\rho}{\rho_0}\right)^{\gamma-1} - 1\right] - \frac{u^2}{2}, \qquad (3.57)$$

and by inserting Eq. (3.57) into Eq. (3.49) we obtain

$$\vartheta = \frac{c_0^2}{\gamma - 1}\left[\left(\frac{\rho}{\rho_0}\right)^{\gamma-1} - 1\right] - \frac{2 - \gamma}{2}u^2. \qquad (3.58)$$

Thus, by inserting Eq. (3.58) into Eqs. (3.56), the jump condition can be expressed in terms of ρ and u.

In Fig. 3.4 we compare the jump condition (3.56) (red curve) to the jump conditions derived from the basic equations for a perfect gas (blue curve) and a fluid with a quadratic equation of state (cyan curve). The last-mentioned jump conditions are given by Eqs. (3.24) and (3.40), respectively. The curves in the figures are obtained by eliminating ρ_l from the jump conditions, setting $\rho_r = \rho_0$ and $u_r = 0$, and plotting u_l versus v. The blue curve is identical to the blue curve in Fig. 3.2. Despite the fact that the higher order equation is exact in the case of a perfect gas, we see that the corresponding jump condition (red curve) is not identical to that derived from the Euler equations for a perfect gas (blue curve). The reason for this disagreement is that the derivation of the lossless higher order wave equation from the Euler equations, relies on manipulations that depend on smoothness. Thus, the two models are not equivalent for solutions with shocks, cf. Section 3.2.2. Finally, we note that the jump conditions which correspond to Eqs. (3.39) and (3.50) include unphysical branches (dashed curves), see discussion in Appendix C.
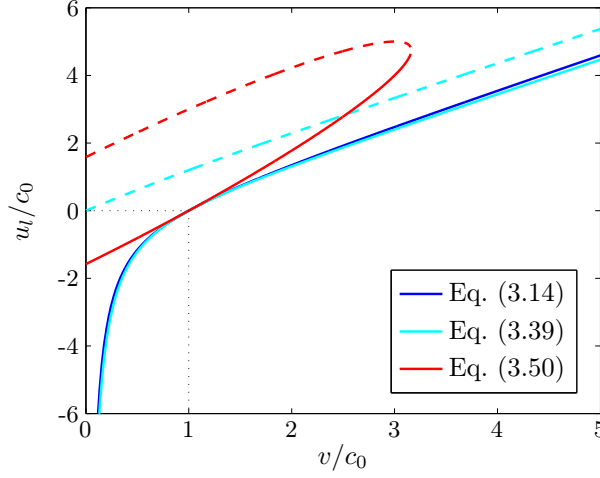
Fig. 3.4. Comparison of the Rankine-Hugoniot jump conditions (3.24), (3.40) and (3.56) corresponding to the systems of equations (3.14), (3.39) and (3.50), respectively. The following parameters are used: $\rho_r = \rho_0$, $u_r = 0$, $\gamma = 1.4$ and $B/A = 0.4$.

Due to the fact that the lossless version of the higher order wave equation is exact with respect to the Euler equations for a perfect gas, it is expected that the two models are equivalent for smooth solutions. In order to investigate this behavior we perform numerical simulations of the two models, using the following smooth Gaussian pulse as initial condition

$$\rho(x,0) = 1 + D_1 \exp(-x^2), \qquad u(x,0) = D_2, \tag{3.59}$$

where D_1 and D_2 are constants. Invoking Eq. (3.57) we find the corresponding initial condition for η as

$$\eta(x,0) = \frac{[1 + D_1 \exp(-x^2)]^{\gamma-1} - 1}{\gamma - 1} + \frac{D_2^2}{2}. \tag{3.60}$$

The result of the numerical simulation of the Euler equations is shown in Fig. 3.5. The numerical solution, and all subsequent numerical solutions, are computed using the COMSOL MULTIPHYSICS® software package,[5] which is a set of algorithms based on the finite element method for discretizing and solving partial differential equations. The COMSOL MULTIPHYSICS code that computes the numerical solutions shown in Figs. 3.5–3.7 can be found in Appendix D. In Fig. 3.6 we plot the L^1-norm of the difference between the numerical solutions of the two models for u, as a function of time. That is to say, we plot the quantity

$$\mathcal{L}^1_{\mathrm{error}}(t) = \frac{1}{N} \sum_{i=0}^{N-1} |u_{\mathrm{HOE}}(x_i,t) - u_{\mathrm{Euler}}(x_i,t)|, \tag{3.61}$$

where N is the number of computational elements used, x_i is the center of each element and HOE denotes the lossless Higher Order acoustic wave Equation.

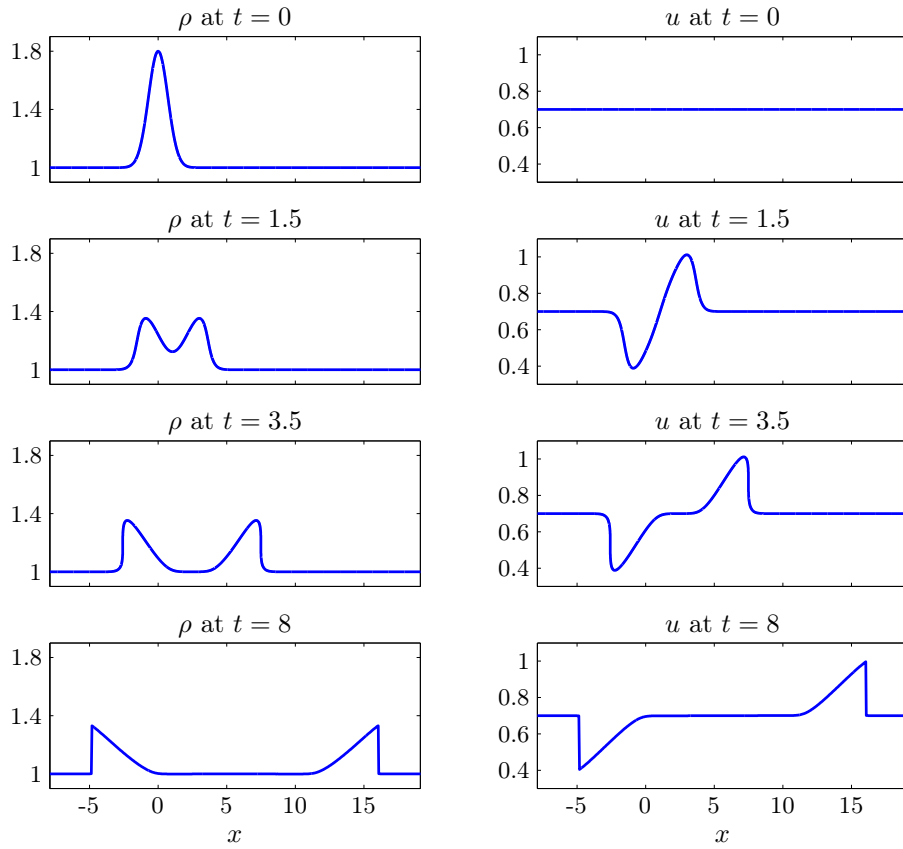
[5] http://www.comsol.com

Fig. 3.5. Numerical simulation of the Euler equations (3.21) for a perfect gas subject to the initial condition (3.59) with $D_1 = 0.8$ and $D_2 = 0.7$. The solution is shown at four different instants in time. The following parameter is used: $\gamma = 1.4$.
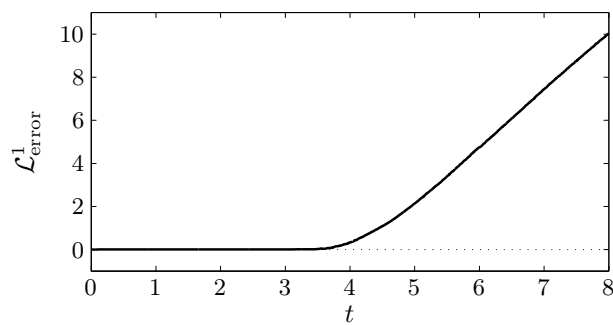

Fig. 3.6. L^1-norm, defined in Eq. (3.61), of the difference between the numerical solution shown in Fig. 3.5 and the corresponding numerical solution of the lossless higher order acoustic wave equation (2.33).

From Fig. 3.6 we see that there exists an instant in time $t_c \approx 3.5$, such that the difference between the two numerical solutions is practically zero when $t < t_c$, and grows with time when $t > t_c$. We assume that t_c corresponds to the instant in time at which shocks form in the solutions. Accordingly, Fig. 3.6 clearly demonstrates that the the two models, i.e. Eqs. (2.33) and (3.21), are equivalent for smooth solutions, but not equivalent for solutions with shocks. Details of the difference between the two solutions are clearly evident from Fig. 3.7, which shows both solutions at $t = 8$. From the figure we see that the shock in the higher order equation (red curve) have traveled a shorter distance than the shock in the Euler equations (blue curve). This behavior is in agreement with the shock jump conditions, since in Fig. 3.4 we observe that for a fixed value of u_l, the propagation velocity of a shock in the higher order equation is smaller than the propagation velocity of a shock in the Euler equations.
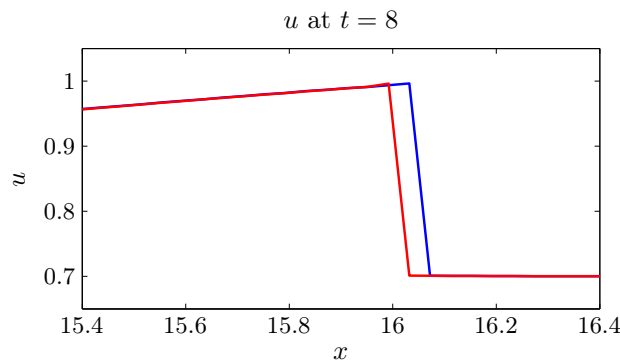
Fig. 3.7. Comparison of the numerical solutions of the Euler equations (blue line) and the higher order acoustic wave equation (red line) at $t = 8$.

3.5.2 Dissipative Case

The thermoviscous shock solution of Eq. (3.46) is studied in detail in the manuscript in Appendix C. Our derivation of the exact traveling wave solution is based on the following solution ansatz

$$\psi(x,t) = \Psi(\xi) - u_1 x + \eta_1 t, \tag{3.62}$$

where $\xi = x - vt$, and u_1 and η_1 are arbitrary constants. Compared to the usual traveling wave assumption $\psi(x,t) = \Psi(\xi)$, the inclusion of $-u_1 x + \eta_1 t$ in Eq. (3.62) leads to a solution with increased flexibility in the asymptotic boundary conditions for $u = -\psi_x$ and $\eta = \psi_t$. This increased flexibility is necessary in order for the equations for asymptotic boundary conditions and the propagation velocity of the smooth shock solution to be consistent with the Rankine-Hugoniot jump condition introduced above. The asymptotic boundary conditions and the propagation velocity of the thermoviscous shock solution must satisfy Eqs. (21) in Appendix C. These equations are found to be *equivalent* to the jump condition (3.56). Thus, the asymptotic boundary conditions of the thermoviscous shock solution of Eq. (3.46) satisfy the jump condition for

the lossless shock solution of Eqs. (3.50). These jump conditions disagree with
the jump condition of the Navier-Stokes equations (3.14). The reason for this
disagreement is that all nonlinear dissipative terms are neglected in the deriva-
tion of the higher order equation (3.46), cf. Section 3.2.4. In order to obtain a
wave equation of which the corresponding jump condition agrees with that of
Eqs. (3.14), one should keep all nonlinear dissipative terms. We did make some
attempts to derive such a wave equation. However, it turns out that such a
derivation become unfeasible.

The structure of the thermoviscous shock solution obtained is given by
Eq. (23) in Appendix C. Note that the structure of this equation is identi-
cal to the structure of Eq. (3.41), that was derived from the basic equations
for a fluid with a quadratic equation of state. However, the coefficients in the
two equations differ. In Fig. 3.8 we compare the structure of the thermoviscous
shock solution derived from the higher order acoustic wave equation (red curve)
to that derived from the basic equations for a perfect gas (blue curve). Identical
parameters are used in the two figures, that is the two shocks propagate at the
same speed. The difference in the asymptotic boundary conditions of the shocks
is in accordance with the disagreement between the jump conditions discussed
above, see Fig. 3.4. Finally, we note that there is a qualitative difference be-
tween the two shock profiles. In the case of the basic equations (blue curve), the
shock structure is more smooth on the front of the shock and less smooth on the
back of the shock. On the other hand, in the case of the higher order equation
(red curve), the shock structure is less smooth on the front of the shock and
more smooth on the back of the shock. In the case of weak shocks propagating
at velocities near the small signal sound velocity c_0, it is found that both shock
solutions resemble the structure of the hyperbolic tangent.

Interestingly, the red curve in Fig. 3.8 is remarkably similar to those shown
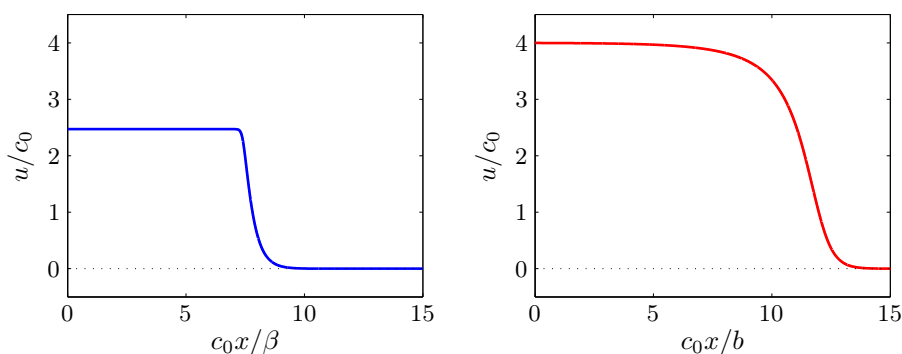in Fig. 1 of Jordan (2006), which depict poroacoustic travelling waveforms.

Fig. 3.8. Profiles of the shock solutions of Eq. (3.14) (blue line) and Eq. (3.46) (red
line). The following parameters were used: $\rho_r = \rho_0$, $u_r = 0$, $v = 3c_0$ and $\gamma = 1.4$.

3.6   The Weakly Nonlinear Wave Equations

In the following we give some results related to the thermoviscous shock solutions
of the straightforward weakly nonlinear equation, the Kuznetsov equation and
the Hamiltonian weakly nonlinear equation that are introduced in Section 2.4.
The thermoviscous shock solution of the Kuznetsov equation is studied recently
in detail by Jordan (2004). The thermoviscous shock solution of the Hamiltonian
weakly nonlinear equation is studied in detail in the manuscript in Appendix A.

   Generally, the thermoviscous shock profiles can be obtained by invoking the
solution ansatz (3.62). For each of the three weakly nonlinear wave equations,
the structure of the thermoviscous shock can be expressed explicitly in terms
of the hyperbolic tangent function, see e.g. Eq. (23) in Appendix A. Hence, in
contrast to the shock profiles discussed in the previous sections, the profile of
the shocks derived from the weakly nonlinear equations is independent of the
strength of the shocks. The equations for the asymptotic boundary conditions
may be written in following way. In the case of the straightforward weakly
nonlinear equation we find

$$u_l = \frac{v^2 - 2u_r v - c_0^2 - (\gamma - 1)\eta_r}{v\left(1 + \dfrac{\gamma - 1}{2c_0^2}\right)} + u_r, \qquad (3.63)$$

for the Kuznetsov equation we obtain

$$u_l = \frac{\left(1 - \dfrac{\gamma - 1}{c_0^2}\eta_r\right)v^2 - 2u_r v - c_0^2 - \eta_r}{v\left(1 + \dfrac{\gamma - 1}{2c_0^2}v^2\right)} + u_r, \qquad (3.64)$$

and in the case of the Hamiltonian weakly nonlinear equation we find the fol-
lowing

$$u_l = \frac{\left(1 - \dfrac{\gamma - 2}{c_0^2}\eta_r\right)v^2 - 2u_r v - c_0^2 - \eta_r}{v\left(\dfrac{3}{2} + \dfrac{\gamma - 2}{2c_0^2}v^2\right)} + u_r. \qquad (3.65)$$

cf. Eq. (29) in Appendix A. In Figs. 3.9 and 3.10 we compare these three jump
conditions to the jump conditions corresponding to the basic equations and the
higher order wave equation. In the case of $\gamma = 1.4$ and $B/A = 0.4$, i.e. Fig. 3.9,
we see that the jump condition corresponding to the straightforward weakly
nonlinear equation (magenta curve) is the one which is closest to the reference
(or exact) jump conditions obtained from the basic equations (blue and cyan
curves). It is somewhat surprising that the straightforward weakly nonlinear
equation gives a better performance than the higher order equation, since the
straightforward weakly nonlinear equation is obtained by neglecting the cubic
nonlinear term in the higher order equation, cf. Section 2.4. As a matter of
fact, it is reasonable to expect the higher order equation to give the highest
accuracy of the two. However, in the derivation of the higher order equation

we neglect nonlinear contributions in the dissipative terms, and in Section 3.2.4 we demonstrated that neglecting such terms leads to unpredictable changes in the corresponding jump condition. This is in fact the explanation why the shock jump condition corresponding to the straightforward nonlinear equation may give a higher accuracy than the shock jump condition corresponding to the higher order equation. In the case of $\gamma = 11$ and $B/A = 10$, i.e. Fig. 3.10, we see that the higher order equation gives a slightly better performance than the straightforward weakly nonlinear equation. Note that $\gamma = 11$ lies outside the range of single-phase perfect gases, for which $1 < \gamma < 1.7$, but may be applicable to certain multi-phase gases, see Makarov and Ochmann (1996a). In both Figs. 3.9 and 3.10, the Kuznetsov equation and the Hamiltonian weakly nonlinear equation performs worse than the straightforward weakly nonlinear equation.
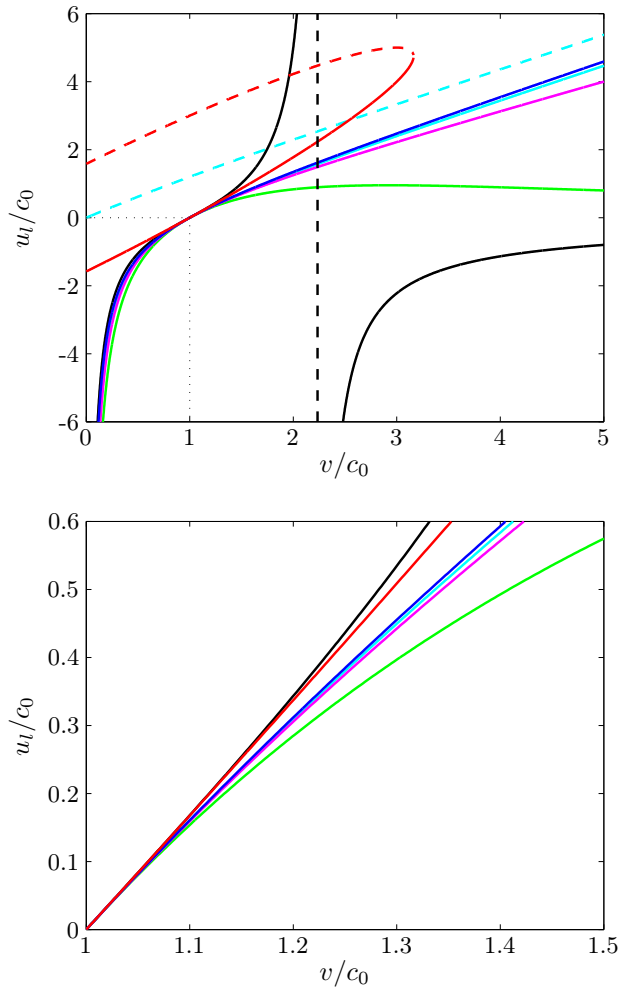
Fig. 3.9. Comparison of the jump conditions (3.24), (3.40), (3.56), (3.63), (3.64) and (3.65) corresponding to the basic equations for a perfect gas (3.14) (blue curve), the basic equations for a fluid with a quadratic equation of state (3.39) (cyan curve), the higher order wave equation (3.46) (red curve), the straightforward weakly nonlinear equation (2.48) (magenta curve), the Kuznetsov equation (2.49) (green curve) and the Hamiltonian weakly nonlinear equation (2.52) (black curve), respectively. The following parameters are used: $\rho_r = \rho_0$, $u_r = 0$, $\gamma = 1.4$ and $B/A = 0.4$. The two figures show the same data on different scales.
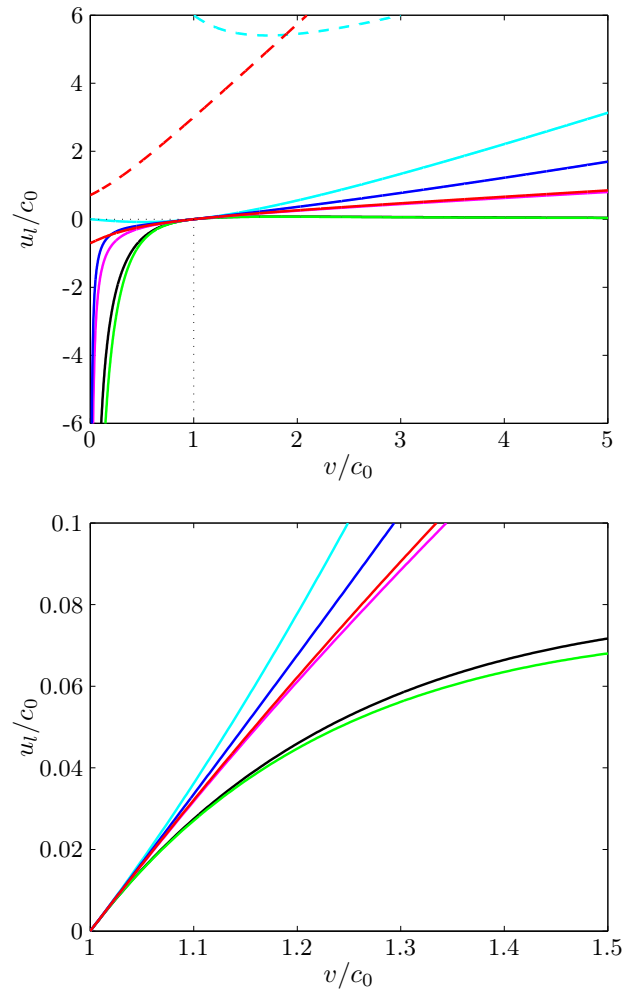
Fig. 3.10. Continued from Fig. 3.9. The following parameters are used: $\gamma = 11$ and $B/A = 10$. Note that red and magenta curves, and the black and green curves, respectively, coincide for $v > c_0$ in the topmost plot.

Chapter 4

Stability Analysis

In this chapter we discuss stability properties of solutions to the nonlinear acoustic equations introduced in Chapter 2. The question of stability is what will happen if a given solution is slightly perturbed. Does the solution recover to its original shape, or does the disturbance grow until the initial solution is lost? In particular we are going to investigate the stability properties of an elementary solution in which the fluid particle velocity u take a constant value for all x and t, and the fluid density ρ take a constant value for all x and t. It turns out that the stability properties of more complex solutions can be related to the stability properties of the elementary solution.

4.1 Euler's Equations for a Perfect Gas

We consider the solution

$$\rho(x,t) = L, \qquad u(x,t) = K, \tag{4.1}$$

where K and L are arbitrary constants. Equations (4.1) represent an exact solution of Euler's equations for a perfect gas (3.21). In order to investigate the linear stability properties of this solution we introduce perturbations $\bar{\rho}(x,t)$ and $\bar{u}(x,t)$ in the following way

$$\rho(x,t) = L + \epsilon\bar{\rho}(x,t), \qquad u(x,t) = K + \epsilon\bar{u}(x,t), \tag{4.2}$$

where $\epsilon \ll 1$. Inserting Eqs. (4.2) into Eqs. (3.21) and keeping terms up to first order in ϵ yields the following linear equations for the perturbations

$$\bar{\rho}_t + L\bar{u}_x + K\bar{\rho}_x = 0, \tag{4.3a}$$

$$L\bar{u}_t + K\bar{\rho}_t + 2KL\bar{u}_x + \left[K^2 - c_0^2\left(\frac{L}{\rho_0}\right)^{\gamma-1}\right]\bar{\rho}_x = 0. \tag{4.3b}$$

Differentiating Eqs. (4.3) with respect to x and t yields

$$\bar{\rho}_{xt} + L\bar{u}_{xx} + K\bar{\rho}_{xx} = 0, \tag{4.4a}$$

$$\bar{\rho}_{tt} + L\bar{u}_{xt} + K\bar{\rho}_{xt} = 0, \tag{4.4b}$$

$$L\bar{u}_{xt} + K\bar{\rho}_{xt} + 2KL\bar{u}_{xx} + \left[K^2 - c_0^2\left(\frac{L}{\rho_0}\right)^{\gamma-1}\right]\bar{\rho}_{xx} = 0, \qquad (4.4c)$$

$$L\bar{u}_{tt} + K\bar{\rho}_{tt} + 2KL\bar{u}_{xt} + \left[K^2 - c_0^2\left(\frac{L}{\rho_0}\right)^{\gamma-1}\right]\bar{\rho}_{xt} = 0. \qquad (4.4d)$$

These four equations can be combined to yield the following two equations for the perturbations $\bar{\rho}$ and $\bar{u}$

$$\bar{\rho}_{tt} + 2K\bar{\rho}_{xt} + \left[K^2 - c_0^2\left(\frac{L}{\rho_0}\right)^{\gamma-1}\right]\bar{\rho}_{xx} = 0, \qquad (4.5a)$$

$$\bar{u}_{tt} + 2K\bar{u}_{xt} + \left[K^2 - c_0^2\left(\frac{L}{\rho_0}\right)^{\gamma-1}\right]\bar{u}_{xx} = 0. \qquad (4.5b)$$

Inserting the single Fourier mode $e^{i(kx-\omega t)}$, where k is the wave number and ω is the angular frequency, into either of Eqs. (4.5), we obtain the following dispersion relation

$$\omega = 2Kk \pm \sqrt{4c_0^2 k^2\left(\frac{L}{\rho_0}\right)^{\gamma-1}}. \qquad (4.6)$$

Since $L > 0$ and $\rho_0 > 0$, we find that the imaginary part of ω is always zero. Accordingly, the Fourier mode $e^{i(kx-\omega t)}$ will be purely oscillatory in nature. Thus, the solutions of Eqs. (4.5) will never grow in time, i.e. the solution (4.1) of Eqs. (3.21) is never linearly unstable.

4.2 Nonlinear Acoustic Wave Equations

In order to study the linear stability properties of solutions to the dissipative wave equations for the velocity potential ψ, we consider the solution

$$\psi(x,t) = -Kx + Lt, \qquad (4.7)$$

where K and L are arbitrary constants. Hence, the partial derivatives of ψ take the constant values $u(x,t) = K$ and $\eta(x,t) = L$. The linear stability analyses of the wave equations is basically along the same lines as the analysis of the Euler equations in the previous section. Details of the analyses in the case of the Hamiltonian weakly nonlinear wave equation and the higher order wave equation are given in the manuscripts in Appendix A and C, respectively. For each of the wave equations it turns out that there exists a stability criterion that must be fulfilled in order for the solution (4.7) to be asymptotically stable. If the stability criterion is not met, a small perturbation of the solution will grow with time. In the following we summarize the criteria obtained. In the case of the higher order acoustic wave equation (2.24) we find that the following criteria must be met in order for the solution (4.7) to be asymptotically stable

$$\frac{\gamma+1}{2}K^2 - (\gamma-1)L - c_0^2 < 0. \qquad (4.8)$$

In the case of the straightforward weakly nonlinear equation (2.48) we find

$$L > \frac{c_0^2}{\gamma - 1}. \tag{4.9}$$

For the Kuznetsov equation (2.49) we find

$$-c_0^2 < L < \frac{c_0^2}{\gamma - 1}. \tag{4.10}$$

In the case of the Hamiltonian weakly nonlinear equation (2.52) we find one criterion that applies to $\gamma - 1 < 1$ and a different one that applies to $\gamma - 1 > 1$ as

$$\gamma - 1 > 1 : \qquad -c_0^2 < L < \frac{c_0^2}{\gamma - 2} \tag{4.11}$$

$$\gamma - 1 < 1 : \qquad -c_0^2 < L < \infty. \tag{4.12}$$

Note that none of these stability criteria depend on the thermoviscous dissipation parameter b. From the details of the analysis it follows that the above stability criteria apply equally well to the lossless and dissipative versions of the wave equations.

In the following we are going to demonstrate that the above stability criteria can be applied to more general solutions than the elementary one discussed above. In particular we demonstrate that if just some part of a solution violates the stability criteria, the solution is unstable. In the case of the higher order equation that is to say, that the solution is unstable if the quantity

$$g(x, t) = \frac{\gamma + 1}{2} u(x, t)^2 - (\gamma - 1)\eta(x, t) - c_0^2 \tag{4.13}$$

is positive at just a single point, or in a limited region in space and time. The quantity g is obtained by substituting $L = \eta(x, t)$ and $K = u(x, t)$ into Eq. (4.8). As an example to demonstrate this behavior in the case of the lossless higher order equation, we repeat the numerical simulation in Figs. 3.5–3.7 for a slightly different value of D_2. From the numerical solution shown in Fig. 4.1 we see that at $t = 0$ and $t = 0.48$, $g < 0$ everywhere on the spatial domain. At $t = 0.74$ we observe an instability in the solution around $x = 1.6$. Furthermore, we see that $g > 0$, just in the spatial neighborhood of the instability. The instability grows rapidly and causes the numerical algorithm to fail further integration in time. This behavior demonstrates that, indeed, the solution is unstable if just some part of the solution violates the stability criterion. The occurrence of instability is not observed in the numerical simulation in Figs. 3.5–3.7. This observation is in agreement with the above stability criterion, since in that simulation it was found that $g < 0$ for all x and t.

From the analysis of the previous chapters we know that the lossless higher order wave equation (2.33) and the Euler equations (3.21) for a perfect gas are equivalent for smooth solutions. Thus, it is somewhat surprising that instabilities occur in solutions of the higher order equation, whereas the same kind of instablilities never occur in solutions of the Euler equations. In order

to investigate this behavior we solve the Euler equations subject to the same initial conditions as in Fig. 4.1. Then, we plot the L^1-norm of the difference between the numerical solutions of the two models for u, as a function of time, see Fig. 4.2. From the figure we see that when $t < t_s$, where $t_s \approx 0.73$, the difference between the two solutions is practically zero. For $t > t_s$ the difference between the two solutions grows rapidly. t_s is the instant in time at which the instability sets in, in the solution of the higher order equation. The solution of the Euler equations show no instability and the solution resembles the solution in Fig. 3.5, also for $t > t_s$.
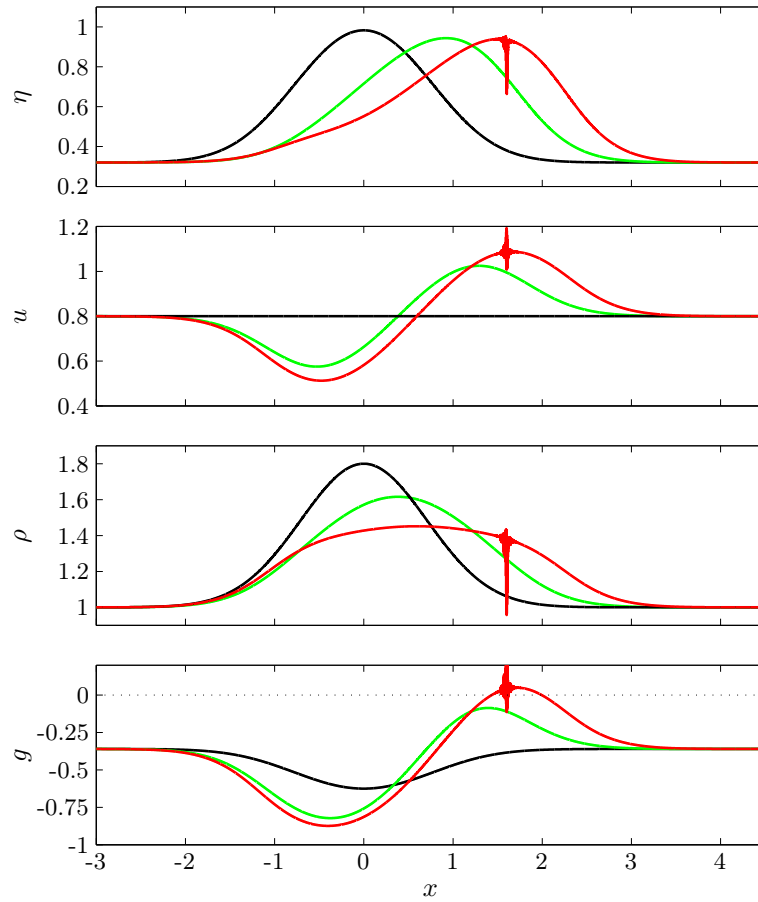
Fig. 4.1. Numerical simulation of the lossless higher order acoustic wave equation (2.33) subject to the initial condition (3.60) with $D_1 = 0.8$ and $D_2 = 0.8$. The solution is shown at three different instants in time: $t = 0$ (black curve), $t = 0.48$ (green curve), and $t = 0.74$ (red curve). ρ and g are defined by Eqs. (2.35) and (4.13), respectively.
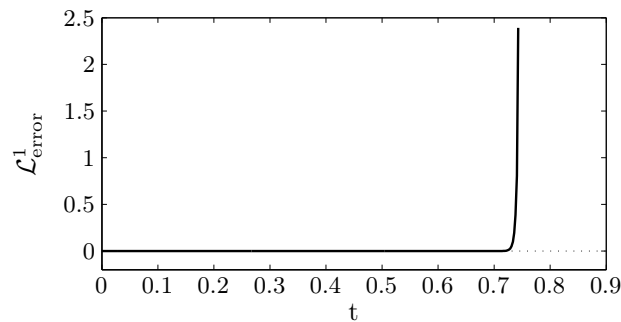

Fig. 4.2. L^1-norm, defined in Eq. (3.61), of the difference between the numerical solution shown in Fig. 4.1 and the corresponding numerical solution of the Euler equations (3.21).

Chapter 5

Wave Steepening and Shock Formation

In this chapter we are going to study progressive-wave motion generated by a source at one end of a one-dimensional semi-infinite domain. Our study is limited to the case of sinusoidal source excitation. Furthermore, our study is limited to the case of lossless fluids. Due to nonlinear terms in the model equations, steepening of the waveform occurs, since larger amplitude portions of the waveform travels faster than lower amplitude portions. This steepening causes discontinuities, or shocks, to develop in the waveform. We are going to demonstrate that these shocks satisfy the Rankine-Hugoniot jump conditions discussed in Chapter 3. In particular we are going to compare solutions of the lossless higher order acoustic wave equation and the Euler equations for a perfect gas. These models are equivalent for smooth solutions, but not equivalent for solutions with shocks. In a recent paper Christov et al. (2007) compare and assess the accuracy of three lossless weakly nonlinear acoustic wave equations, through a numerical study of shock formation. In the second section of this chapter, we shall study the accuracy of the Hamiltonian weakly nonlinear wave equation proposed in Section 2.4.3, by comparing its solution to the results reported by Christov and coworkers.

5.1   The Euler Equations and the Higher Order Equation

We start by considering the Euler equations for a perfect gas (3.21) subject to the initial conditions

$$\rho(x, t = 0) = \rho_0, \qquad u(x, t = 0) = 0, \tag{5.1}$$

which reflect the fact that the medium ahead of the wave front is in its equilibrium state. For the left boundary condition we choose

$$u(x = 0, t) = c_0 \sin \pi t, \tag{5.2}$$

which is a natural choice when studying, for example, the motion of pistons. In order to simulate a semi-infinite domain, we chose the spatial domain on which the equations are solved to have a length l, which is large enough so that reflections from the right boundary do not occur. The boundary condition on the right boundary is chosen to be $u(x = l, t) = 0$. Throughout this chapter we take $\gamma = 1.4$, which corresponds to air at 20℃. From the numerical solution of the problem, which is shown Fig. 5.1, we observe the following: at $t = 0.3$ the solution is smooth (i.e. there is no shock in the solution), at $t = 0.9$ a shock occurs in the solution, and at $t = 1.5$ the shock is fully developed.

In Chapter 3 we demonstrated that the Euler equations (3.21) for a perfect gas and the lossless higher order acoustic wave equation (2.33) are equivalent for smooth solutions, but not equivalent for solutions with shocks. In order to investigate this behavior we solve Eq. (2.33) subject to the above boundary and initial conditions, and compare the solution to that of the Euler equations. In particular we plot in Fig. 5.2 the L^1-norm of the difference between the two solutions for u, as a function of time. That is to say, we plot the quantity (3.61). From Fig. 5.2 we see that there exists an instant in time $t_c \approx 0.5$, such that the difference between the two numerical solutions is practically zero when $t < t_c$, and grows with time when $t > t_c$. We assume that t_c corresponds to the instant in time at which shocks form in the solutions. Accordingly, Fig. 5.2 clearly demonstrates that the Eqs. (2.33) and (3.21) are equivalent for smooth solutions, but not equivalent for solutions with shocks. Details of the difference between the two solutions are clearly evident from Fig. 5.3, which shows both solutions at $t = 1.5$.

In order to gain further insight into the process of shock formation, and the difference between two models (i.e. the Euler equations and the higher order equation), we plot in Fig. 5.4 the spatial positions of the wave fronts of the progressive disturbances as function of time. That is to say, we draw the contour lines determined by $u = 0+$. The slope of these contour lines represent the propagation velocity of the wave fronts. From the figures we see that for $0 < t < t_c$, the wave fronts in the solutions of both models propagate at the small-signal speed of sound c_0. As the shocks form at $t = t_c$, the wave fronts start to accelerate because the propagation velocity of the shocks is greater that the small-signal sound velocity. At $t = 1.5$ the propagation velocities of the fully developed shocks is found to be $1.57 \times c_0$ in the case of the Euler equations, and $1.47 \times c_0$ in case of the higher order equation. At $t = 1.5$ the fully developed shock in the solution of the Euler equations jumps between u_r and u_l in u, and between ρ_r and ρ_l in ρ, as indicated in Fig. 5.1. In order to investigate if this shock satisfies the Rankine-Hugoniot jump condition we insert $\rho_r = \rho_0$, $u_r = 0$ and the value of u_l read off from the numerical solution into Eqs. (3.24), which are the jump condition corresponding to the Euler equations (3.21) for a perfect gas. The values of ρ_l and v obtained by solving the resulting equations agree perfectly well with those observed in the numerical solution. Hence, we have demonstrated that the fully developed shock in the solution of the Euler equations satisfies the Rankine-Hugoniot jump condition of the governing equations. In a similar manner we found that the fully developed shock observed in the solution of

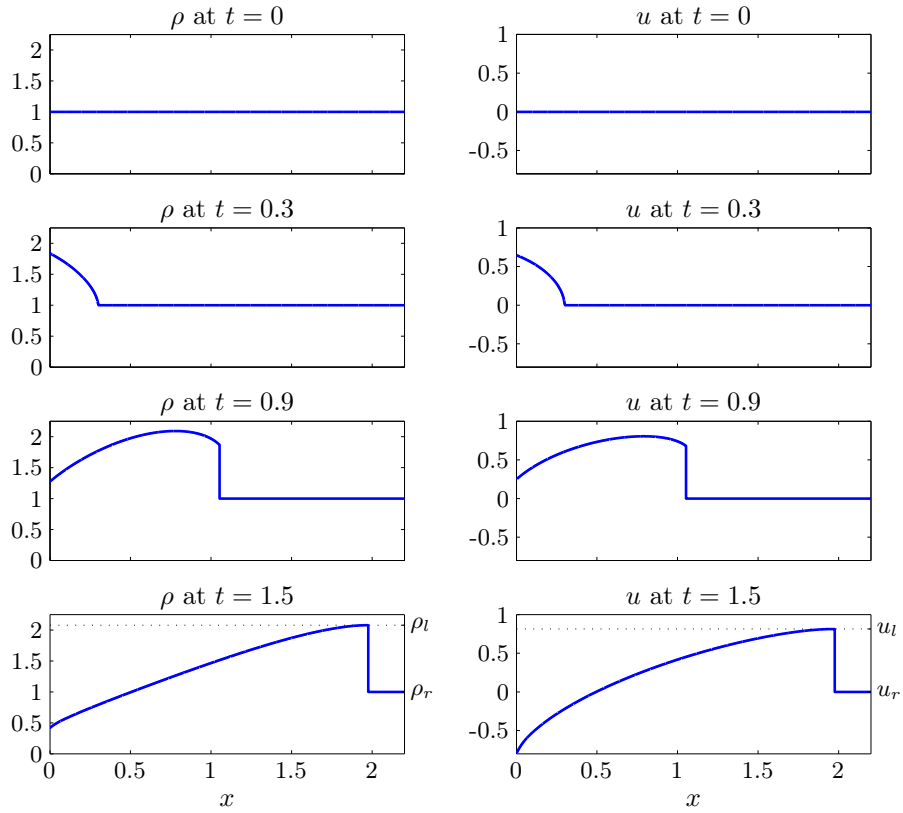the higher order acoustic wave equation satisfies the corresponding Rankine-Hugoniot jump condition (3.56).

Fig. 5.1. Numerical simulation of the Euler equations (3.21) for a perfect gas subject to the initial and boundary conditions (5.1) and (5.2). The solution is shown at four different instants in time. The fully developed shock observed at $t = 1.5$ jumps between ρ_r and ρ_l in ρ, and between u_r and u_l in u.
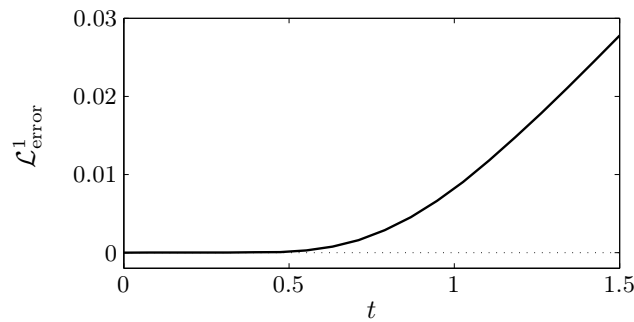

Fig. 5.2. L^1-norm, defined in Eq. (3.61), of the difference between the numerical solution shown in Fig. 5.1 and the corresponding numerical solution of the lossless higher order acoustic wave equation (2.33).
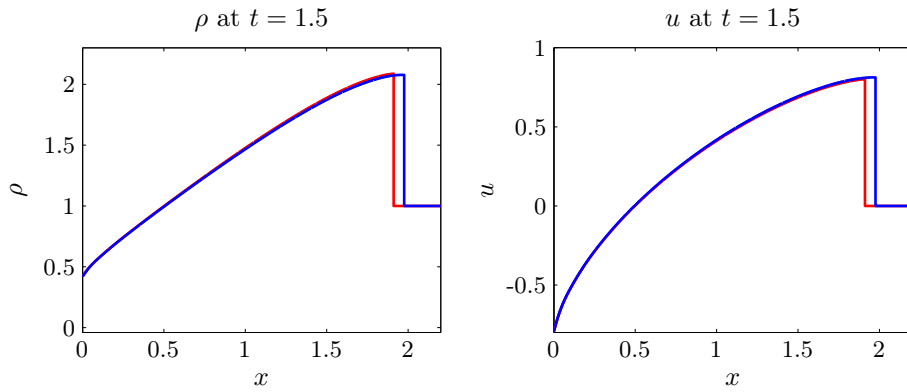
Fig. 5.3. Comparison of the numerical solutions of the Euler equations (blue line) and the higher order acoustic wave equation (red line) at $t = 1.5$.
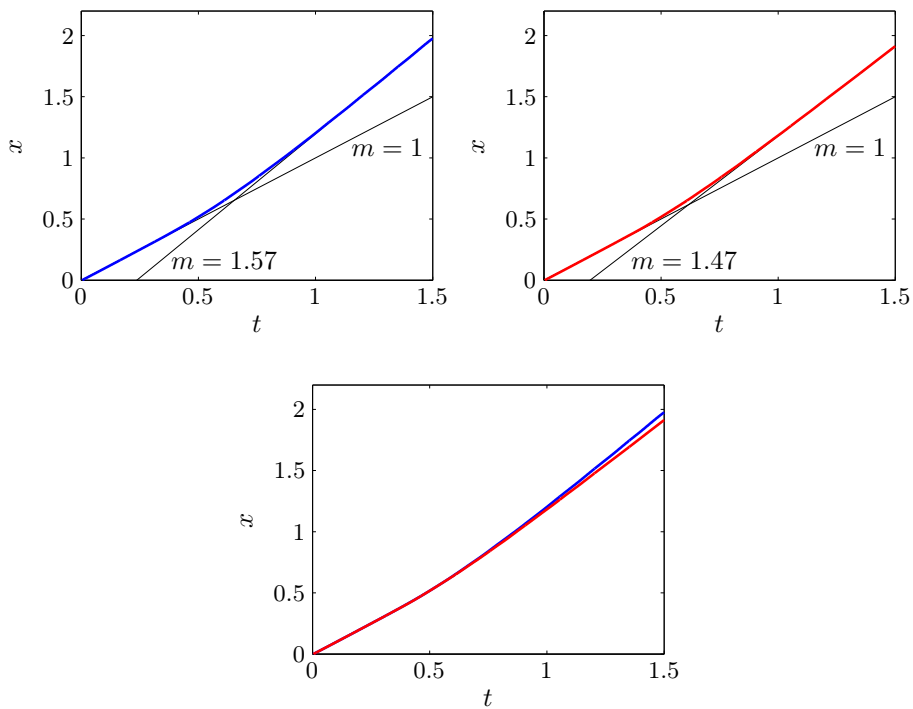
Fig. 5.4. Spatial positions of the wave fronts of the progressive disturbances as function of time. m denotes the slopes of the straight lines. The color convention is the same as in Fig. 5.3.

5.2 Accuracy of the Hamiltonian Weakly Nonlinear Equation

In their recent paper Christov et al. (2007) compare three lossless weakly nonlinear acoustic wave equations to the 'exact' Euler equations through a numerical study of shock formation, and assess the accuracy of the approximate equations. The three weakly nonlinear equations considered by Christov et al. are the straightforward weakly nonlinear equation, the Kuznetsov equation and the Lighthill-Westervelt equation (Westervelt, 1963). The two first equations are introduced in Chapter 2. The latter of the three equations is a well-established model equation in nonlinear acoustics. However, Christov and coworkers conclude that the Lighthill-Westervelt equation gives the poorest performance of the three equations in their study of shock formation. Accordingly, the Lighthill-Westervelt equation is not discussed here. The investigations conducted by Christov and coauthors do not include the Hamiltonian weakly nonlinear equation (2.52). In order to assess the accuracy of this equation compared to the straightforward weakly nonlinear equation and Kuznetsov's equation, we are going to reproduce some of the results reported by Christov et al., and additionally include the Hamiltonian weakly nonlinear equation in our study.

In their study Christov and coworkers introduced the following dimensionless variables denoted by tilde

$$
\begin{aligned}
\tilde{x} = x/L, \qquad \tilde{t} = t(c_0/L), \qquad \tilde{\psi} = \psi/(u_{\max}L), \\
\tilde{p} = p/(\rho_0 c_0^2), \qquad \tilde{\rho} = \rho/\rho_0, \qquad \tilde{u} = u/u_{\max},
\end{aligned}
\tag{5.3}
$$

where $u_{\max} = \max|u|$ and L denote characteristic speed and length, respectively. In terms of these variables (omitting the tilde) the Euler equations (3.21) become

$$
\begin{bmatrix} \rho \\ \rho u \end{bmatrix}_t + \begin{bmatrix} \varepsilon \rho u \\ \varepsilon \rho u^2 + \rho^\gamma/(\gamma \varepsilon) \end{bmatrix}_x = 0,
\tag{5.4}
$$

and the lossless higher order acoustic wave equation (2.33) becomes

$$
\psi_{tt} - c_0^2 \psi_{xx} = \varepsilon(\gamma-1)\psi_{xx}\psi_t + 2\varepsilon\psi_{xt}\psi_x - \varepsilon^2 \frac{\gamma+1}{2}\left(\psi_x\right)^2 \psi_{xx}.
\tag{5.5}
$$

Here $\varepsilon = u_{\max}/c_0$ is the Mach number of the flow. From Eq. (5.5) follows directly the non-dimensional versions of the weakly nonlinear equations, cf. Section 2.4. In terms of the non-dimensional variables (again omitting the tilde) the density (2.35) becomes

$$
\rho = \left[1 + \varepsilon(\gamma-1)\left(\psi_t - \varepsilon\frac{(\psi_x)^2}{2}\right)\right]^{\frac{1}{\gamma-1}},
\tag{5.6}
$$

which is the exact relationship between ρ and ψ in the context of Eq. (5.5). Making a Taylor expansion of Eq. (5.6) around $(\eta, u) = (0, 0)$ and neglecting terms that are second and higher order in ε yields

$$
\rho = 1 + \varepsilon\eta,
\tag{5.7}
$$

where $\eta = \psi_t$. It is not immediately clear which one of Eqs. (5.6) and (5.7) is the best suitable to apply, in order to compute ρ within the context of the weakly nonlinear equations. In order to assess which one of them is the most favorable, we use both relationships to compute ρ in the following numerical simulations. Following Christov et al. (2007) we solve the equations subject to the following initial and boundary conditions

$$\rho(x, t = 0) = 1, \qquad u(x, t = 0) = 0, \qquad u(x = 0, t) = \sin \pi t. \qquad (5.8)$$

Note that these conditions are the dimensionless versions of the initial conditions (5.1) applied above. For the numerical simulation below we take $\varepsilon = 0.26503$. For this value of ε the predicted time of shock formation is $t = 1$ (Christov et al., 2007). The results of our numerical simulations are shown at different instants in time through Figs. 5.5–5.8.

In Figs. 5.5, 5.6 and 5.7 we apply Eq. (5.6) in order to compute ρ from the solutions of the weakly nonlinear equations. In Fig. 5.8 we apply Eq. (5.7) in order to compute ρ from the solutions at $t = 1$ and $t = 2$ of the weakly nonlinear equations. By comparing the two cases, i.e. comparing the topmost plot in Fig. 5.5 to the topmost plot in Fig. 5.8, and comparing the topmost plot in Fig. 5.6 to the lowermost plot in Fig. 5.8, we observe that the solutions of the three weakly nonlinear equations (green, magenta and black curves) come closer to the solution of the 'exact' Euler equations (blue curve) when we use Eq. (5.6) to compute ρ. Furthermore, the plots of ρ are more consistent with the plots of u, in the case of using Eq. (5.6). Thus, we suggest that ρ is best computed by the use of Eq. (5.6). Christov and coworkers applied Eq. (5.7) to compute ρ from the solutions of the weakly nonlinear equations. In Figs. 5.6 and 5.8 we plot a number of data points read off from the numerical results presented by these authors. We see that there is a fine agreement between our numerical solution, and the data points taken from Christov et al.. The numerical results reported by Christov and coworkers extend up to $t = 2$. Thus there is no figure corresponding to Fig. 5.7 in their paper.

From our numerical simulations we observe the following. At $t = 1$ the solution of the Hamiltonian weakly nonlinear equation (black curve) is the one which is closest to the Euler equations (blue curve). At $t = 2$ the Hamiltonian weakly nonlinear equation and the straightforward equation matches the shock in the Euler equations more or less equally well. The solution of the Hamiltonian weakly nonlinear equation is closest to the solution of the Euler equations on the smooth part of the solution. At $t = 4$ the straightforward equation matches the shock in the Euler equations best. The solution of the Hamiltonian weakly nonlinear equation is still closest to the solution of the Euler equations on the smooth part of the solution. Thus we conclude that the Hamiltonian weakly nonlinear equation is the one which performs best for smooth solutions, whereas the straightforward equation is the weakly nonlinear model, which best matches the shock in the Euler equations. This is not surprising, since the shock jump condition for the straightforward weakly nonlinear equation is the one which is closest to the jump condition of the Euler equations, cf. Fig. 3.9.
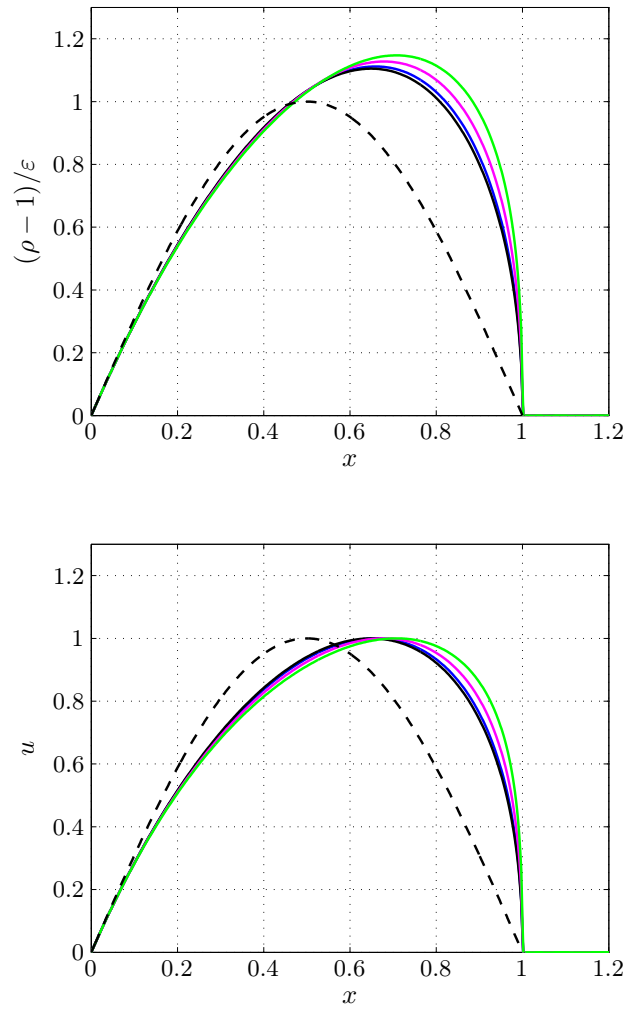
Fig. 5.5. Snapshots of the scaled dimensionless acoustic density $(\rho-1)/\varepsilon$ and velocity u at $t = 1$. The color convention is as follows: in blue is the Euler equations (3.14) for a perfect gas, in magenta is the lossless version of the straightforward weakly nonlinear equation (2.48), in green is the lossless version of the Kuznetsov equation (2.49), in solid black is the lossless Hamiltonian weakly nonlinear equation (2.51), in dashed black is the linear wave equation. For the three weakly nonlinear equations, the density ρ is obtained using Eq. (5.6).
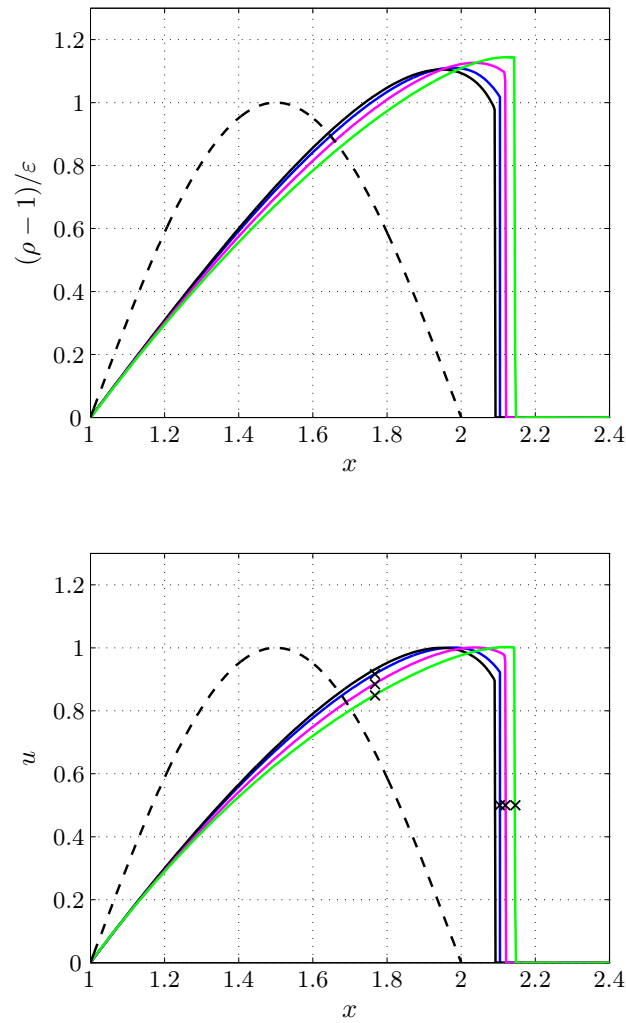
Fig. 5.6. Snapshots of the scaled dimensionless acoustic density $(\rho-1)/\varepsilon$ and velocity u at $t = 2$. The color convention is the same as in Fig. 5.5. For the three weakly nonlinear equations, the density ρ is obtained using Eq. (5.6). The crosses represent data points taken from graphs presented in Christov et al. (2007).
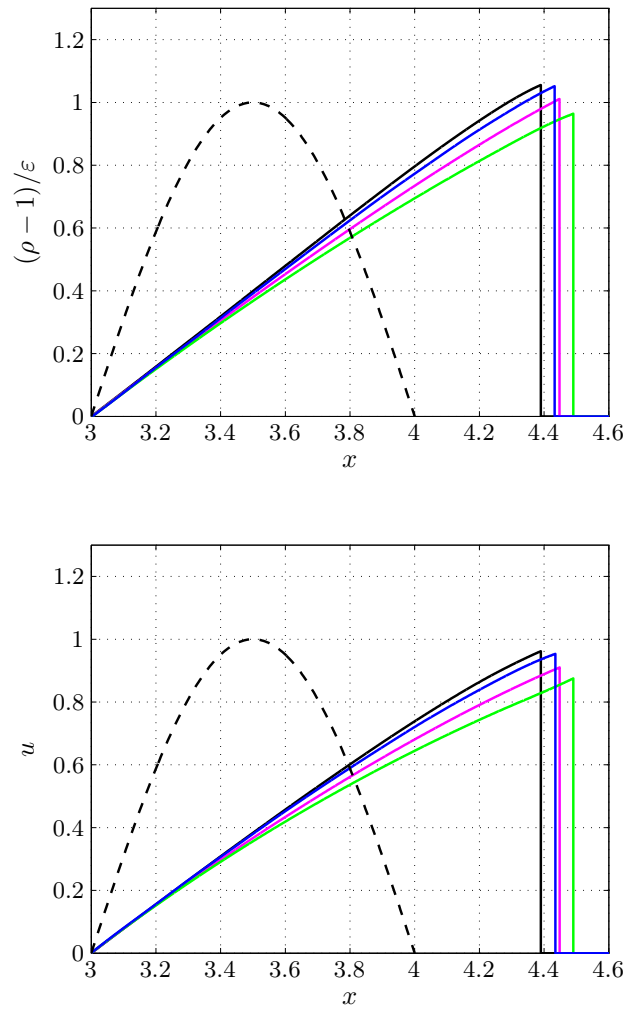
Fig. 5.7. Snapshots of the scaled dimensionless acoustic density $(\rho - 1)/\varepsilon$ and velocity u at $t = 4$. The color convention is the same as in Fig. 5.5. For the three weakly nonlinear equations, the density ρ is obtained using Eq. (5.6).
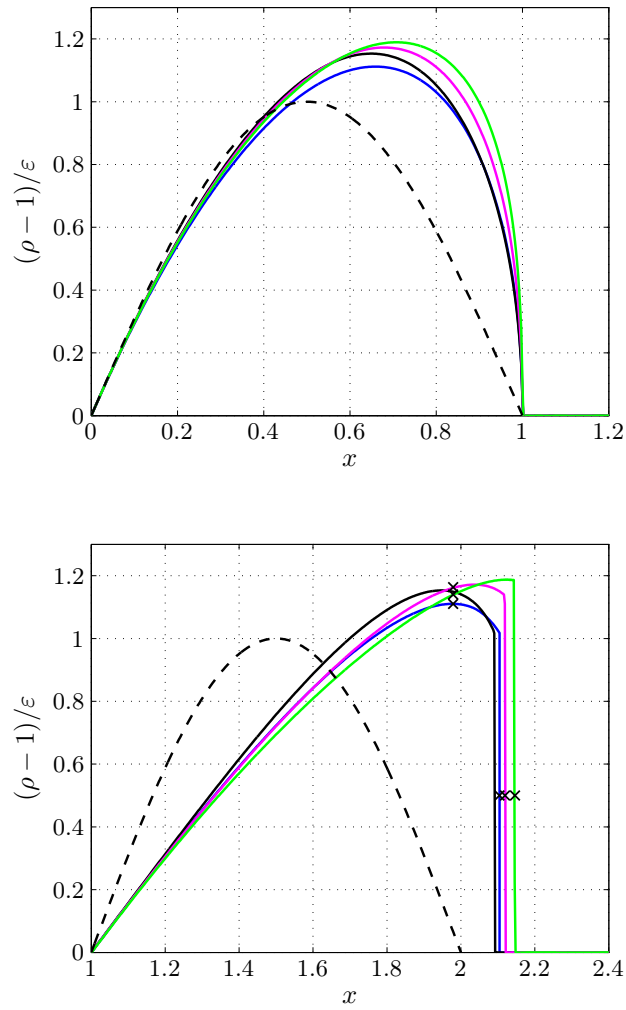
Fig. 5.8. Snapshots of the scaled dimensionless acoustic density $(\rho - 1)/\varepsilon$ at $t = 1$ (topmost) and $t = 2$ (lowermost). The color convention is the same as in Fig. 5.5. For the three weakly nonlinear equations, the density ρ is obtained using Eq. (5.7). The crosses represent data points taken from graphs presented in Christov et al. (2007).

Chapter 6

Compound Waves

Compound waves are solutions that are compounded by two or more waves. Problems of compound waves include shock interactions, such as head-on colliding shocks and overtaking shocks. Solutions to the Riemann problem are compound waves as well. The Riemann problem is simply a given equation together with very special initial data consisting of piecewise constant functions with a single jump discontinuity. In the following we introduce the notion of a rarefaction wave, which often occurs in problems with compound waves. We study the Riemann problem and problems with colliding shocks.

6.1   Rarefaction Waves (loss-less case)

The problems of compound waves we are going to study include two types of waves, namely shocks and rarefaction waves. Rarefaction waves are waves that rarefy the fluid through which they propagate, as opposed to shocks which compress the fluid. That is, rarefaction waves decrease the fluid density, and shocks increase the fluid density. A rarefaction wave separates two constant states of the fluid. The two constant states to the left and right of the rarefaction wave are separated by smooth functions which depend on x/t, as opposed to the jump discontinuity that separates the constant states to the left and right of a shock. For the system of conservation laws (3.1) the rarefaction wave has the form

$$q(x,t) = \begin{cases} q_l & \text{if } x/t \leq z_2, \\ Q(x/t) & \text{if } z_2 \leq x/t \leq z_1, \\ q_r & \text{if } x/t \geq z_1, \end{cases} \qquad (6.1)$$

where q_l and q_r represent the constant states to the left and right of the rarefaction wave, and z_1 and z_2 are constants. In section 4 in Appendix C we derive an exact rarefaction wave solution to the lossless higher order equation (2.33). The derivation is based on the assumption that $u = -\psi_x$ and $\eta = \psi_t$ are functions of x/t. We find that the constant values of u and η to the left and to the right of the rarefaction wave, must satisfy Eq. (40) in Appendix C. This equation can be written in terms of ρ and u by invoking Eq. (2.35). In Fig. 6.1 we show a

numerical simulation of the lossless higher order wave equation for initial data that corresponds to a rarefaction wave. Due to the fact that the lossless higher order wave equation and the Euler equations for a perfect gas are equivalent for smooth solutions (cf. Section 2.2.6), it is expected that the rarefaction wave solution of the Euler equations (3.21) is identical to the rarefaction wave solution of the higher order equation. This behavior was verified by performing a numerical simulation of the Euler equations with initial data identical to those in Fig. 6.1. The numerical solution of the Euler equations was found to be identical to the numerical solution in Fig. 6.1. Thus, the rarefaction wave solutions of the lossless higher order equation and the Euler equations for a perfect gas are identical.
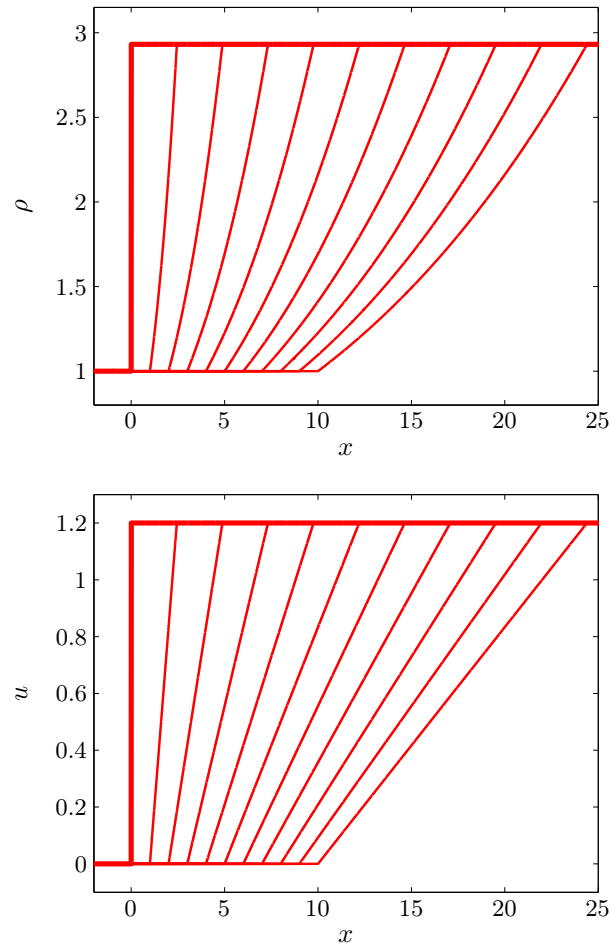

Fig. 6.1. Numerical simulation of the lossless higher order acoustic wave equation (2.33) with initial data (shown in bold line) corresponding to a rarefaction wave. The solution solution is shown at eleven instants during $t \in [0, 10]$. The following parameter is used: $\gamma = 1.4$.

6.2   Thermoviscous shocks and rarefaction waves

6.2.1   The Riemann Problem

Consider a given equation with the piecewise-constant initial data

$$\rho(x,0) = \left\{ \begin{array}{ll} \rho_a, & \text{if } x < 0, \\ \rho_b, & \text{if } x > 0, \end{array} \right. \qquad u(x,0) = \left\{ \begin{array}{ll} u_a, & \text{if } x < 0, \\ u_b, & \text{if } x > 0, \end{array} \right. \qquad (6.2)$$

where ρ_a, ρ_b, u_a and u_b are constants. This is the Riemann problem. The special case of the Riemann problem with $u_a = u_b = 0$ corresponds to a shock tube problem. That is a tube in which a gas at low pressure and a gas at high pressure are separated using a diaphragm. In Fig. 6.2 we show a numerical simulation of the viscous basic equations (3.14) for a perfect gas with such initial data. We see that the solution is compounded by a rarefaction wave that propagates to the left and a shock that propagates to the right. The asymptotic boundary conditions of each of the two waves and the propagation velocity of the shock can be predicted by analytical calculations. These calculations rely on the equations for the asymptotic boundary conditions of the shock and rarefaction wave, details are given in Section 6 in Appendix C. The book by LeVeque (2002) gives helpful and thorough details on the solution of the Riemann problem. Note that, in general, the equations for the asymptotic boundary conditions of the shock (i.e. the shock jump condition) and the rarefaction wave do not depend on the dissipation parameters. Accordingly, asymptotic boundary conditions and propagation velocities observed in the solutions of Riemann problems are not influenced by the presence of dissipation in the governing equations.

6.2.2   Interacting Shocks

In Figs. 6.3 and 6.4 we show numerical simulations of Eq. (3.14) for two examples of colliding shocks. In Fig. 6.3 we simulate two shocks that propagate at different speeds in the same direction. The shocks collide once the faster one catches up with the slower one. Each of the two shocks that make up the initial condition is an exact solution defined by Eq. (3.30) with its asymptotic boundary conditions satisfying the shock jump condition (3.24). From the numerical solution of the problem we see that a rarefaction wave and a shock emerge from the collision. These two waves propagate to the left and right, respectively, away from the point of collision. The simulation in Fig. 6.4 is similar to the one in Fig. 6.3. Although, in this example the two shocks in the initial condition propagate towards each other and make a head-on collision at a later instant in time. From the result of the numerical simulation we see that the collision results in two shocks that propagate away from each other. The contour plot reveals that these shocks travel at a higher speed compared to the speed of the shocks before the collision.

Generally, the properties of the waves that emerge from the collisions, i.e. asymptotic boundary conditions and shock propagation velocities, can be predicted by analytical calculations. At the time when the two shocks collide, the solution represents a Riemann problem. Thus, the problem of predicting

the waves after the collision is reduced to that of solving a Riemann problem. Figs. 6.2, 6.3 and 6.4 are numerical simulations of Eq. (3.14). The corresponding simulations of the higher order acoustic wave equation (2.24) are performed in Appendix C. In the case of the Riemann problem and the problem with head-on colliding shocks, the two models behave qualitatively in the same manner, but with quantitative differences between the solutions of the two models. In the case of overtaking shocks, however, there is a qualitative difference between the two models. In the case of the higher order equation we observe that two shocks emerge from the collision, whereas in the case of Eq. (3.14) we observe that a rarefaction wave and a shock emerges from the collision. For the specific choice of γ, this qualitative difference between the two models is found to remain, also if the shocks before the collision are chosen arbitrarily weak. These differences between the two models are due to the fact that the two models have different shock jump conditions.

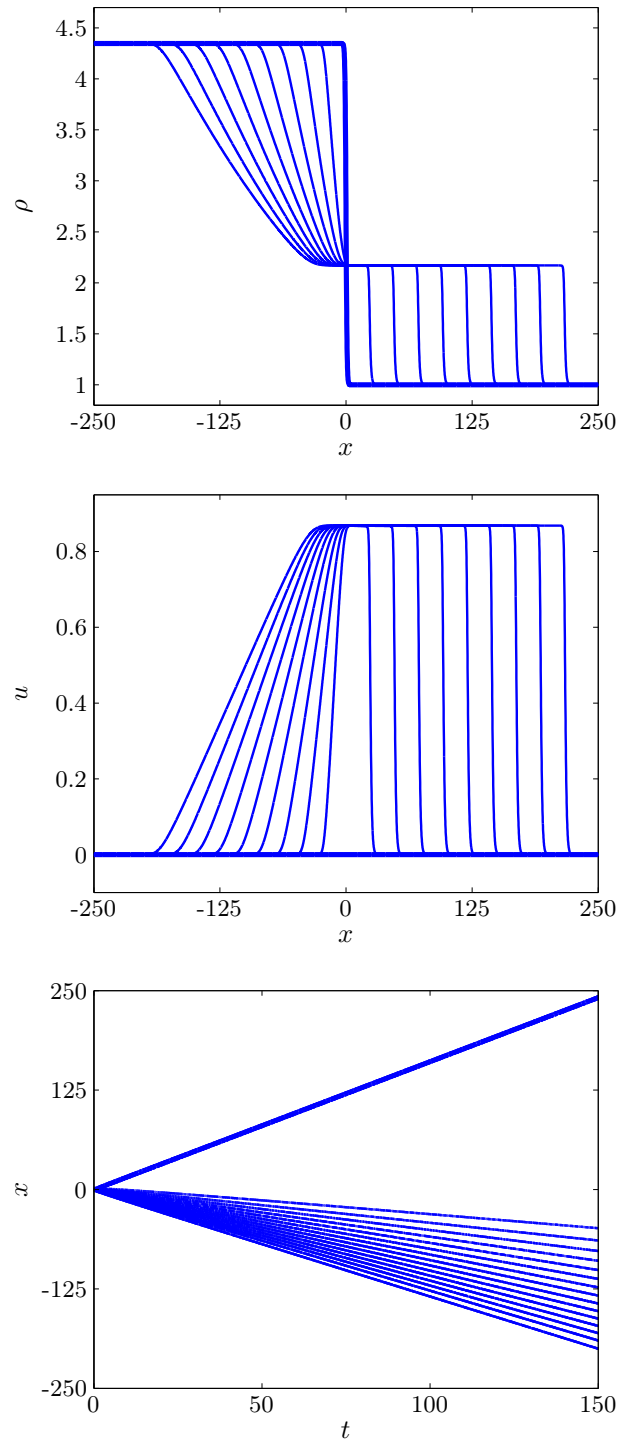**Fig. 6.2.** Numerical simulation of Eq. (3.14) with initial data (shown in bold line) corresponding to a Riemann problem. The following parameter is used: $\gamma = 1.4$.

Fig. 6.3. Numerical simulation of Eq. (3.14) with initial data (shown in bold line) corresponding to two overtaking shocks. The following parameter is used: $\gamma = 6$. Lowermost: contour lines given by $u = Z_i$, where Z_i are constants.
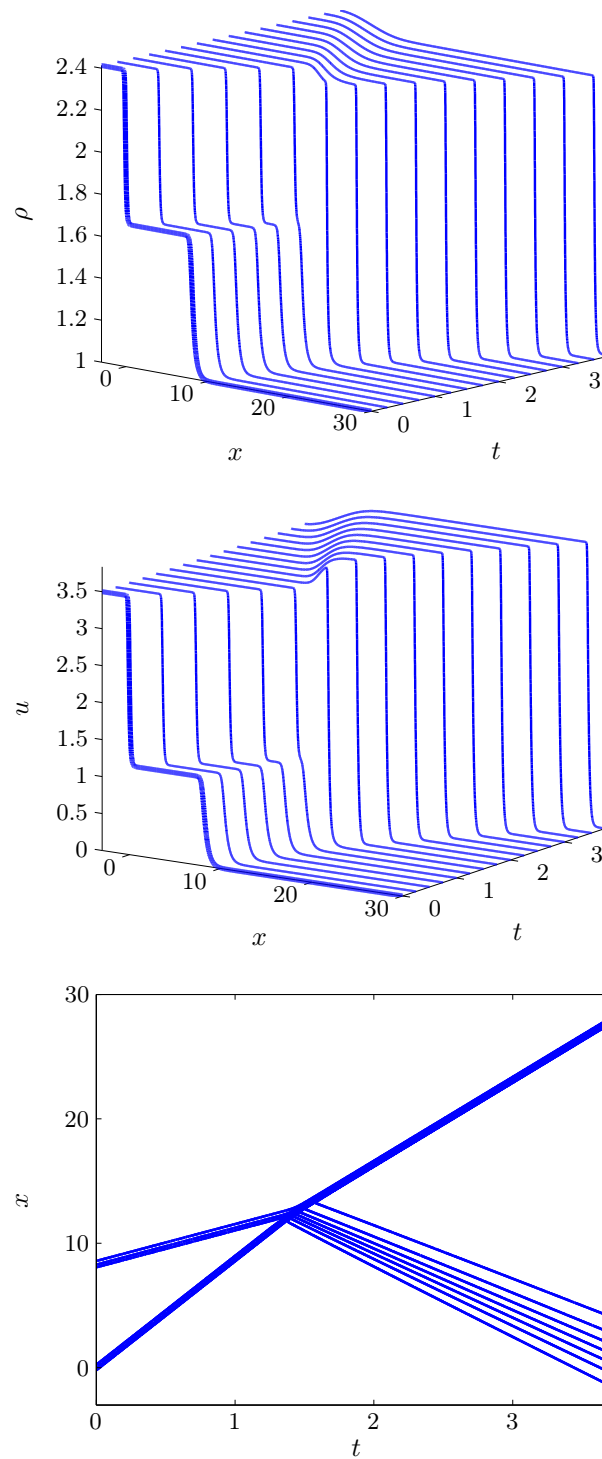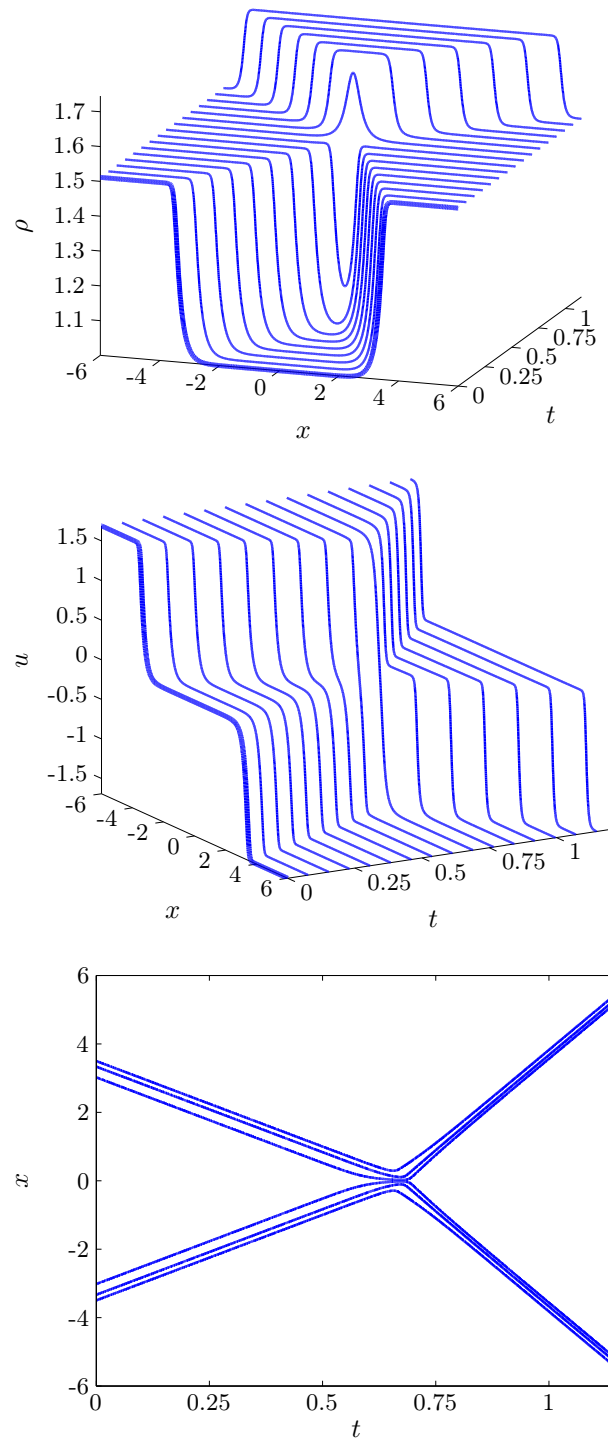
Fig. 6.4. Numerical simulation of Eq. (3.14) with initial data (shown in bold line) corresponding to two head-on colliding shocks. The following parameter is used: $\gamma = 11$. Lowermost: contour lines given by $u = Z_i$, where Z_i are constants.

Chapter 7

Nonlinear Standing Waves and Other Exact Solutions

Standing waves are of great importance within the field of nonlinear acoustics. If acoustical resonators are driven at, or near, one of their resonance frequencies, the amplitude of the acoustical field inside the resonator becomes very high. Within the theory of lossless linear acoustics it is well-known that the amplitude goes to infinity at the resonance frequencies. However, in real situations the amplitude at resonance becomes finite due to dissipative effects. In typical situations dissipation is small and the amplitude encountered will be large. Accordingly, nonlinear effects come into play and may give rise to standing shocks inside the resonator. Much of the basic theory for nonlinear standing waves is due to Chester (1964), who studied resonant oscillations in closed tubes. A study of nonlinear standing waves based on a perturbation approach applied to the Kuznetsov equation is given in the book by Enflo and Hedberg (2002).

It is a well-known fact that acoustical standing waves (and acoustical waves in general) may generate a flow field in which the particle velocities are not simply sinusoidal, and a pattern of time-independent vortical flows or steady circulations is often found in the body of compressible media. Such flow patterns are known as acoustic streaming (Nyborg, 1998). Acoustic streaming is not studied here, however it was originally experimental results on acoustic resonances and acoustic streaming in microfluidic systems (Hagsäter et al., 2007, 2008) that motivated us to investigate standing waves.

In this chapter we investigate nonlinear standing waves in a one-dimensional acoustical resonator having one closed end, and one end periodically oscillating. The analysis is based on numerical simulations of our Hamiltonian weakly nonlinear equation (2.52).[1] If we drive the oscillator at one of its resonance frequencies, and choose the amplitude of the periodic excitation and the thermoviscous dissipation parameter appropriately, the solution consists of a number of standing shocks inside the oscillator. The particular structure of the standing

---

[1]It is believed that the analysis of this chapter can be carried out equally well for the other three wave equations introduced in Chapter 2, i.e. the higher order acoustic wave equation, the straightforward weakly nonlinear equation and the Kuznetsov equation.

shocks observed in the oscillator inspired us to introduce a new solution ansatz, in order to search for new exact solutions of the governing equation. We are going to demonstrate that application of this new solution ansatz leads to new exact solutions, that resemble the standing shocks observed in the oscillator. Whether these new exact solutions are related to nonlinear standing waves is yet to be investigated.

7.1   Nonlinear Standing Waves in a Closed Tube

We consider our Hamiltonian weakly nonlinear equation (2.52), which we repeat here for convenience

$$\psi_{tt} - c_0^2 \psi_{xx} = \psi_t \psi_{xx} + \frac{\gamma - 2}{c_0^2} \psi_{tt} \psi_t + 2\psi_{xt}\psi_x + b\psi_{xxt}. \qquad (7.1)$$

Equation (7.1) is applied to a finite domain of length 1 with the boundary conditions formulated for the fluid particle velocity $u = -\psi_x$ in the following way

$$u(x = 0, t) = D \sin 2\pi t, \qquad u(x = 1, t) = 0, \qquad (7.2)$$

where $D = 0.01 \times c_0$. In our numerical simulation we let the amplitude of the periodic excitation rise from 0 to D during a finite time interval (for practical reasons), and run the simulation until the steady state is reached. Throughout this chapter we take $\gamma = 1.4$. Figures 7.1 and 7.2 show the numerical solution obtained during one cycle of oscillation within the steady state. In Fig. 7.3 we plot η as function of time at the right boundary of the oscillator, together with the excitation in u at the left boundary. In the example shown in the figures we excite the second eigenmode of the system, which gives rise to two standing shocks. Generally, exciting the nth eigenmode results in n standing shocks. Our numerical results agree qualitatively with the results presented in Chester (1964) and Enflo and Hedberg (2002).

Interestingly, wave patterns similar to the nonlinear standing wave patterns observed in the acoustical resonator have been found in the the perturbed sine-Gordon equation as a model for long Josephson junctions (Pagano et al., 1988).
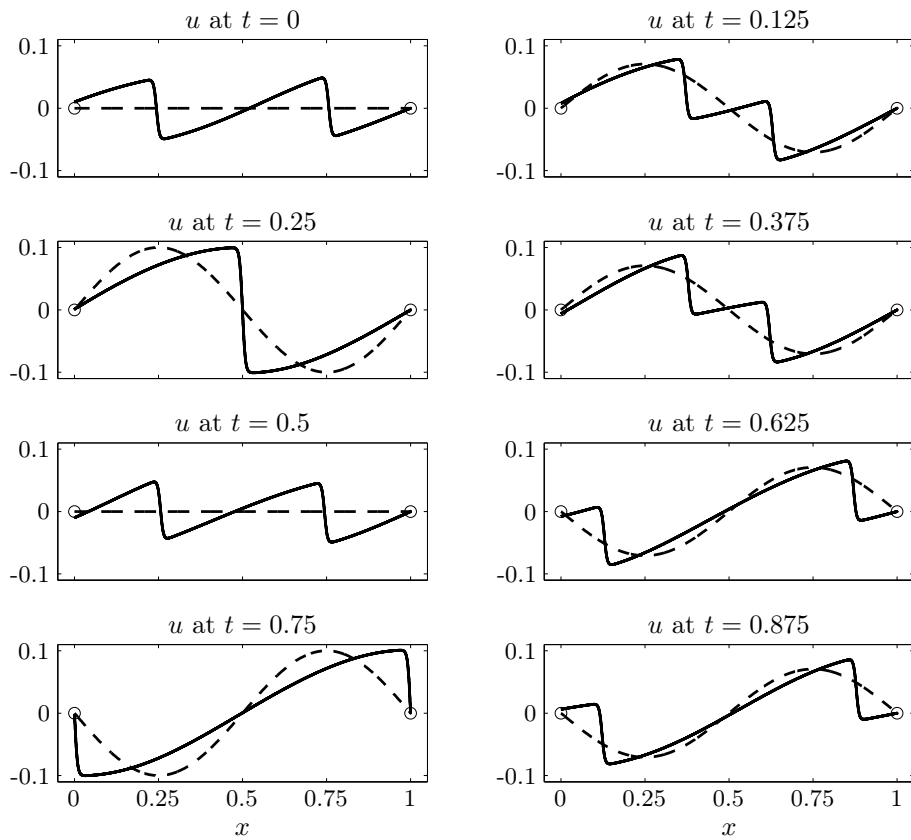
Fig. 7.1. Numerical simulation of Eq. (7.1) subject to the boundary conditions (7.2). The solution is shown at eight different instants during one cycle of oscillation. The eigenmode of the corresponding linear problem is shown in dashed line. The following parameters are used: $b = 5 \times 10^{-4}$, $\gamma = 1.4$.
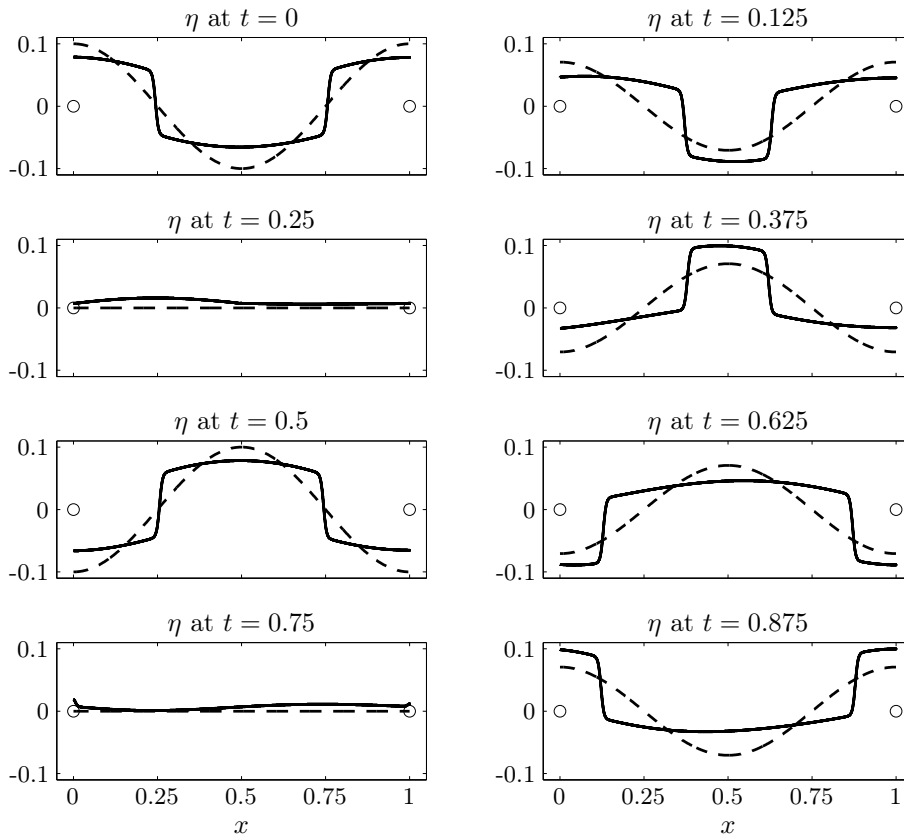
Fig. 7.2. Continued from Fig. 7.1.

Fig. 7.3. Continued from Fig. 7.2. Blue line, left y-axis: $u(x = 0, t)$. Green line, right y-axis: $\eta(x = 1, t)$. The one cycle of oscillation between the dashed lines corresponds to the one shown in Figs. 7.1 and 7.2.

7.2   Other Exact Solutions

The standing shocks observed in the above numerical simulation resemble sums of traveling shocks and functions that are linear in x and t, i.e. traveling shocks with sloping lines on each side of the shock. In order to search for exact solutions, we introduce the following solution ansatz
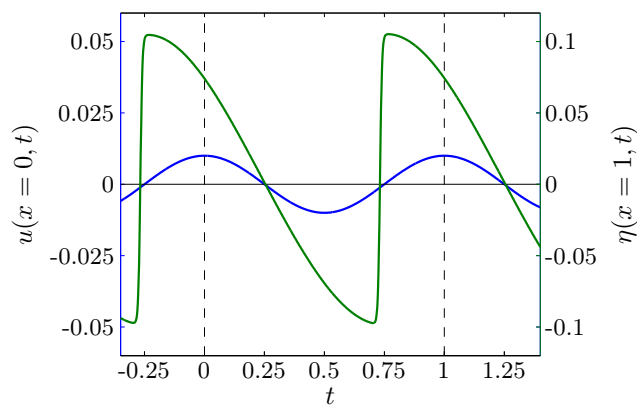
$$\psi(x,t) = \Psi(\xi) + a_1 x + a_2 t + a_3 xt + a_4 \frac{x^2}{2} + a_5 \frac{t^2}{2}, \qquad (7.3)$$

where $\xi = x - vt$. Note that Eq. (7.3) is an extension of the solution ansatz (3.62), that was used to derive the thermoviscous shock solutions. The ansatz (7.3) takes into account terms of second order in x and t that were not included in Eq. (3.62). Taking the derivatives of Eq. (7.3) with respect to x and t, respectively, yields

$$u(x,t) = \Phi(\xi) - a_1 - a_3 t - a_4 x, \qquad \eta(x,t) = v\Phi(\xi) + a_2 + a_3 x + a_5 t, \quad (7.4)$$

where $\Phi = -\Psi'$ and prime denotes differentiation with respect to ξ. Inserting Eq. (7.3) into Eq. (7.1) yields

$$b\Psi''' + \left(3 + \frac{\gamma - 2}{c_0^2} v^2\right) \Psi'' \Psi' + \left(2a_1 - \frac{\gamma - 2}{c_0^2} v a_2 - \frac{a_2 - v^2 + c_0^2}{v}\right) \Psi''$$

$$+ \left(a_4 + \frac{\gamma - 2}{c_0^2} a_5 - \frac{2a_3}{v}\right) \Psi' + (\alpha_1 \Psi'' + \alpha_2) x + (\alpha_3 \Psi'' + \alpha_4) t$$

$$- \frac{1}{v} \left(2a_1 a_3 + a_2 a_4 + c_0^2 a_4 + \frac{\gamma - 2}{c_0^2} a_2 a_5 - a_5\right) = 0, \quad (7.5)$$

where

$$\alpha_1 = a_3 - 2va_4 + \frac{\gamma - 2}{c_0^2} v^2 a_3, \quad \alpha_2 = 3a_3 a_4 + \frac{\gamma - 2}{c_0^2} a_3 a_5,$$

$$\alpha_3 = a_5 - 2va_3 + \frac{\gamma - 2}{c_0^2} v^2 a_5, \quad \alpha_4 = a_4 a_5 + 2a_3^2 + \frac{\gamma - 2}{c_0^2} a_5^2. \qquad (7.6)$$

Equation (7.5) depends explicitly on both x and t. However, in each of the following four cases, Eq. (7.5) reduces to an ordinary differential equation with ξ being the only independent variable:

(i) $(\alpha_3 \Psi'' + \alpha_4)/(\alpha_1 \Psi'' + \alpha_2) = -v$.
(ii) $\alpha_1 = 0$, $\alpha_3 = 0$ and $\alpha_4/\alpha_2 = -v$.
(iii) $\alpha_2 = 0$, $\alpha_4 = 0$ and $\alpha_3/\alpha_1 = -v$.
(iv) $\alpha_1 = 0$, $\alpha_2 = 0$, $\alpha_3 = 0$ and $\alpha_4 = 0$.

The first case yields $\Psi'' =$ constant, which we are not going to investigate further. Inserting Eqs. (7.6) into the second case yields a system of three nonlinear equations for the four unknowns a_3, a_4, a_5 and v. These equations were solved using the software package MAPLE™.[2] Remarkably, it turns out that the solution implies that $\alpha_2 = 0$ and $\alpha_4 = 0$. In a similar manner it turns out that the

---

[2] http://www.maplesoft.com

solution of the third case implies that $\alpha_1 = 0$ and $\alpha_3 = 0$. Thus, the second, third and fourth cases have the same solution. In these cases we obtain

$$a_3 = \frac{a_5}{3v}, \qquad a_4 = \frac{a_5}{9v^2}, \qquad v^2 = -\frac{c_0^2}{3(\gamma - 2)}, \qquad (7.7)$$

where a_5 can be chosen arbitrarily. By inserting Eqs. (7.7) into Eq. (7.5), and invoking $\Phi = -\Psi'$ we obtain

$$b\Phi'' - \frac{8}{3}\Phi'\Phi + \left(2a_1 + v - \frac{c_0^2}{v} - \frac{2a_2}{3v}\right)\Phi'$$
$$- \frac{8a_5}{9v^2}\Phi - \frac{a_5}{v} + \frac{2a_1 a_5}{3v^2} - \frac{(2a_2 - c_0^2)a_5}{9v^3} = 0. \quad (7.8)$$

The solution $\Phi(\xi)$ of this equation represents, when inserted into Eqs. (7.4), an exact solution of Eq. (7.1). However, Eq. (7.8), which is a second order nonlinear ordinary differential equation (ODE), cannot be readily solved using analytical techniques. Thus, we are going to solve the equation by application of numerical tools, in order to determine Φ. Two examples of numerical solutions of Eq. (7.8) are shown in Fig. 7.4. These numerical solutions are obtained using the MATLAB solver `ode45`.
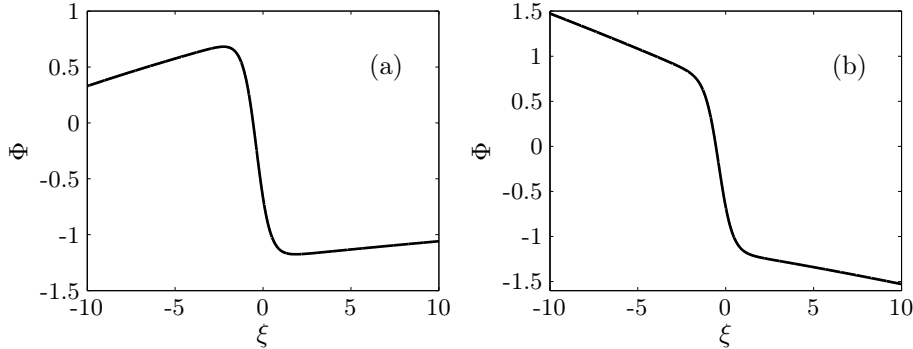

Fig. 7.4. Numerical solutions of Eq. (7.8). $a_1 = 0$, $a_2 = 0$, (a): $a_5 = -0.05$, (b): $a_5 = 0.1$. a_3, a_4 and v are given by Eq. (7.7). $\gamma = 1.4$.

Once Φ is computed we insert the result, that is the numerical solution which is a set of data points, into Eqs. (7.4) in order to obtain $u(x, t)$ and $\eta(x, t)$. Furthermore, we obtain the function Ψ by numerically integrating Φ with respect to ξ. Then, by inserting the data points obtained in this manner into Eq. (7.3) we obtain $\psi(x, t)$. In order to verify that the solution obtained actually represents an exact solution of Eq. (7.1), we apply the solution as initial condition in numerical simulations of Eq. (7.1). In our simulations we let the boundary conditions depend on t in such a way that the boundary conditions matches the exact solution. The results of the numerical simulations are shown in Figs. 7.5 and 7.6. Indeed, the numerical solutions presented in these figures verify that the solutions we have obtained are exact solutions of the form (7.3).

According to the discussion in Chapter 2, Eq. (7.1) is basically an approximation to the Navier-Stokes equations (3.14) for a perfect gas, and to Eqs. (3.39)

in the case of a fluid with a quadratic equation of state. Hence, on the basis of the above results it would be very relevant to consider the following solution ansatz

$$\rho(x,t) = P(x - vt) + a_1 x + a_2 t, \qquad u(x,t) = U(x - vt) + a_3 x + a_4 t. \quad (7.9)$$

Investigations of whether substitution of Eqs. (7.9) into Eqs. (3.14) and (3.39) leads to exact solutions is left for further studies.
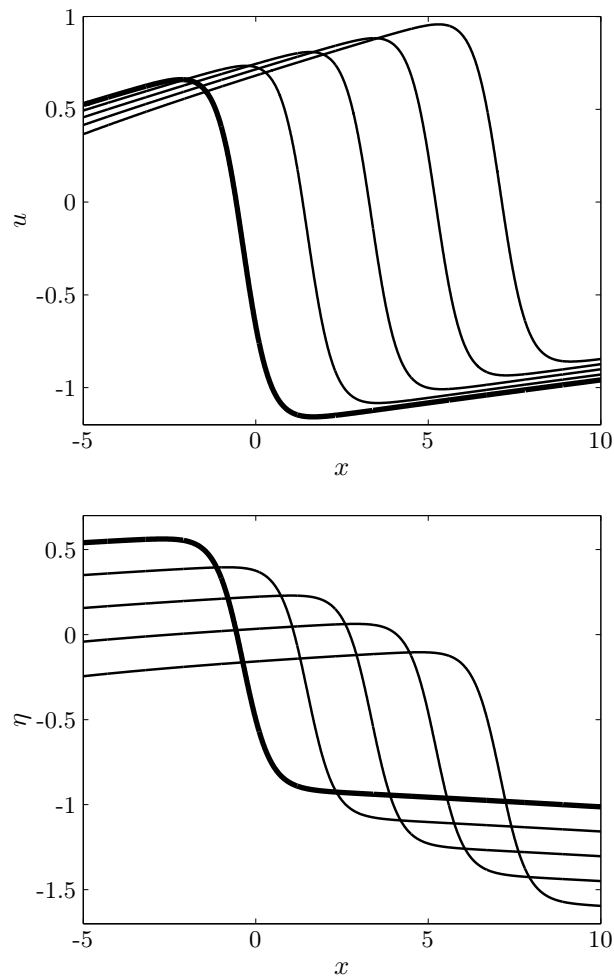

Fig. 7.5. Numerical simulation of Eq. (7.1). The initial condition (shown in bold line) and the boundary conditions are obtained from the numerical solution given in Fig. 7.4(a). The solution is shown at five instants during $t \in [0, 10]$.
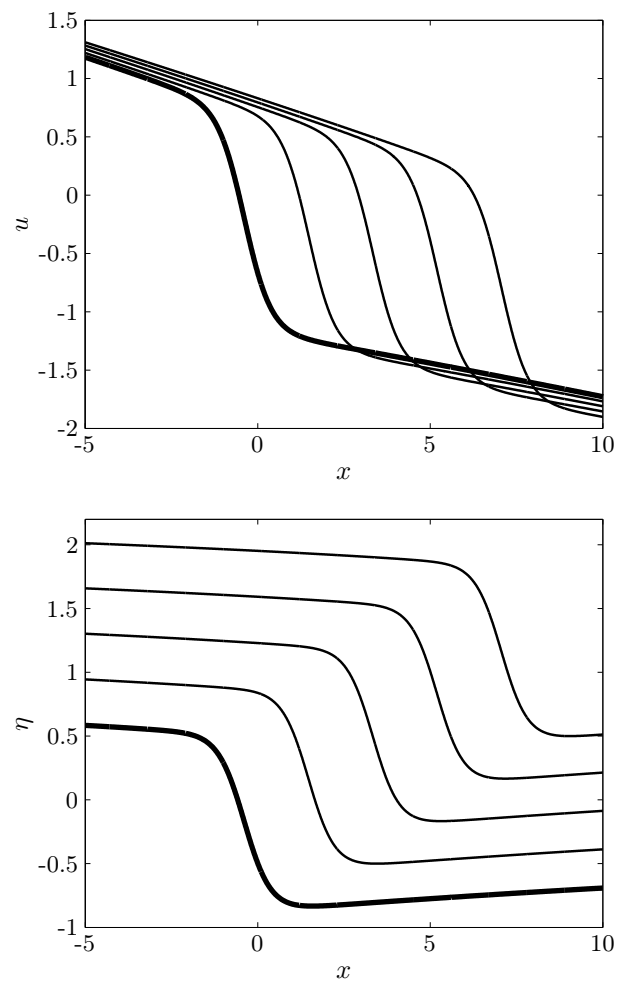
Fig. 7.6. Continued from Fig. 7.5. The initial and boundary conditions are obtained from the solution given in Fig. 7.4(b).

Chapter 8

Conclusions

We have studied four nonlinear acoustical wave equations that apply to both perfect gasses and arbitrary fluids with a quadratic equation of state. The wave equations are derived by applying various approximation schemes to the basic compressible Navier-Stokes equations. Detailed investigations of shock solutions have demonstrated that caution must be taken if the governing equations are subjected to manipulations that depend on smoothness, or if nonlinear dissipative terms are neglected in the equations. Such manipulations and approximations are found to have unexpected influence on the shock jump conditions. Hence, we found a straightforward weakly nonlinear wave equation to be more accurate than a higher order wave equation for the purpose of shock modeling. However, in the case of smooth solutions the higher order equation is the most accurate, as one would expect.

By investigating the linear stabiliy properties of solutions to the wave equations, certain stability criteria for each of the four wave equations are obtained. If these stability criteria are violated instabilities occur in the solutions of the wave equations. It was demonstrated that such instabilities do not occur in the basic equations from which the wave equations are derived.

Problems with compound waves have been studied. In particular we investigated shock interactions and the classical Riemann problem. The solutions to these problems may include two types of waves, namely shocks and rarefaction waves. Problems of compound waves was solved by invoking shock jump conditions and corresponding equations for rarefaction waves. Numerical studies of acoustical resonators revealed the presence of standing shocks inside the resonator. The particlular wave pattern observed in acoustical resonator, inspired us to derive new exact generalized shock solutions.

Bibliography

Aanonsen, S. I., Barkve, T., Tjøtta, J. N., and Tjøtta, S. (1984). Distortion and harmonic generation in the nearfield of a finite amplitude sound beam. *J. Acoust. Soc. Am.*, 75(3):749–768.

Arfken, G. B. and Weber, H. J. (2001). *Mathematical Methods for Physicists*. Academic Press.

Beyer, R. T. (1974). *Nonlinear Acoustics*. Navy Sea Systems Command, Washington, D.C.

Beyer, R. T. (1998). The parameter B/A. In Hamilton, M. F. and Blackstock, D. T., editors, *Nonlinear Acoustics*, chapter 2, pages 25–39. Academic Press, San Diego.

Chapman, C. J. (2000). *High Speed Flow*. Cambridge University Press.

Chester, W. (1964). Resonant oscillations in closed tubes. *J. Fluid Mech.*, 18:44–64.

Christov, I., Christov, C. I., and Jordan, P. M. (2007). Modeling weakly nonlinear acoustic wave propagation. *Q. J. Mechanics. Appl. Math.*, 60(4):473–495.

Corless, R. M., Gonnet, G. H., Hare, D. E. G., Jeffrey, D. J., and Knuth, D. E. (1996). On the Lambert W function. *Adv. Comput. Math.*, 5(4):329–359.

Crighton, D. G. (1979). Model equations of nonlinear acoustics. *Ann. Rev. Fluid Mech.*, 11:11–33.

Enflo, B. O. and Hedberg, C. M. (2002). *Theory of Nonlinear Acoustics in Fluids*. Kluwer Academic, Dordrecht.

Gent, R. (1997). *Applied Physics and Technology of Diagnostic Ultrasound*. Milner Publishing, Prospect.

Goldstein, H., Poole, C., and Safko, J. (2001). *Classical Mechanics*. Addison Wesley, 3rd edition.

Hagsäter, S. M., Jensen, T. G., Bruus, H., and Kutter, J. P. (2007). Acoustic resonances in piezo-actuated microfluidic chips: full-image micro-piv experiments and numerical simulations. *Lab Chip*, 7:1336–1344.

Hagsäter, S. M., Lenshof, A., Skafte-Pedersen, P., Kutter, J. P., Laurell, T., , and Bruus, H. (2008). Acoustic resonances in straight micro channels: Beyond the 1d-approximation. *Lab Chip*, 8:1178–1184.

Hamilton, M. F. and Morfey, C. L. (1998). Model equations. In Hamilton, M. F. and Blackstock, D. T., editors, *Nonlinear Acoustics*, chapter 3, pages 41–64. Academic Press, San Diego.

Jordan, P. M. (2004). An analytical study of Kuznetsov's equation: diffusive solitions, shock formation, and solution bifurcation. *Phys. Lett. A*, 326:77–84.

Jordan, P. M. (2006). Finite amplitude acoustic travelling waves in a fluid that saturates a porous medium: Acceleration wave formation. *Phys. Lett. A*, 355:216–221.

Kuznetsov, V. P. (1971). Equations of nonlinear acoustics. *Sov. Phys. Acoust.*, 16:467–470.

Landau, L. D. and Lifshitz, E. M. (1987). *Fluid mechanics*. Pergamon, Oxford.

Lax, P. D. (1957). Hyperbolic systems of conservation laws. II. *Comm. Pure Appl. Math.*, 10:537–566.

LeVeque, R. J. (2002). *Finite volume methods for hyperbolic problems*. Cambridge University Press, Cambridge.

Li, D. (2004). Analysis on linear stability of oblique shock waves in steady supersonic flow. *J. Differential Equations*, 207(1):195–225.

Lide, D. R., editor (2007). *CRC Handbook of Chemistry and Physics, Internet Version 2007, (87th Edition), http://www.hbcpnetbase.com*. Taylor and Francis, Boca Raton.

Lighthill, M. J. (1956). Viscosity effects in sound waves of finite amplitude. In *in Surveys in Mechanics*, pages 250–351. University Press.

Makarov, S. and Ochmann, M. (1996a). Nonlinear and thermoviscous phenomena in acoustics, part I. *Acustica*, 82:579–606.

Makarov, S. and Ochmann, M. (1996b). Nonlinear and thermoviscous phenomena in acoustics, part II. *Acustica*, 83:197–222.

Nyborg, W. L. (1998). Acoustic streaming. In Hamilton, M. F. and Blackstock, D. T., editors, *Nonlinear Acoustics*, chapter 7, pages 207–231. Academic Press, San Diego.

Ockendon, H. and Ockendon, J. R. (2004). *Waves and Compressible Flow*. Springer.

Pagano, S., Sørensen, M. P., Christiansen, P. L., and Parmentier, R. D. (1988). Stability of fluxon motion in long josephson junctions at high bias. *Phys. Rev. B*, 38(7):4677–4687.

Rudenko, O. V. and Soluyan, S. I. (1977). *Theoretical foundations of nonlinear acoustics*. Consultants Bureau, New York.

Schecter, S., Marchesin, D., and Plohr, B. J. (1996). Structurally stable Riemann solutions. *J. Differential Equations*, 126(2):303–354.

Smoller, J. (1994). *Shock waves and reaction-diffusion equations*, volume 258 of *Grundlehren der Mathematischen Wissenschaften [Fundamental Principles of Mathematical Sciences]*. Springer-Verlag, New York, second edition.

Söderholm, L. H. (2001). A higher order acoustic equation for the slightly viscous case. *Acustica*, 87:29–33.

Westervelt, P. J. (1963). Parametric acoustic array. *J. Acoust. Soc. Amer.*, 35:535–537.

Yang, X. and Cleveland, R. O. (2005). Time domain simulation of nonlinear acoustic beams generated by rectangular pistons with application to harmonic imaging. *J. Acoust. Soc. Am.*, 117(1):113–123.

Zabolotskaya, E. A. and Khokhlov, R. V. (1969). Quasi-plane waves in the nonlinear acoustics of confined beams. *Sov. Phys. Acoust.*, 15:35–40.

Zakharov, V. E. and Kuznetsov, E. A. (1997). Hamiltonian formalism for nonlinear waves. *Physics-Uspekhi*, 40:1087–1116.

Appendix A

Manuscript posted on arXiv June, 2008

Analytical and numerical modeling of front propagation and interaction of fronts in nonlinear thermoviscous fluids including dissipation

Anders R. Rasmussen* and Mads P. Sørensen
Department of Mathematics, Technical University of Denmark, DK-2800 Kongens Lyngby, Denmark

Yuri B. Gaididei
Bogolyubov Institute for Theoretical Physics, 03680 Kiev, Ukraine

Peter L. Christiansen
Department of Informatics and Mathematical Modelling and Department of Physics,
Technical University of Denmark, DK-2800 Kongens Lyngby, Denmark
(Dated: June 3, 2008)

A wave equation, that governs finite amplitude acoustic disturbances in a thermoviscous Newtonian fluid, and includes nonlinear terms up to second order, is proposed. In contrast to the model known as the Kuznetsov equation, the proposed nonlinear wave equation preserves the Hamiltonian structure of the fundamental fluid dynamical equations in the non-dissipative limit. An exact traveling front solution is obtained from a generalized traveling wave assumption. This solution is, in an overall sense, equivalent to the Taylor shock solution of the Burgers equation. However, in contrast to the Burgers equation, the model equation considered here is capable to describe waves propagating in opposite directions. Owing to the Hamiltonian structure of the proposed model equation, the front solution is in agreement with the classical Rankine-Hugoniot relations. The exact front solution propagates at supersonic speed with respect to the fluid ahead of it, and subsonic speed with respect to the fluid behind it, similarly to the fluid dynamical shock. Linear stability analysis reveals that the front is stable when the acoustic pressure belongs to a critical interval, and is otherwise unstable. These results are verified numerically. Studies of head-on colliding fronts demonstrate that the front propagation speed changes upon collision.

I. INTRODUCTION

The "classical" equation of nonlinear acoustics [1], the so-called Kuznetsov equation [2], governs finite amplitude acoustic disturbances in a Newtonian, homogeneous, viscous, and heat conducting fluid. The model equation and its paraxial approximation, the Khokhlov-Zabolotskaya-Kuznetsov (KZK) equation [2, 3], are occasionally encountered within studies related to nonlinear wave propagation. See e.g. the recent works by Jordan [4] who presented the derivation and analysis of an exact traveling wave solution to the one-dimensional Kuznetsov equation, and by Jing and Cleveland [5] who described a three-dimensional numerical code that solves a generalization of the KZK equation, and the references cited in the introductory sections of those papers. Other recent works based on the Kuznetsov equation include: analysis of energy effects accompanying a strong sound disturbance [6], studies of generation of higher harmonics and dissipation based on a 3D finite element formulation [7], and studies of nonlinear wave motion in cylindrical coordinates [8]. The derivations of the Kuznetsov equation [2, 9, 10] and related model equations [11, 12, 13]

are based on the complete system of the equations of fluid dynamics. It has been demonstrated that this system of equations is of Hamiltonian structure in the non-dissipative limit [14]. However, in the non-dissipative limit, the Kuznetsov equation does not retain the Hamiltonian structure.

In this paper we propose a nonlinear wave equation, which, in the non-dissipative limit, preserves the Hamiltonian structure of the fundamental equations. Furthermore, we present the derivation and analysis of an exact traveling front solution, which applies equally well to the proposed nonlinear wave equation and the Kuznetsov equation. The derivation of the exact solution is based on a *generalized* traveling wave assumption, which leads to a wider class of exact solutions compared to the one reported by Jordan [4, 15]. Furthermore, the introduction of the generalized assumption is necessary in order to interpret the results of numerical simulations of head-on colliding fronts presented in this paper. In order to relate our results to the classical literature, we demonstrate that the exact front solution retains a number of properties of the fluid dynamical shock. The paper is structured as follows: The proposed equation and its Hamiltonian structure are discussed in Section II. Section III contains the derivation of our exact traveling front solution and analysis of its stability properties. In Section IV we demonstrate that the front is related the classical shock. Section V presents numerical investigations of the front,

while Section VI contains our conclusions.

II. NONLINEAR WAVE EQUATIONS

Equations governing finite amplitude acoustic disturbances in a Newtonian, homogeneous, viscous and heat conducting fluid may be derived from the following four equations of fluid dynamics: *the equation of motion*

$$\rho\left(\frac{\partial \mathbf{u}}{\partial t} + (\mathbf{u}\cdot\boldsymbol{\nabla})\mathbf{u}\right) = -\boldsymbol{\nabla}p + \eta\Delta\mathbf{u} + \left(\frac{\eta}{3}+\zeta\right)\boldsymbol{\nabla}(\boldsymbol{\nabla}\cdot\mathbf{u}), \quad (1)$$

the equation of continuity

$$\frac{\partial \rho}{\partial t} + \boldsymbol{\nabla}\cdot(\rho\mathbf{u}) = 0, \quad (2)$$

the heat transfer equation

$$\rho T\left(\frac{\partial s}{\partial t} + (\mathbf{u}\cdot\boldsymbol{\nabla})s\right) = \frac{\eta}{2}\left(\frac{\partial u_i}{\partial x_j} + \frac{\partial u_j}{\partial x_i} - \frac{2}{3}\delta_{ij}\frac{\partial u_k}{\partial x_k}\right)^2 + \zeta(\boldsymbol{\nabla}\cdot\mathbf{u})^2 + \kappa\Delta T, \quad (3)$$

and *the equation of state*

$$p = p(\rho, s). \quad (4)$$

Here $\mathbf{x} = (x,y,z)$ are the spatial (Cartesian) coordinates and t denotes time. $\mathbf{u} = (u,q,w)$ is the fluid particle velocity, ρ is the density of the medium, p, s, and T are the thermodynamic variables pressure, entropy and temperature, respectively. η and ζ are the coefficients of shear and bulk viscosity, and κ is the heat conductivity coefficient. Δ is the Laplace operator.

To obtain a nonlinear wave equation all dependent variables except one are eliminated from the system (1)–(4), resulting in a nonlinear wave equation for that single variable [2, 9, 10, 11, 12, 13]. The deviations of ρ, p, s, and T from their equilibrium values, ρ_0, p_0, s_0, and T_0 are assumed to be small, as well as the fluid particle velocity, $|\mathbf{u}|$. The heat conductivity coefficient κ and the viscosities η and ζ are also treated as small quantities. In order to obtain a second order approximation, all equations are written retaining terms up to second order in the small quantities. It is assumed that the flow is rotation free, $\boldsymbol{\nabla}\times\mathbf{u} = 0$, thus

$$\mathbf{u} \equiv -\boldsymbol{\nabla}\psi, \quad (5)$$

where ψ is the velocity potential. Furthermore, it has become customary to use the following approximation for the equation of state [16]

$$p - p_0 = c_0^2(\rho-\rho_0) + \frac{c_0^2}{\rho_0}\frac{B/A}{2}(\rho-\rho_0)^2 + \left(\frac{\partial p}{\partial s}\right)_{\rho,s=s_0}(s-s_0), \quad (6)$$

TABLE I: Values of c_0, B/A, and b for three different substances. The values for b are rough estimates obtained from Eq. (8) neglecting the influence of bulk viscosity and thermal losses.

Substance	c_0 (m s^{-1})	B/A	b (m^2 s^{-1})
Water	1483 (20℃)[a]	5.0 (20℃)[b]	1.3×10^{-6} (20℃)[c]
Air	343 (20℃)[a]	0.4 (20℃)[b,d]	21×10^{-6} (27℃)[c]
Soft tissue	1540[e]	9.6 (37℃)[b,f]	N/A

[a] Ref. 19
[b] Ref. 17
[c] Values for ρ_0 and η are obtained from Ref. 19.
[d] Diatomic gas
[e] Ref. 20
[f] Human breast fat

where B/A is the fluid nonlinearity parameter [17] and $c_0^2 \equiv (\partial p/\partial\rho)_{s,\rho=\rho_0}$ is the small-signal sound speed. Then, from Eqs. (1)–(6) we obtain the following nonlinear wave equation

$$\frac{\partial^2\psi}{\partial t^2} - c_0^2\Delta\psi = \frac{\partial\psi}{\partial t}\Delta\psi + \frac{\partial}{\partial t}\left(b\Delta\psi + (\boldsymbol{\nabla}\psi)^2 + \frac{B/A-1}{2c_0^2}\left(\frac{\partial\psi}{\partial t}\right)^2\right), \quad (7)$$

where b is the diffusivity of sound [18]

$$b \equiv \frac{1}{\rho_0}\left\{\frac{4}{3}\eta + \zeta + \kappa\left(\frac{1}{C_V}-\frac{1}{C_p}\right)\right\}, \quad (8)$$

and C_V and C_p denote the heat capacities at constant volume and pressure, respectively. Typical values of the physical parameters c_0, B/A, and b are given in Table I. In the first order approximation, Eq. (7) reduces to

$$\frac{\partial^2\psi}{\partial t^2} = c_0^2\Delta\psi. \quad (9)$$

Introducing Eq. (9) in the first term on the right hand side of Eq. (7), the Kuznetsov equation [2]

$$\frac{\partial^2\psi}{\partial t^2} - c_0^2\Delta\psi = \frac{\partial}{\partial t}\left(b\Delta\psi + (\boldsymbol{\nabla}\psi)^2 + \frac{B/A}{2c_0^2}\left(\frac{\partial\psi}{\partial t}\right)^2\right), \quad (10)$$

is obtained.

In absence of dissipation, i.e. $\eta = \zeta = 0$, Eqs. (1) and (2) possess Hamiltonian structure [14]. This property is, however, *not* retained in Eq. (10) with $b=0$, i.e. the non-dissipative limit of the Kuznetsov equation is not Hamiltonian. In contrast, Eq. (7) *does* retain the Hamiltonian structure in the non-dissipative limit. Accordingly, the equation may be derived from the Lagrangian density

$$\mathcal{L} = \frac{(\psi_t)^2}{2} - c_0^2\frac{(\boldsymbol{\nabla}\psi)^2}{2} - \frac{B/A-1}{6c_0^2}(\psi_t)^3 - \frac{\psi_t(\boldsymbol{\nabla}\psi)^2}{2}, \quad (11)$$

using the Euler-Lagrange equation[1]. From the Legendre transformation [22] we obtain the corresponding Hamiltonian density as

$$\mathcal{H} = c_0^2 \frac{(\boldsymbol{\nabla}\psi)^2}{2} + \frac{(\psi_t)^2}{2} - \frac{B/A - 1}{3c_0^2} (\psi_t)^3, \qquad (12)$$

which may be integrated to yield the total Hamiltonian

$$H = \int_{-\infty}^{+\infty} \int_{-\infty}^{+\infty} \int_{-\infty}^{+\infty} \mathcal{H} \, dx \, dy \, dz. \qquad (13)$$

Taking the time derivative of H in Eq. (13) with $\mathcal{H}$ replaced by Eq. (12), and using Eq. (7), one can obtain a simple expression for dH/dt. Doing this in one spatial dimension we obtain after some calculations

$$\frac{dH}{dt} = \left[c_0^2 \psi_t \psi_x + (\psi_t)^2 \psi_x \right]_{-\infty}^{+\infty} - b \int_{-\infty}^{+\infty} (\psi_{xt})^2 \, dx. \qquad (14)$$

In Eq. (14), which is sometimes called the energy balance equation, we observe that the first terms on the right hand side correspond to energy in- and output at the two boundaries, and that the last term accounts for energy dissipation inside the system.

In the remaining portion of this paper we shall limit the analysis to one-dimensional plane fields, in which case the proposed model equation (7) reduces to

$$\psi_{tt} - c_0^2 \psi_{xx} = \psi_t \psi_{xx}$$
$$+ \frac{\partial}{\partial t} \left(b\psi_{xx} + (\psi_x)^2 + \frac{B/A - 1}{2c_0^2} (\psi_t)^2 \right), \quad (15)$$

where subscripts indicate partial differentiation.

Finally, for later reference we give the second-order expressions for the acoustic density, $\rho - \rho_0$, and acoustic pressure, $p - p_0$, in terms of the velocity potential, ψ. From the equations of motion (1) and state (6), subject to the basic assumptions of the derivation of the two model equations (7) and (10), we obtain

$$\rho - \rho_0 = \frac{\rho_0}{c_0^2} \left(\psi_t - \frac{(\psi_x)^2}{2} - \frac{B/A - 1}{2c_0^2} (\psi_t)^2 - b\psi_{xx} \right), \qquad (16)$$

---

[1] Letting $\eta = \zeta = 0$, $\mathbf{u} = -\boldsymbol{\nabla}\psi$, and $p = \rho^\gamma/\gamma$ in Eqs. (1–2), and (4), respectively, one can derive the Lagrangian density

$$\mathcal{L}_{PEE} = \frac{c_0^4}{\gamma} \left(1 + \frac{\gamma - 1}{c_0^2} \left(\psi_t - \frac{(\boldsymbol{\nabla}\psi)^2}{2} \right) \right)^{\frac{\gamma}{\gamma - 1}},$$

corresponding to the potential Euler equation (PEE) given in Ref. 21. Expanding $\mathcal{L}_{PEE}$ to third order and letting $\gamma = B/A + 1$ we obtain Eq. (11).

and

$$p - p_0 = \rho_0 \left(\psi_t - \frac{(\psi_x)^2}{2} + \frac{1}{2c_0^2} (\psi_t)^2 \right) - \left(\frac{4}{3}\eta + \zeta \right) \psi_{xx}, \qquad (17)$$

respectively. It should be noted that Eqs. (16) and (17) are derived from the fundamental equations, thus, the expressions are not specific to any of the two model equations (7) and (10).

III. EXACT TRAVELING FRONT SOLUTION

Recently, a standard traveling wave approach was applied to the one-dimensional approximation of the Kuznetsov equation (10) to reveal an exact traveling wave solution [4, 15]. In this section we extend the standard approach by introducing a generalized traveling wave assumption and analyze the stability properties of the solution.

A. Generalized traveling wave analysis

We introduce the following generalized traveling wave assumption

$$\psi(x,t) = \Psi(x - vt) - \lambda x + \sigma t$$
$$\equiv \Psi(\xi) - \lambda x + \sigma t, \qquad (18)$$

where λ and σ are arbitrary constants, v denotes the wave propagation velocity, and $\xi \equiv x - vt$ is a wave variable. The inclusion of $-\lambda x + \sigma t$ in Eq. (18) leads to a wider class of exact solutions, compared to the one obtained from the assumption $\psi = \Psi(x - vt)$, which is the standard one. Furthermore, the introduction of the generalized assumption is necessary in order to interpret the results of numerical simulations of head-on colliding fronts presented in Section V B. Inserting Eq. (18) into the nonlinear wave equation (15) we obtain the ordinary differential equation

$$\left(v^2 - c_0^2 \right) \Psi'' = \left(-v\Psi' + \sigma \right) \Psi'' - v \frac{d}{d\xi} \left\{ b\Psi'' \right.$$
$$\left. + (\Psi' - \lambda)^2 + \frac{B/A - 1}{2c_0^2} (-v\Psi' + \sigma)^2 \right\}, \quad (19)$$

where prime denotes ordinary differentiation with respect to ξ. Integrating once and introducing $\Phi \equiv -\Psi'$, Eq. (19) reduces to

$$C = vb\Phi' - \left(\frac{3}{2} + \frac{B/A - 1}{2c_0^2} v^2 \right) v\Phi^2 +$$
$$\left\{ \left(1 - \frac{B/A - 1}{c_0^2} \sigma \right) v^2 - 2\lambda v - c_0^2 - \sigma \right\} \Phi, \quad (20)$$

where C is a constant of integration. Requiring that the solution satisfy $\Phi' \to 0$ as $\xi \to \pm\infty$, and either

$$\Phi \to \begin{cases} \theta, & \xi \to +\infty \\ 0, & \xi \to -\infty \end{cases} \quad \text{or} \quad \Phi \to \begin{cases} 0, & \xi \to +\infty \\ \theta, & \xi \to -\infty \end{cases}, \quad (21)$$

where θ is an arbitrary constant, lead us to $C = 0$ and

$$\frac{B/A - 1}{2c_0^2}\theta v^3 - \left(1 - \frac{B/A - 1}{c_0^2}\sigma\right)v^2 + \left(\frac{3}{2}\theta + 2\lambda\right)v + c_0^2 + \sigma = 0. \quad (22)$$

In order to obtain our traveling wave solution, we separate the variables in Eq. (20) subject to $C = 0$, then, using Eq. (22), we find the solution to be the traveling front

$$\Phi = \frac{\theta}{2}\left\{1 - \tanh\left(\frac{2(\xi - x_0)}{l}\right)\right\}, \quad (23)$$

$$l \equiv \frac{4b}{\left(\frac{B/A - 1}{2c_0^2}v^2 + \frac{3}{2}\right)\theta}, \quad (24)$$

where x_0 is an integration constant, $|l|$ is the front thickness, and $0 < \Phi < \theta$. Finally, using $\Phi = -\Psi'$ and inserting Eq. (23) into Eq. (18) we obtain (apart from an arbitrary constant of integration)

$$\psi(x,t) = -\frac{\theta}{2}\left\{\xi - \frac{l}{2}\ln\left(\cosh\frac{2(\xi - x_0)}{l}\right)\right\} - \lambda x + \sigma t, \quad (25)$$

which is the exact solution for the velocity potential.

Traveling tanh solutions, such as the front solution (23), are often called Taylor shocks. The existence of an exact solution of this type to the classical Burgers equation is a well known result [23]. However, the Burgers equation is restricted to wave propagation *either* to the left or to the right. The model equation considered in this paper does not suffer from this limitation, as shall be illustrated in Section V B.

Regarding the exact solution derived above, the physical properties of the flow associated with the traveling front are obtained from the partial derivatives of Eq. (25), which are given by

$$-\psi_x = \Phi + \lambda \quad \text{and} \quad \psi_t = v\Phi + \sigma. \quad (26)$$

According to Eq. (5) the fluid particle velocity is obtained as $u = -\psi_x$, and the first order approximation of Eq. (17) yields the acoustic pressure as $p - p_0 \approx \rho_0\psi_t$. The boundary conditions of the front are obtained from Eqs. (23) and (26) as

$$-\psi_x \to \begin{cases} \theta + \lambda, & \xi \to \mp\infty \\ \lambda, & \xi \to \pm\infty \end{cases}, \quad (27a)$$

$$\psi_t \to \begin{cases} v\theta + \sigma, & \xi \to \mp\infty \\ \sigma, & \xi \to \pm\infty \end{cases}, \quad (27b)$$

where upper (lower) signs apply for $l > 0$ ($l < 0$). Hence, the four parameters v, θ, λ, and σ, that was introduced in the derivation of the exact solution, determine the four boundary conditions of the front. From these boundary conditions we find that θ and $v\theta$ correspond to the heights of the jump across the front measured in $-\psi_x$ and ψ_t, respectively, see Fig. 1. At this point it is appropriate to emphasize that, in order for the exact solution to exist, the four parameters v, θ, λ, and σ must satisfy the cubic equation (22). Furthermore, the allowable values of the wave propagation velocity correspond to the *real* roots of this equation. A noticeably property of Eq. (22), which will prove useful later on, is that the equation is invariant under the transformation

$$v \to v, \quad \theta \to -\theta, \quad \lambda \to \theta + \lambda, \quad \sigma \to v\theta + \sigma. \quad (28)$$

Also the boundary conditions (27) are invariant, since, according to Eq. (24), the above transformation leads to $l \to -l$.
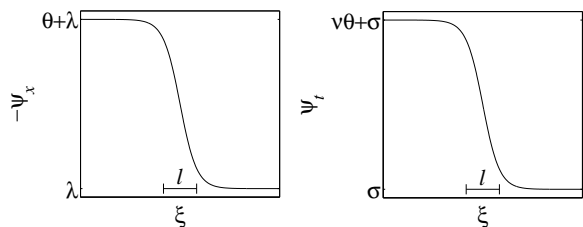

FIG. 1: The exact solution of Eq. (15) represents a traveling front. In order for the solution to exist, the wave propagation velocity, v, the front height, θ, and the two constants, λ and σ, must satisfy Eq. (22). The plot shows a front with $l > 0$.

In order to investigate the relationship between the front height, θ, and the front propagation velocity, v, we solve Eq. (22) with respect to θ to obtain

$$\theta = \frac{\left(1 - \frac{B/A - 1}{c_0^2}\sigma\right)v^2 - 2\lambda v - c_0^2 - \sigma}{v\left(\frac{3}{2} + \frac{B/A - 1}{2c_0^2}v^2\right)}. \quad (29)$$

For $B/A < 1$ the curve $\theta(v)$ has singularities at

$$v = v_s \equiv \pm\left(\frac{3c_0^2}{1 - B/A}\right)^{1/2}, \quad (30)$$

and for $B/A > 1$ the curve has a maximum[2] at $(v, \theta) = (v_{max}, \theta_{max})$, where v_{max} is obtained as

$$v_{max} = c_0\left(\frac{3B/A + \sqrt{9(B/A)^2 + 12(B/A - 1)}}{2(B/A - 1)}\right)^{1/2}, \quad (31)$$

———

[2] The critical point $(v, \theta) = (v_{max}, \theta_{max})$ was identified by Jordan [4] as the solution bifurcation point.

when $\lambda = 0$ and $\sigma = 0$. These two characteristic properties of the curve are illustrated in Fig. 2.
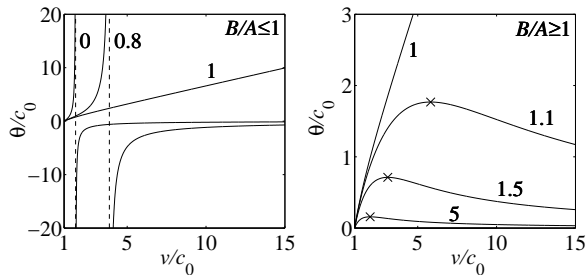

FIG. 2: The plots show the relationship between the front height, θ, and the front propagation velocity, v, given by Eq. (29) with $\lambda = 0$, $\sigma = 0$, and $B/A = \{0, 0.8, 1, 1.1, 1.5, 5\}$ (see labels on the plots). The dashed lines indicate the singularity at $v = v_s$, which is defined in Eq. (30), and crosses indicate the maximum $(\theta, v) = (\theta_{max}, v_{max})$ defined in Eq. (31).

Finally, it should be emphasized that the generalized traveling wave analysis conducted above also applies to the one-dimensional approximation of the Kuznetsov equation (10). In this case Eq. (22) is replaced by[3]

$$\frac{B/A}{2c_0^2}\theta v^3 - \left(1 - \frac{B/A}{c_0^2}\sigma\right)v^2 + (\theta + 2\lambda)\,v + c_0^2 = 0, \quad (32)$$

and Eq. (24) by

$$l = \frac{4b}{\left(\dfrac{B/A}{2c_0^2}v^2 + 1\right)\theta}. \quad (33)$$

Apart from these changes, a generalized traveling wave analysis of the Kuznetsov equation is basically identical to that of Eq. (15).

The Hamiltonian structure, however, is unique to the proposed nonlinear wave equation (7) and its one-dimensional approximation Eq. (15). In order to establish a relationship between the exact solution, derived in this section, and the Hamiltonian structure of the governing equation, we insert Eq. (25) into Eq. (14) and the one-dimensional approximations of Eqs. (12) and (13). Then, after some calculations, we find that Eq. (14) reduces to the cubic equation (22). Hence, the exact traveling front solution of the proposed Hamiltonian model equation (15) satisfies the energy balance equation (14).

B. Linear stability analysis

In order to gain insight into the stability properties of the traveling front solution we initially consider the

_____

[3] Eliminating λ and σ from Eq. (32) makes the equation equivalent to the previously reported result [4]

constant solution

$$-\psi_x = K \qquad \text{and} \qquad \psi_t = L, \quad (34)$$

which satisfies the nonlinear wave equation (15). The two constants K and L are arbitrary. In order to investigate the linear stability properties of this solution, we add small perturbation terms to the constant values as

$$-\psi_x = K - \varepsilon\chi_x \qquad \text{and} \qquad \psi_t = L + \varepsilon\chi_t, \quad (35)$$

where $\chi = \chi(x,t)$ and $\varepsilon \ll 1$. Then, inserting Eqs. (35) into Eq. (15) and keeping terms up to first order in ε we obtain the following linear perturbation equation

$$\left(1 - \frac{B/A - 1}{c_0^2}L\right)\chi_{tt} - \left(c_0^2 + L\right)\chi_{xx} = b\chi_{xxt} - 2K\chi_{xt}. \quad (36)$$

Inserting the single Fourier mode

$$\chi(x,t) = D\,e^{i(kx - \omega t)}, \quad (37)$$

where D is the amplitude, k is the wave number, and ω is the angular frequency, into Eq. (36), we obtain the following dispersion relation

$$\left(\frac{B/A - 1}{c_0^2}L - 1\right)\omega^2 + \left(2Kk - ibk^2\right)\omega + \left(c_0^2 + L\right)k^2 = 0. \quad (38)$$

The constant solution (34) is asymptotically stable only if all solutions of Eq. (36) approach zero as $t \to \infty$. This is the case when the imaginary part of both roots in Eq. (38), ω_1 and ω_2, are negative. It can be shown that for $B/A > 1$ the only requirement in order for the imaginary part of both roots to be negative is

$$-c_0^2 < L < \frac{c_0^2}{B/A - 1}. \quad (39)$$

When $B/A < 1$ the only requirement for both roots to have a negative imaginary part is

$$-c_0^2 < L < \infty. \quad (40)$$

Hence, the stability properties of the constant solution (34) are determined exclusively by L, i.e. the constant value of ψ_t. Recall that the acoustic pressure is proportional to ψ_t, thus, the level of the acoustic pressure determines the stability properties of the solution.

In order for the front solution to be stable, it is a necessary condition that both left and right asymptotic values of ψ_t, given by Eq. (27b), belong to the interval (39) when $B/A > 1$, and the interval (40) when $B/A < 1$. In Section V A we shall further investigate this stability criterion by means of numerical simulations.

IV. FRONT-SHOCK RELATIONSHIP

Within fluid dynamics, a shock denotes a sharp change of the physical quantities. A shock propagates at supersonic speed with respect to the fluid ahead of it, while it remains subsonic with respect to the fluid behind it. The physical quantities of the flow on each side of the shock are connected by the Rankine-Hugoniot relations, which are conservation equations for mass, momentum and energy. In the following we shall demonstrate that the front solution of the proposed Hamiltonian model equation (15) retains these properties.

A. The Rankine-Hugoniot relations

Using square brackets to denote the change in value of any quantity across a shock, e.g.

$$[\rho] = \rho_{\mathrm{a}} - \rho_{\mathrm{b}}, \tag{41}$$

where b denotes the value behind the shock and a denotes the value ahead of it, the Rankine-Hugoniot relations may be written as [24]

$$\mathrm{mass}: \quad [\rho(u-v)] = 0, \tag{42}$$

$$\mathrm{momentum}: \quad \left[p + \rho(u-v)^2\right] = 0, \tag{43}$$

$$\mathrm{energy}: \quad \left[h + (u-v)^2/2\right] = 0, \tag{44}$$

where v is the shock propagation velocity and h is the enthalpy.

We now replace u, ρ, p, and h with expressions in terms of ψ_x and ψ_t, and write all equations retaining terms up to second order. Upon setting $u = -\psi_x$ and substituting Eqs. (16) and (17) into Eqs. (42) and (43) we thus obtain

$$\left[\left(\frac{(\psi_x)^2}{2} + \frac{B/A-1}{2c_0^2}(\psi_t)^2\right)v \right. \\ \left. - \psi_t(\psi_x + v) - c_0^2\psi_x\right] = 0, \quad (45)$$

and

$$\left[\frac{B/A-1}{2c_0^2}(\psi_t)^2 v^2 - \psi_t v^2 - 2\psi_t\psi_x v \right. \\ \left. - \frac{(\psi_t)^2}{2} - 2c_0^2\psi_x v - c_0^2\psi_t\right] = 0, \quad (46)$$

respectively. The dissipative terms involving κ, ζ, and η do not appear in Eqs. (45) and (46), since $\psi_{xx} \to 0$ ahead of and behind the front. The changes in ψ_x and ψ_t across the front are obtained from the boundary conditions (27). Assuming that $l > 0$ and $v > 0$, and using the notation introduced in Eq. (41) we may write

$$[\psi_x] = \theta, \qquad [\psi_t] = -v\theta. \tag{47a}$$

Furthermore, changes in products of ψ_x and ψ_t are

$$\left[(\psi_x)^2\right] = -\theta^2 - 2\theta\lambda, \tag{47b}$$

$$\left[(\psi_t)^2\right] = -v^2\theta^2 - 2v\theta\sigma, \tag{47c}$$

$$\left[\psi_x\psi_t\right] = v\theta^2 + v\theta\lambda + \theta\sigma. \tag{47d}$$

Inserting Eqs. (47) into Eqs. (45) and (46) both conservation equations reduce to the cubic equation (22). This striking result leads to the conclusion, that Eq. (22) implies conservation of mass and momentum. At this point it should be noted that the generalized traveling wave analysis of the Kuznetsov equation (10) leads to the cubic equation (32), which is not in agreement with the conservation equations for mass and momentum.

In order to handle the enthalpy in the condition for energy conservation (44) we shall make use of the following fundamental thermodynamic relationship [24]

$$\boldsymbol{\nabla}h = \frac{\boldsymbol{\nabla}p}{\rho}. \tag{48}$$

Using the equation of motion (1), subject to the basic assumptions of the derivation of the model equations in Section II, we obtain from Eq. (44)

$$[\psi_t + v\psi_x] = 0. \tag{49}$$

Alternatively, Eq. (49) follows directly from the generalized traveling wave assumption (18). Hence, the traveling wave assumption implies energy conservation in the flow.

B. Sub-/supersonic speeds of propagation

In order to determine whether the traveling front solution, derived in Section III A, propagates at sub- or supersonic speed with respect to the fluid ahead of it and the fluid behind it, we need to introduce the speed of sound in these regions of the fluid. Without loss of generality, we may consider only fronts propagating in the positive direction, $v > 0$, since Eq. (15) is invariant under the transformation $x \to -x$. Furthermore, we shall limit the analysis to stable fronts, i.e. ψ_t must belong to the interval (39) when $B/A > 1$, and the interval (40) when $B/A < 1$. Then, letting $\theta \to 0$ in Eq. (22) and solving for v yields the small signal propagation velocity, which is equivalent to the speed of sound, c. Introducing $\lambda = K$ and $\sigma = L$ we obtain

$$v = c(K, L) \equiv \frac{K + \sqrt{K^2 + \left(L + c_0^2\right)\left(1 - \dfrac{B/A-1}{c_0^2}L\right)}}{1 - \dfrac{B/A-1}{c_0^2}L}, \tag{50}$$

where K and L denote the constant levels of $-\psi_x$ and ψ_t, respectively, at which the speed of sound (50) is evaluated. Inserting the boundary conditions of the front into

Eq. (50), i.e. substituting Eq. (27a) for K and Eq. (27b) for L, we obtain the speed of sound ahead of, c_a, and behind, c_b, the front

$$c_{\substack{a\\b}} = c(\lambda, \sigma), \tag{51}$$

$$c_{\substack{b\\a}} = c(\theta + \lambda, v\theta + \sigma), \tag{52}$$

where upper (lower) subscripts apply for $l > 0$ ($l < 0$). Note that, under the transformation (28), Eq. (52) transforms into Eq. (51). Hence, without loss of generality we shall consider only Eq. (51) in the following.

In order to compare the front propagation velocity, v, to c_a and c_b we make the following observations. Inserting Eq. (29) into Eq. (24) yields

$$l = \frac{4bv}{\left(1 - \dfrac{B/A - 1}{c_0^2}\sigma\right)v^2 - 2\lambda v - c_0^2 - \sigma}. \tag{53}$$

The denominator in Eq. (53) becomes zero when $v = c(\lambda, \sigma)$, where $c(\lambda, \sigma)$ is given by Eq. (50). Then, given that $v > 0$, we obtain from Eq. (53) that

$$v > c(\lambda, \sigma) \Leftrightarrow l > 0 \quad \text{and} \quad v < c(\lambda, \sigma) \Leftrightarrow l < 0. \tag{54}$$

Finally, from Eqs. (51) and (54) it follows that

$$v > c_a \quad \text{and} \quad v < c_b. \tag{55}$$

Hence, in all cases, the propagation velocity of the exact traveling front solution is supersonic with respect to the fluid ahead of the front, and subsonic with respect to the fluid behind it.

V. NUMERICAL RESULTS

All numerical calculations rely on a commercially available software package[4], which is based on the finite element method. For convenience we introduce the following non-dimensional variables, denoted by tilde

$$\tilde{\psi}(\tilde{x}, \tilde{t}) = \frac{1}{b}\psi(x, t), \qquad \tilde{x} = \frac{c_0}{b}x, \qquad \tilde{t} = \frac{c_0^2}{b}t. \tag{56}$$

Under this transformation we may write Eq. (15) as

$$\psi_{tt} - \psi_{xx} = \psi_t\psi_{xx} + \frac{\partial}{\partial t}\left(\psi_{xx} + (\psi_x)^2 + \frac{B/A - 1}{2}(\psi_t)^2\right), \tag{57}$$

where the tildes have been omitted. From a comparison of Eqs. (15) and (57), we find that the results of the previous sections subject to $b = 1$ and $c_0 = 1$ apply to

---

[4] COMSOL version 3.2a, http://www.comsol.com (2005)

Eq. (57). Non-dimensional versions of the parameters, v, θ, λ, and σ, also indicated by tilde, become

$$\tilde{\lambda} = \frac{\lambda}{c_0}, \qquad \tilde{\sigma} = \frac{\sigma}{c_0^2}, \qquad \tilde{\theta} = \frac{\theta}{c_0}, \qquad \tilde{v} = \frac{v}{c_0}. \tag{58}$$

In the following analysis we consider only the non-dimensional formulation of the problem. For notational simplicity we shall omit the tildes.

A. Investigation of the front stability criterion

In order to investigate, numerically, the stability properties of the front, we chose as initial condition for the numerical solution, the exact solution given by Eqs. (25) and (26), and choose v, θ, λ, σ, and B/A such that Eq. (22) is satisfied. For the sake of clarity, we shall limit the numerical investigations to the specific case of $\lambda = 0$, $\sigma = 0$, $v > 0$, and $l > 0$, which, according to Eq. (27), corresponds to fronts propagating to the right into an unperturbed fluid.

A first numerical simulation is presented in Fig. 3. Evidently, the numerical algorithm successfully integrates the initial condition forward in time. This finding indicates that, for the specific choice of parameters, $v = 1.4$, $\theta = 0.127$, and $B/A = 5$, the front exists and is stable. A second numerical simulation is presented in Fig. 4. This initial condition is given a larger velocity, $v = 1.7$, and a larger height, $\theta = 0.153$, while $B/A = 5$ remains unchanged compared to the first example. The parameters are chosen such that Eq. (22) remains satisfied. Apparently, the numerical algorithm fails when integrating the solution forward in time, which indicates that the front is unstable for the specific choice of parameters. Given that $\sigma = 0$ and $l > 0$, the left and right asymptotes of the front are given by $\psi_t = v\theta$ and $\psi_t = 0$, respectively, according to Eq. (27b). Clearly, the right value belongs to the interval (39), thus, it does not causes instability of the front. However, if the left value, $v\theta$, lies outside the interval (39), it causes instability of the front. Inserting the value of B/A from the two examples above into Eq. (39), we find that in the first and second example, $v\theta$ lies inside and outside the interval (39), respectively. Hence, the behavior observed in Figs. 3 and 4 agrees with the stability criterion introduced in Section III B.

A large number of numerical simulations have been performed in order to systematically investigate the stability properties of the front. Within each simulation the parameters in the initial condition are, again, chosen such that Eq. (22) is satisfied. The result of this investigation is presented in Fig. 5. Still, $\sigma = 0$ and $l > 0$, such that the left asymptotic value of the front is given by $\psi_t = v\theta$. For $B/A > 1$ the stability threshold curve in the $(B/A, v)$-plane is obtained when $v\theta$ equals the upper bound of the interval (39). Using Eq. (29) we obtain

$$v\theta = \frac{1}{B/A - 1} \Rightarrow v = \frac{\sqrt{(B/A - 1)(2\,B/A + 1)}}{B/A - 1}. \tag{59}$$

For $B/A < 1$, the stability threshold curve is given by Eq. (30), since $v\theta$ lies within (outside) the interval (40) when $v < v_s$ ($v > v_s$), according to Eq. (29). The two stability threshold curves are included in Fig. 5. The fine agreement between the numerical results and the stability threshold curves indicates that the stability criterion, introduced in Section III B, is both necessary *and* sufficient in order for the front solution to be stable.
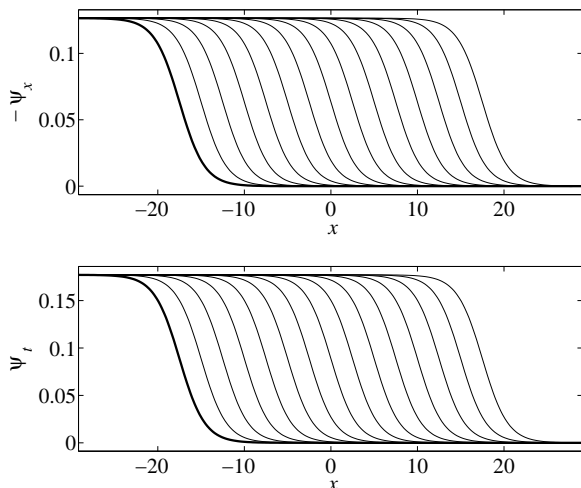

FIG. 3: The initial condition at $t = 0$ (bold line) is obtained from Eqs. (25) and (26) subject to $v = 1.4$, $\theta = 0.127$, $\lambda = 0$, $\sigma = 0$, and $B/A = 5$, which satisfy Eq. (22). The numerical solutions are shown over the time interval $0 \leq t \leq 25$.
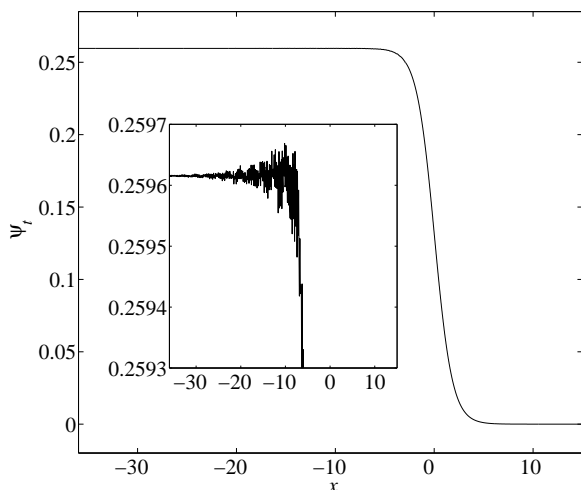

FIG. 4: The numerical algorithm fails to integrate this solution forward in time (insert shows magnification). See caption of Fig. 3. $v = 1.7$, $\theta = 0.153$, $\lambda = 0$, $\sigma = 0$, and $B/A = 5$. The numerical solution is shown at time $t = 3.8 \times 10^{-3}$.
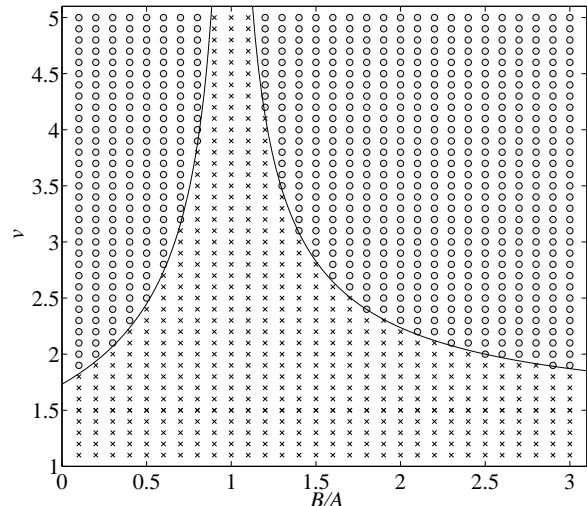

FIG. 5: Each point in the $(B/A, v)$-plane represents a numerical simulation, with the initial condition obtained from Eqs. (25) and (26) subject to $\lambda = 0$, $\sigma = 0$, and θ given by Eq. (29). Crosses and circles indicate stable and unstable solutions, respectively (compare with Figs. 3 and 4). Solid lines represent the stability threshold curves given by Eqs. (30) and (59).

B. Head-on colliding fronts

The numerical simulation presented in Fig. 6 shows the result of a head-on collision between two fronts. From the simulation we observe that two new fronts emerge upon the collision. The contour plot reveals that these fronts travel at a higher speed, compared to the speed of the fronts before the collision. For other choices of initial condition, we found the outcome of the head-on collision to be fronts traveling at lower speed, compared to that of the fronts before the collision.

In order to analyze solutions of Eq. (15) that comprise two fronts, we assume that these fronts belong to the class of exact front solutions derived in Section III A above. Investigations of the fronts that emerge upon a head-on collision have made it clear that this assumption is true, only when the generalized traveling wave assumption is considered, in contrast to the standard traveling wave assumption. Then, for each of the two fronts in the solution we introduce four new parameters, v, θ, λ, and σ, which must satisfy Eq. (22) as

$$\frac{B/A - 1}{2}\theta_i v_i^3 - (1 - (B/A - 1)\sigma_i)\, v_i^2$$
$$+ \left(\frac{3}{2}\theta_i + 2\lambda_i\right) v_i + \sigma_i + 1 = 0, \qquad i = 1, 2, \quad (60)$$

where subscript 1 and 2 denote parameters associated with waves positioned to the left and right, respectively. Furthermore, we require that solutions comprising two fronts are continuous and satisfy the following set of ar-

bitrary boundary conditions

$$-\psi_x \to \begin{cases} P, & x \to -\infty \\ Q, & x \to +\infty \end{cases}, \quad \psi_t \to \begin{cases} R, & x \to -\infty \\ S, & x \to +\infty \end{cases}.$$
(61)

Assuming that $l_1 > 0$ and $l_2 < 0$, we find, using Eq. (27), that the these requirements lead to the following conditions

$$\lambda_1 = \lambda_2 = P - \theta_1 = Q - \theta_2, \quad (62a)$$

$$\sigma_1 = \sigma_2 = R - v_1\theta_1 = S - v_2\theta_2, \quad (62b)$$

$$\theta_1 + \theta_2 = P - Q, \quad v_1\theta_1 + v_2\theta_2 = R - S. \quad (62c)$$

Then, we substitute the boundary values found in Fig. 6 for P, Q, R, and S in Eqs. (62), and substitute the value of B/A into Eq. (60). Finally, solving the system of equations (60) and (62), we obtain the results listed in Table II. The solution in the first row of the table corresponds to the initial fronts found in Fig. 6. The solution in the second row corresponds to two unstable fronts, according the stability criterion discussed above. The two fronts that emerge upon the head-on collision are defined by the values found in the third row of the table. Hence, the fronts after the collision travel at the velocities $-v_1 = v_2 = 1.76$, which is in agreement with the velocities determined from the slope of the contour lines in Fig. 6.

VI. CONCLUSIONS

A nonlinear wave equation that governs finite amplitude acoustic disturbances in a thermoviscous Newtonian fluid, and includes nonlinear terms up to second order, has been presented. The single dependent variable is the velocity potential. It has been demonstrated that, in the non-dissipative limit, the equation preserves the Hamiltonian structure of the fundamental fluid dynamical equations, hence, the model equation is associated with corresponding Lagrangian and Hamiltonian densities. Furthermore, we found that the Kuznetsov equation is an approximation of the proposed nonlinear wave equation. However, in the non-dissipative limit the Kuznetsov equation is not Hamiltonian. Exact traveling front solutions, for the partial derivatives with respect to space and time of the dependent variable, has been obtained using a generalized traveling wave assumption. This generalized assumption leads to a wider class of exact solutions compared the one obtained from a standard traveling wave assumption, since the generalized assumption includes two arbitrary constants, which are added to the partial derivatives. As a result of the generalized traveling wave analysis we found that, in order for the front to exist, its boundary values, its propagation velocity, and the physical parameters of the problem must satisfy a given cubic equation in the front propagation velocity. The derivation of the exact solution applies equally
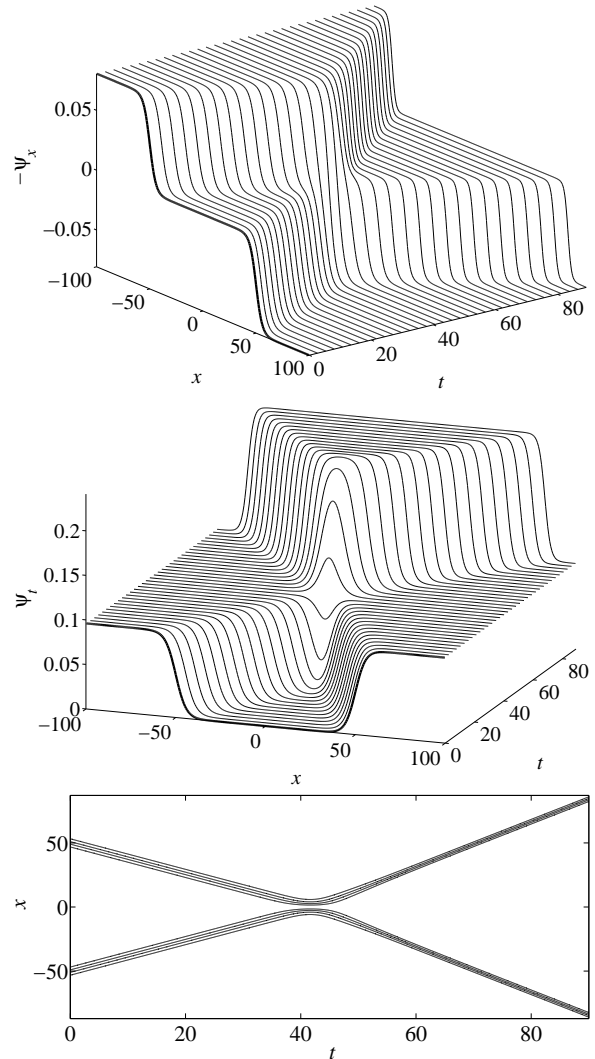

FIG. 6: The initial condition (bold lines in the two topmost plots), corresponds to two fronts that make a head-on collision at $t = 42$. The initial fronts are defined by $v_1 = -v_2 = 1.19$, $\theta_1 = -\theta_2 = 8.07 \times 10^{-2}$, $\lambda_1 = \lambda_2 = 0$, $\sigma_1 = \sigma_2 = 0$, and $B/A = 5$, where subscript 1 and 2 relate to fronts positioned the left and right, respectively. For each of the two fronts the parameters satisfy Eq. (22). Lowermost: contour lines given by $-\psi_x = Z$, where Z takes 4 equidistantly spaced values across each front.

well to the proposed Hamiltonian model equation and the Kuznetsov equation. Results for both equations have been given.

It has been demonstrated that the overall stability properties of the front are determined by the stability of the two asymptotic tails of the front. A linear stability analysis of these steady parts of the solution revealed that the front is stable when the partial derivative with respect to time, which is proportional to the acoustic pressure, belongs to a critical interval, and is otherwise unstable. This stability criterion has been verified numerically, by

TABLE II: Solution of Eqs. (60) and (62) subject to $P = -Q = 8.07 \times 10^{-2}$, $R = S = 9.60 \times 10^{-2}$, and $B/A = 5$ (compare with Fig. 6).

Solution	v_1	θ_1	v_2	θ_2	$\lambda_1 = \lambda_2$	$\sigma_1 = \sigma_2$
1	1.19	8.07×10^{-2}	-1.19	-8.07×10^{-2}	0	0
2	-3.25	8.07×10^{-2}	3.25	-8.07×10^{-2}	0	35.8×10^{-2}
3	-1.76	8.07×10^{-2}	1.76	-8.07×10^{-2}	0	23.8×10^{-2}

using the exact front solution as initial condition in a number of numerical simulations.

It has been demonstrated that, in all cases, the front propagates at supersonic speed with respect to the fluid ahead of it, while it remains subsonic with respect to the fluid behind it. The same properties have been reported for the classical fluid dynamical shock. Furthermore, it has been demonstrated that the cubic equation, mentioned above, is equivalent to the well established Rankine-Hugoniot relations, which connect the physical quantities on each side of a shock. However, this result was accomplished only when considering the cubic equation obtained from the analysis of the proposed Hamiltonian wave equation. The generalized traveling wave analysis based on the Kuznetsov equation is not in agreement with the Rankine-Hugoniot relations. Estimates of the front thickness may be obtained using the values for the diffusivity of sound listed in Table. I. In water and air front thicknesses are found to be of the order 10^{-9} and 10^{-7} meters, respectively. However, caution should be taken with these estimates, as the small length scales violates the continuum assumption of the governing equations.

Numerical simulations of two head-on colliding fronts have demonstrated that two new fronts emerge upon the collision, and that these fronts, in the general case, travel at speeds, which are different from the speeds of the fronts before the collision. It has been demonstrated that the velocities of the fronts after the collision may be calculated, based on information about the fronts before the collision. However, in order to accomplish this calculation, it has proven necessary to introduce the generalized traveling wave assumption in the derivation of the front solution.

In future studies, it would be rewarding to further investigate a variety of interacting fronts, other than the head-on collision reported in this paper. Also a search for other types of wave solutions, might learn us more about the properties of the proposed Hamiltonian model equation and the Kuznetsov equation.

Acknowledgments

[1] S. I. Aanonsen, T. Barkve, J. N. Tjøtta, and S. Tjøtta, "Distortion and harmonic generation in the nearfield of a finite amplitude sound beam", J. Acoust. Soc. Am. **75**, 749–768 (1984).
[2] V. P. Kuznetsov, "Equations of nonlinear acoustics", Sov. Phys. Acoust. **16**, 467–470 (1971).
[3] E. A. Zabolotskaya and R. V. Khokhlov, "Quasi-plane waves in the nonlinear acoustics of confined beams", Sov. Phys. Acoust. **15**, 35–40 (1969).
[4] P. M. Jordan, "An analytical study of Kuznetsov's equation: diffusive solitons, shock formation, and solution bifurcation", Phys. Lett. A **326**, 77–84 (2004).
[5] Y. Jing and R. O. Cleveland, "Modeling the propagation of nonlinear three-dimensional acoustic beams in inhomogeneous media", J. Acoust. Soc. Am. **122**, 1352–1364 (2007).
[6] J. Wójcik, "Conservation of energy and absorption in acoustic fields for linear and nonlinear propagation", J. Acoust. Soc. Am. **104**, 2654–2663 (1998).
[7] J. Hoffelner, H. Landes, M. Kaltenbacher, and R. Lerch, "Finite element simulation of nonlinear wave propagation in thermoviscous fluids including dissipation", IEEE Trans. Ultrason., Ferroelect., Freq. Contr. **48**, 779–786 (2001).
[8] A. Shermenev, "Separation of variables for the nonlinear wave equation in cylindrical coordinates", Physica D **212**, 205–215 (2005).
[9] B. O. Enflo and C. M. Hedberg, *Theory of Nonlinear Acoustics in Fluids* (Kluwer Academic, Dordrecht) (2002).
[10] S. Makarov and M. Ochmann, "Nonlinear and thermoviscous phenomena in acoustics, part II", Acustica **83**, 197–222 (1996).
[11] M. V. Aver'yanov, V. A. Khokhlova, O. A. Sapozhnikov, P. Blanc-Benon, and R. O. Cleveland, "Parabolic equation for nonlinear acoustic wave propagation in inhomogeneous moving media", Acoust. Phys. **52**, 623–632 (2006).
[12] K. Naugolnykh and L. Ostrovsky, *Nonlinear Wave Processes in Acoustics* (Cambridge University Press, Cambridge) (1998).
[13] L. H. Söderholm, "A higer order acoustic equation for the slightly viscous case", Acustica **87**, 29–33 (2001).
[14] V. E. Zakharov and E. A. Kuznetsov, "Hamiltonian formalism for nonlinear waves", Physics-Uspekhi **40**, 1087–1116 (1997).

[15] P. M. Jordan, "Bifurcations of diffusive soliton solutions to Kuznetsov's equation", J. Acoust. Soc. Am. **113**, 2283–2283 (2003).

[16] S. Makarov and M. Ochmann, "Nonlinear and thermoviscous phenomena in acoustics, part I", Acustica **82**, 579–606 (1996).

[17] R. T. Beyer, "The parameter B/A", in *Nonlinear Acoustics*, edited by M. F. Hamilton and D. T. Blackstock, chapter 2, 25–39 (Academic Press, San Diego) (1998).

[18] M. F. Hamilton and C. L. Morfey, "Model equations", in *Nonlinear Acoustics*, edited by M. F. Hamilton and D. T. Blackstock, chapter 3, 41–64 (Academic Press, San Diego) (1998).

[19] D. R. Lide, ed., *CRC Handbook of Chemistry and Physics, Internet Version 2007, (87th Edition), `http://www.hbcpnetbase.com`* (Taylor and Francis, Boca Raton) (2007).

[20] R. Gent, *Applied Physics and Technology of Diagnostic Ultrasound* (Milner Publishing, Prospect) (1997).

[21] I. Christov, C. I. Christov, and P. M. Jordan, "Modeling weakly nonlinear acoustic wave propagation", Q. J. Mechanics. Appl. Math. **60**, 473–495 (2007).

[22] H. Goldstein, C. Poole, and J. Safko, *Classical Mechanics*, 3 edition (Addison Wesley) (2001).

[23] M. F. Hamilton, D. T. Blackstock, and A. D. Pierce, "Progressive waves in lossless and lossy fluids", in *Nonlinear Acoustics*, edited by M. F. Hamilton and D. T. Blackstock, chapter 3, 65–150 (Academic Press, San Diego) (1998).

[24] L. D. Landau and E. M. Lifshitz, *Fluid mechanics* (Pergamon, Oxford) (1987).

Appendix B

Manuscript submitted to
Proc. ECMI 2008
(accepted July, 2009)

Analytical and Numerical Modelling of Thermoviscous Shocks and Their Interactions in Nonlinear Fluids Including Dissipation

A.R. Rasmussen[1], M.P. Sørensen[1], Yu.B. Gaididei[2], and P.L. Christiansen[3]

[1] Department of Mathematics, Technical University of Denmark, DK-2800 Kongens Lyngby, Denmark
[2] Bogolyubov Institute for Theoretical Physics, 03680 Kiev, Ukraine
[3] Department of Informatics and Mathematical Modelling and Department of Physics, Technical University of Denmark, DK-2800 Kongens Lyngby, Denmark

Summary. A wave equation, that governs finite amplitude acoustic disturbances in a thermoviscous Newtonian fluid, and includes nonlinear terms up to second order, is proposed. The equation preserves the Hamiltonian structure of the fundamental fluid dynamical equations in the non-dissipative limit. An exact thermoviscous shock solution is derived. This solution is, in an overall sense, equivalent to the Taylor shock solution of the Burgers equation. However, in contrast to the Burgers equation, the model equation considered here is capable to describe waves propagating in opposite directions. Studies of head-on colliding thermoviscous shocks demonstrate that the propagation speed changes upon collision.

1 Introduction

The "classical" equation of nonlinear acoustics, the so-called Kuznetsov equation [7], governs finite amplitude acoustic disturbances in a Newtonian, homogeneous, viscous, and heat conducting fluid. This equation arises in the modelling of biomedical ultrasound [5] and modelling of jet engines [2], to mention a few examples. The derivations of the Kuznetsov equation [7] and related model equations [8] are based on the complete system of the equations of fluid dynamics. It has been demonstrated that this system of equations is of Hamiltonian structure in the absence af dissipation [9]. However, in the non-dissipative limit, the Kuznetsov equation does not retain the Hamiltonian structure.

In this paper we propose a nonlinear wave equation, which, in the non-dissipative limit, preserves the Hamiltonian structure of the fundamental equations. We present the derivation and analysis of an exact thermoviscous shock solution. The derivation of the exact solution is based on a *generalized* travelling wave assumption, which leads to a wider class of exact solutions

compared to the one reported by Jordan [6] for the Kuznetsov equation. Furthermore, the introduction of the generalized assumption is necessary in order to interpret the results of numerical simulations of head-on colliding thermoviscous shocks presented in this paper.

2 Nonlinear wave equations

Equations governing finite amplitude acoustic disturbances in a Newtonian, homogeneous, viscous and heat conducting fluid may be derived from four equations of fluid dynamics. Namely, the equation of motion, the equation of continuity, the heat transfer equation and an equation of state. To obtain a nonlinear wave equation all dependent variables except one are eliminated from this system of equations, resulting in a nonlinear wave equation for that single variable. Retaining nonlinear terms up to the second order, we obtained a nonlinear wave equation, which we write here for the case of one-dimensional plane fields

$$\psi_{tt} - c_0^2 \psi_{xx} = \psi_t \psi_{xx} + \frac{\partial}{\partial t} \left(b\psi_{xx} + (\psi_x)^2 + \frac{B/A - 1}{2c_0^2} (\psi_t)^2 \right). \tag{1}$$

From the velocity potential $\psi = \psi(x,t)$ one can obtain the fluid particle velocity as $u = -\psi_x$ and the acoustic pressure as $p \approx \psi_t$. The parameter b is the diffusivity of sound (or thermoviscous dissipation parameter) [4], c_0 is the small-signal sound speed, and B/A is the fluid nonlinearity parameter [1]. In the first order approximation Eq. (1) reduces to $\psi_{tt} = c_0^2 \psi_{xx}$. Introducing this in the first term on the right hand side of Eq. (1), the Kuznetsov equation [7]

$$\psi_{tt} - c_0^2 \psi_{xx} = \frac{\partial}{\partial t} \left(b\psi_{xx} + (\psi_x)^2 + \frac{B/A}{2c_0^2} (\psi_t)^2 \right), \tag{2}$$

is obtained.

The Euler equations of fluid dynamics possess Hamiltonian structure [9]. This property is, however, *not* retained in Eq. (2) with $b = 0$, i.e. the non-dissipative limit of the Kuznetsov equation is not Hamiltonian. In contrast, Eq. (1) *does* retain the Hamiltonian structure in the non-dissipative limit. Accordingly, the equation may be derived from the Lagrangian density

$$\mathcal{L} = \frac{(\psi_t)^2}{2} - c_0^2 \frac{(\psi_x)^2}{2} - \frac{B/A - 1}{6c_0^2} (\psi_t)^3 - \frac{\psi_t (\psi_x)^2}{2}, \tag{3}$$

using the Euler-Lagrange equation. Using the Legendre transformation the corresponding Hamiltonian density can be obtained

$$\mathcal{H} = \frac{\partial \mathcal{L}}{\partial \psi_t} \psi_t - \mathcal{L}. \tag{4}$$

3 Exact thermoviscous shock solution

Recently, a standard travelling wave approach was applied to the one-dimensional approximation of the Kuznetsov equation (2) to reveal an exact travelling wave solution [6]. In this section we extend the standard approach by introducing the following generalized travelling wave assumption

$$
\begin{aligned}
\psi(x,t) &= \Psi(x - vt) - \lambda x + \sigma t \\
&\equiv \Psi(\xi) - \lambda x + \sigma t,
\end{aligned}
\tag{5}
$$

where λ and σ are arbitrary constants, v denotes the wave propagation velocity, and $\xi \equiv x - vt$ is a wave variable. The inclusion of $-\lambda x + \sigma t$ in Eq. (5) leads to a wider class of exact solutions, compared to the one obtained from the assumption $\psi = \Psi(x - vt)$, which is the standard one. Furthermore, the introduction of the generalized assumption is necessary in order to interpret the results of numerical simulations of head-on colliding thermoviscous shocks presented in Section 4. Inserting Eq. (5) into the nonlinear wave equation (1), integrating once and introducing $\Phi \equiv -\Psi'$ we obtain the ordinary differential equation

$$
C = vb\Phi' - \left(\frac{3}{2} + \frac{B/A - 1}{2c_0^2} v^2 \right) v\Phi^2 +
$$
$$
\left\{ \left(1 - \frac{B/A - 1}{c_0^2} \sigma \right) v^2 - 2\lambda v - c_0^2 - \sigma \right\} \Phi, \quad (6)
$$

where prime denotes differentiation with respect to ξ and C is a constant of integration. Requiring that the solution satisfy $\Phi' \to 0$ as $\xi \to \pm\infty$, and either

$$
\Phi \to \begin{cases} \theta, \ \xi \to +\infty \\ 0, \ \xi \to -\infty \end{cases} \quad \text{or} \quad \Phi \to \begin{cases} 0, \ \xi \to +\infty \\ \theta, \ \xi \to -\infty \end{cases}, \tag{7}
$$

where θ is an arbitrary constant, lead us to $C = 0$ and

$$
\frac{B/A - 1}{2c_0^2} \theta v^3 - \left(1 - \frac{B/A - 1}{c_0^2} \sigma \right) v^2 + \left(\frac{3}{2}\theta + 2\lambda \right) v + c_0^2 + \sigma = 0. \tag{8}
$$

In order to obtain our travelling wave solution we solve Eq. (6) subject to $C = 0$ by separation of variables, and by invoking Eq. (8) we find the solution to be

$$
\Phi = \frac{\theta}{2} \left\{ 1 - \tanh\left(\frac{2(\xi - x_0)}{l} \right) \right\}, \tag{9}
$$

$$
l \equiv \frac{4b}{\left(\dfrac{B/A - 1}{2c_0^2} v^2 + \dfrac{3}{2} \right) \theta}, \tag{10}
$$

where x_0 is an integration constant, $|l|$ is the shock thickness, and $0 < \Phi < \theta$. Finally, using $\Phi = -\Psi'$ and inserting Eq. (9) into Eq. (5) we obtain (apart from an arbitrary constant of integration)

$$\psi(x,t) = -\frac{\theta}{2}\left\{\xi - \frac{l}{2}\ln\left(\cosh\frac{2(\xi - x_0)}{l}\right)\right\} - \lambda x + \sigma t, \qquad (11)$$

which is the exact solution for the velocity potential.

Travelling tanh solutions, such as the solution (9), are often called Taylor shocks or thermoviscous shocks. The existence of an exact solution of this type to the classical Burgers equation is a well known result [3]. However, the Burgers equation is restricted to wave propagation *either* to the left *or* to the right. The model equation considered in this paper does not suffer from this limitation, as shall be illustrated in Section 4.

Taking the partial derivatives of Eq. (11), we find that the fluid particle velocity, $u = -\psi_x$, and the acoustic pressure, $p \approx -\psi_t$, are given by

$$-\psi_x = \Phi + \lambda \quad \text{and} \quad \psi_t = v\Phi + \sigma. \qquad (12)$$

Note that, according to Eqs. (7) and (12), the asymptotic boundary conditions for $-\psi_x$ and ψ_t are determined by v, θ, λ, and σ, which must satisfy Eq (8).

4 Head-on colliding thermoviscous shocks

The numerical simulation presented in Fig. 1 shows the result of a head-on collision between two thermoviscous shocks[4]. From the simulation we observe that two new waves emerge upon the collision. The contour plot reveals that these travel at a higher speed, compared to the speed of the waves before the collision. For other choices of initial condition, we found the outcome of similar head-on collisions to be two thermoviscous shocks travelling at lower speed, compared to that before the collision.

In order to analyze solutions of Eq. (1) that comprise two thermoviscous shocks, we assume that each of these belong to the class of exact solutions derived in Section 3. Investigations of the thermoviscous shocks that emerge upon a head-on collision have made it clear that this assumption is true, only when the generalized travelling wave assumption is used, in contrast to the standard travelling wave assumption. For each of the two thermoviscous shocks in the solution we introduce four new parameters, v, θ, λ, and σ, which must satisfy Eq. (8) as

$$\frac{B/A - 1}{2}\theta_i v_i^3 - (1 - (B/A - 1)\sigma_i)\, v_i^2$$
$$+ \left(\frac{3}{2}\theta_i + 2\lambda_i\right)v_i + \sigma_i + 1 = 0, \qquad i = 1, 2, \quad (13)$$

---

[4] Non-dimensional variables $\tilde{x} = c_0 x/b$, $\tilde{t} = c_0^2 t/b$, and $\tilde{\psi}(\tilde{x}, \tilde{t}) = \psi(x,t)/b$ were introduced prior to the numerical computation.
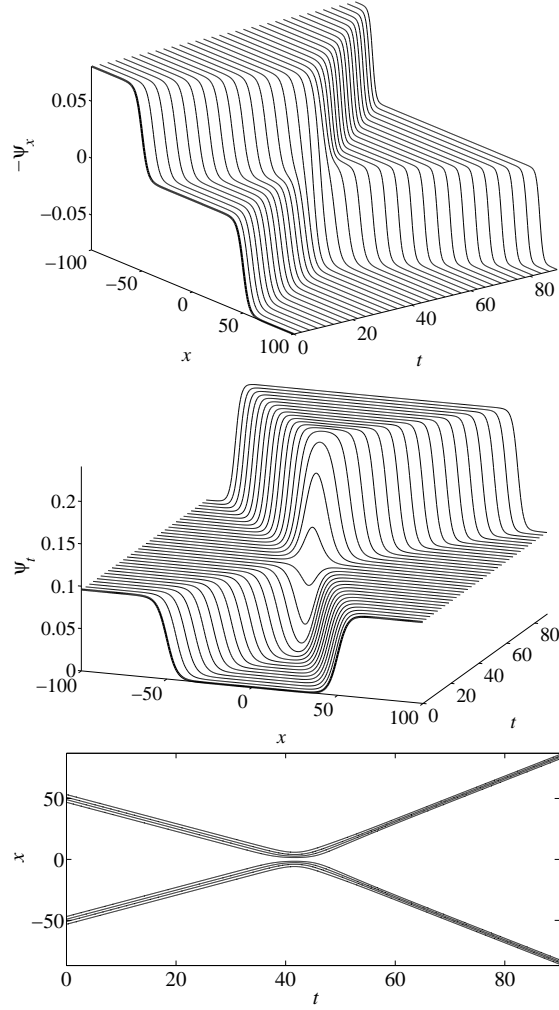
Fig. 1. The initial condition (bold lines in the two topmost plots) corresponds to two thermoviscous shocks that travel at $v = \pm 1.19$ and make a head-on collision at $t = 42$. The nonlinearity parameter was set to $B/A = 5$. Lowermost: contour lines given by $-\psi_x = Z$, where Z takes 4 equidistantly spaced values across each wave.

where subscript 1 and 2 denote parameters associated with waves positioned to the left and right, respectively. Furthermore, we require that solutions comprising two waves are (I) continuous and (II) satisfy the following set of arbitrary boundary conditions

$$-\psi_x \to \begin{cases} P, \ x \to -\infty \\ Q, \ x \to +\infty \end{cases}, \quad \psi_t \to \begin{cases} R, \ x \to -\infty \\ S, \ x \to +\infty \end{cases}. \tag{14}$$

Assuming that $l_1 > 0$ and $l_2 < 0$, we find (using the boundary conditions for each of the two waves) that the two requirements lead to the following conditions

$$\lambda_1 = \lambda_2, \qquad\qquad\qquad \sigma_1 = \sigma_2, \qquad\qquad (15a)$$

$$P = \theta_1 + \lambda_1, \qquad\qquad\qquad Q = \theta_2 + \lambda_2, \qquad\qquad (15b)$$

$$R = v_1\theta_1 + \sigma_1, \qquad\qquad\qquad S = v_2\theta_2 + \sigma_2, \qquad\qquad (15c)$$

Finally, we substitute the boundary values of $-\psi_x$ and ψ_t at $x = \pm 100$ in Fig. 1 for P, Q, R, and S in Eqs. (15), substitute the value of B/A into Eq. (13), and solve the resulting system of equations for v_1, θ_1, λ_1, σ_1, v_2, θ_2, λ_2, and σ_2. Following these steps we find that the waves after the collision travel at the velocities $-v_1 = v_2 = 1.76$ compared to $v_1 = -v_2 = 1.19$ before the collision. This finding is fine in agreement with the velocities determined from the slope of the contour lines in Fig. 1.

5 Conclusions

An exact thermoviscous shock solutions has been obtained using a generalized travelling wave assumption. This generalized assumption leads to a wider class of exact solutions compared to the one obtained from a standard travelling wave assumption and in turn this enable us to predict the outcome of two head-on colliding shocks. Analytical results for the wave speeds after the collision was in fine agreement with numerical observations. In future studies, it would be rewarding to further investigate interacting thermoviscous shocks, e.g. collisions between shocks travelling in the same directions.

References

1. R.T. Beyer, in *Nonlinear Acoustics* edited by M.F. Hamilton and D.T. Blackstock (Academic Press, 1998)
2. R. Fernando, R. Marchiano, F. Coulouvrat and Y. Druon, Nonlinear Acoustics—Fundamentals and Applications, Proceedings of the 18th ISNA, 99–102 (2008)
3. M.F. Hamilton, D.T. Blackstock and A.D. Pierce, in *Nonlinear Acoustics* edited by M.F. Hamilton and D.T. Blackstock (Academic Press, 1998)
4. M.F. Hamilton and C.L. Morfey, in *Nonlinear Acoustics* edited by M.F. Hamilton and D.T. Blackstock (Academic Press, 1998)
5. J. Hoffelner, H. Landes, M. Kaltenbacher and R. Lerch, IEEE Trans. Ultrason., Ferroelect., Freq. Contr. **48** 779–786 (2001)
6. P.M. Jordan, Phys. Lett. A **326** 77–84 (2004)
7. V.P. Kuznetsov, Sov. Phys. Acoust. **16** 467–470 (1971)
8. K. Naugolnykh and L. Ostrovsky, *Nonlinear Wave Processes in Acoustics* (Cambridge University Press, 1998).
9. V.E. Zakharov and E.A. Kuznetsov, Physics-Uspekhi **40** 1087–1116 (1997)

Appendix C

Manuscript for J. Acoust. Soc. Am.

Compound waves in a higher order nonlinear model of thermoviscous fluids

Anders Rønne Rasmussen and Mads Peter Sørensen
Department of Mathematics, Technical University of Denmark
DK-2800 Kongens Lyngby, Denmark

Yuri B. Gaididei
Bogolyubov Institute for Theoretical Physics
03143 Kiev, Ukraine

Peter Leth Christiansen
Informatics and Mathematical Modelling and Department of Physics
Technical University of Denmark
DK-2800 Kongens Lyngby, Denmark

April 30, 2009

Abstract

A generalized traveling wave ansatz is used to investigate compound shock waves in a higher order nonlinear model of a thermoviscous fluid. The fluid velocity potential is written as a traveling wave plus a linear function of space and time. The latter offers the possibility of predicting the outcome of interacting shock waves, i.e. shock jump heights and wave velocities after collisions and overtakes. The stability of the linear solution part is investigated and a criterion for its stability is determined. For a number of instances, the numerical results show formation of rarefraction waves. By using a similarity transformation, analytical expressions for these rarefraction waves are found in the limit of no dissipation. Examples of compound shock waves are illustrated by numerical simulations.

1   Introduction

Shock waves appearing in thermoviscous fluids are solitary waves resulting from balancing nonlinearity with viscous and heat conducting effects. The traveling wave approach has predominantly been used for nonlinear partial differential equations of Hamiltonian type and for reaction diffusion problems. However, it is well known that the traveling wave ansatz can be used to find shock waves in Burgers' equation. Despite this fact it has only recently been appreciated that the solitary wave approach is well suited for studies of various models of thermoviscous shocks. Jordan [1] determined a traveling wave solution for the Kuznetsov equation [2] and later on successfully invoked the traveling wave approach for studies of nonlinear viscoelastic media [3, 4]. In order to investigate high Mach number shock wave propagation, Chen et al. [5] investigated a higher-order equation derived by Söderholm [6], allowing for a more accurate assessment of traveling wave velocities.

In this paper compound shock waves are investigated in the model for thermoviscous fluids proposed by Söderholm [6]. The studies are based on a generalization

1

of the traveling wave ansatz for the velocity potential by adding a function linear in the space and time variables to the traveling wave part [7]. The solution of the resulting ordinary differential equation is given implicitly, in contrast to the explicit solutions found for the Kuznetsov equation in [1] and a third order approximation to acoustic waves in thermoviscous fluid in [7]. The generalized ansatz makes it possible to determine analytically the outcome of head-on colliding and overtaking shock waves. In order to illustrate the solitary wave properties (or quasi soliton nature) of the traveling shock waves, collision and overtake simulation experiments are performed for the shocks. The traveling wave shock solutions are equivalent to the Taylor shock solution of the Burgers equation. However, in contrast to the Burgers equation the model studied here allows counter propagating shocks. The paper is organized as follows: In chapter 2 the model equation is presented, in chapter 3 a generalized traveling wave ansatz is used to determine an implicit shock wave solution and in chapter 4 rarefraction waves are investigated. In chapter 5 stability properties are studied and finally chapter 6 deals with compound waves.

2 Model equation

In this investigation we use a model derived by Söderholm [6]. The wave propagation phenomena are restricted to the case of plane waves with finite amplitudes in one spatial dimension and in a homogeneous medium. The fluid particle velocity field is denoted by $u=u(x,t)$, where x is the space variable and t is time. The wave equation is formulated in terms of the velocity potential $\psi=\psi(x,t)$ defined by

$$u \equiv -\psi_x \, , \tag{1}$$

where subscript denotes partial differentiation. The dynamical equation governing the acoustic wave propagation reads in terms of ψ [6]

$$\psi_{tt} - c_0^2 \psi_{xx} = (\gamma - 1)\psi_{xx}\psi_t + 2\psi_{xt}\psi_x - \frac{\gamma + 1}{2} \left(\psi_x\right)^2 \psi_{xx} + b\psi_{xxt} \, . \tag{2}$$

Here γ is the adiabatic index or ratio of the specific heats, c_0 is the small-signal speed of sound, and b is the diffusivity of sound [8], which takes into account thermal and viscous losses. Eq. (2) is the one-dimensional version of the three-dimensional model equation derived by Söderholm [6], taking only first order dissipative effects into account. We consider the first order approximation for the pressure

$$p(x,t) \simeq p_0 + \rho_0 \eta(x,t) \tag{3}$$

where p_0 (ρ_0) is the static pressure (density) and $\eta \equiv \psi_t$. The lossless limit of Eq. (2), which is obtained by letting $b = 0$, appears in a number of works [8, 9, 10, 11, 12]. Some of these authors emphasize the fact that the equation is exact for a lossless perfect gas, which is described by the following equation of state

$$\frac{p}{p_0} = \left(\frac{\rho}{\rho_0}\right)^\gamma \, , \qquad c^2 = \frac{dp}{d\rho} = \gamma \frac{p}{\rho} \, , \qquad c_0^2 = \gamma \frac{p_0}{\rho_0} \, , \tag{4}$$

where ρ is the density and c is the the velocity of sound. For $b = 0$ Eq. (2) is exact in the sense that it can be derived from the Euler equations without introducing any approximations. Accordingly, Christov et al. [13, 14, 15] denoted Eq. (2) with $b = 0$ the potential Euler equation.

The case of a perfect-gas behavior can be extended to arbitrary fluids, including both gases and liquids. The general equation of state is expressed as $p = p(\rho, s)$, where $s = s(x, t)$ is the entropy. We shall expand the equation of state in a Taylor series about $(\rho, s) = (\rho_0, s_0)$, with s_0 being the entropy of the static and unperturbed fluid. Within the field of nonlinear acoustics it has become customary [16] to retain only the following terms in the Taylor series

$$p - p_0 = c_0^2(\rho - \rho_0) + \frac{c_0^2}{\rho_0}\frac{B/A}{2}(\rho - \rho_0)^2 + \frac{\partial p}{\partial s}\bigg|_{\rho=\rho_0, s=s_0}(s - s_0), \qquad (5)$$

where

$$c_0^2 \equiv \frac{\partial p}{\partial \rho}\bigg|_{\rho=\rho_0, s=s_0} \qquad (6)$$

is the small signal sound velocity, and

$$B/A \equiv \frac{\rho_0}{c_0^2}\frac{\partial^2 p}{\partial \rho^2}\bigg|_{\rho=\rho_0, s=s_0} \qquad (7)$$

is the non-dimensional fluid nonlinearity parameter, which is determined by experimental methods. Values of B/A for a wide range of media are given in reference [17]. The expansion contains terms up to second order in $\rho - \rho_0$, but contains only terms up to first order in $s - s_0$ when nonlinear contributions in the dissipative terms are neglected.

A detailed study of the case of an arbitrary fluid, described by the quadratic equation of state (5), is given in Christov et al. [13]. Their analysis leads to a wave equation, which is quite complicated. However, by assuming that the Mach number, $\varepsilon = u_{\max}/c_0$, is small they show that their complicated equation may be approximated by Eq. (2) with $\gamma - 1$ replaced by B/A. The study conducted by Christov and coworkers is carried out for the lossless case, however, their analysis and results readily generalizes to take into account the linear thermoviscous effects discussed above.

Inserting the perfect gas law (4) into Eqs. (6) and (7) one obtains

$$B/A = \gamma - 1. \qquad (8)$$

Hence, there is a direct connection between the ratio of specific heats and the parameter of nonlinearity.

The nonlinear model equation (2) can be simplified by introducing scaled and dimensionless variables, denoted by tilde

$$\tilde{\psi}(\tilde{x}, \tilde{t}) = \frac{1}{b}\psi(x, t), \qquad \tilde{x} = \frac{c_0}{b}x, \qquad \tilde{t} = \frac{c_0^2}{b}t, \qquad (9)$$

where $b > 0$. Under this transformation we may rewrite Eq. (2) as

$$\psi_{tt} - \psi_{xx} = (\gamma - 1)\psi_{xx}\psi_t + 2\psi_{xt}\psi_x - \frac{\gamma + 1}{2}(\psi_x)^2\psi_{xx} + \psi_{xxt}, \qquad (10)$$

where the tildes have been omitted. Equation (10) is used in the numerical simulations in the rest of this paper.

3

3 Thermoviscous shock

We begin our search for thermoviscous shock solutions with the following observation: since Eq. (2) is invariant under the transformation $x \curvearrowright -x$, we need only consider, without loss of generality, right traveling waves. Our derivation is based on the following traveling wave assumption

$$\psi(x,t) = \Psi(\xi) - u_1 x + \eta_1 t, \tag{11}$$

where $\xi = x - vt$ is the traveling wave variable with constant and positive velocity v for right traveling waves, u_1 and η_1 are arbitrary constants. Compared to the solution obtained from the assumption $\psi(x,t) = \Psi(x - vt)$, which is the usual one, the inclusion of $-u_1 x + \eta_1 t$ in Eq. (11) leads to a more general shock solution with additional flexibility in the asymptotic boundary conditions for $u = -\psi_x$ and $\eta = \psi_t$. This increased flexibility turns out to be necessary in order to fully describe problems with interacting waves. Such problems will be treated in Section 6. Taking the derivatives of Eq. (11) with respect to x and t, respectively, yields

$$u(x,t) = \Phi(\xi) + u_1 \qquad \text{and} \qquad \eta(x,t) = v\Phi(\xi) + \eta_1, \tag{12}$$

where

$$\Phi \equiv -\Psi'. \tag{13}$$

We observe that u and η depend on ξ alone and not explicitly on x and t. Hence, u and η are traveling waves in the usual sense.

Inserting Eq. (11) into Eq. (2) yields the following ordinary differential equation (ODE)

$$vb\Psi''' + \alpha{\Psi'}^{3'} - \beta{\Psi'}^{2'} + \delta\Psi'' = 0, \tag{14}$$

where prime denotes differentiation with respect to ξ, and α, β, and δ are defined in the following way

$$\alpha \equiv \frac{\gamma + 1}{6}, \tag{15}$$

$$\beta \equiv \frac{\gamma + 1}{2}(u_1 - v), \tag{16}$$

$$\delta \equiv v^2 - c_0^2 - (\gamma - 1)\eta_1 - 2vu_1 + \frac{\gamma + 1}{2}u_1^2. \tag{17}$$

Integrating once and introducing Eq. (13) reduces Eq. (14) to

$$vb\Phi' + \alpha\Phi^3 + \beta\Phi^2 + \delta\Phi = C, \tag{18}$$

where C is a constant of integration. If we require that the solution must satisfy $\Phi' \to 0$ as $\xi \to \pm\infty$ we have $\Phi \to \theta$ as $\xi \to \pm\infty$, where θ is a constant. From Eq. (18) we find that θ must satisfy

$$\alpha\theta^3 + \beta\theta^2 + \delta\theta = C. \tag{19}$$

4

Clearly, Eq. (19) has three solutions θ_0, θ_1, and θ_2. Without loss of generality we may assume $\theta_0 = 0$, obtain $C = 0$ and

$$\alpha\theta_{1,2}^2 + \beta\theta_{1,2} + \delta = 0. \tag{20}$$

Hence, for θ_1 and θ_2 we have

$$\theta_1 = \frac{-\beta - D}{2\alpha} \qquad \text{and} \qquad \theta_2 = \frac{-\beta + D}{2\alpha}, \tag{21}$$

where $D \equiv \sqrt{\beta^2 - 4\alpha\delta}$. For $C = 0$ we obtain

$$-(\xi - \xi_0)\frac{\delta}{vb} = \ln(|\Phi|) + \frac{\beta - D}{2D}\ln(|\Phi - \theta_1|) - \frac{\beta + D}{2D}\ln(|\Phi - \theta_2|), \tag{22}$$

where ξ_0 is an integration constant. Eq. (22) gives an explicit closed form of the solution of $\xi(\Phi)$. However, from Eq. (22) we cannot, in general, obtain an explicit closed form solution for $\Phi(\xi)$. For numerical purposes, however, one can compute a set of values of ξ from a set of values of Φ, whereafter one can plot Φ versus ξ as shown in Fig. 1. From Eq. (22) we observe, in accordance with the figure, that the solution represents two smooth steps Φ_1 and Φ_2 that satisfy the following asymptotic boundary conditions

$$\Phi_1 \to \begin{cases} \theta_1 & \text{if } \xi \to -\infty \\ \theta_0 = 0 & \text{if } \xi \to +\infty \end{cases} \qquad \text{and} \qquad \Phi_2 \to \begin{cases} \theta_1 & \text{if } \xi \to -\infty \\ \theta_2 & \text{if } \xi \to +\infty \end{cases}. \tag{23}$$

From Eqs. (21) with $u_1 = 0$ and $\eta_1 = 0$ we find that $\theta_1 \to 0$ and $\theta_2 \to 3c_0$ in the limit of $v \to c_0$. Hence, in this limit the difference between the left and right asymptotic boundary conditions of Φ_1 tends to 0. This is the small amplitude behavior, which agrees with linear acoustics. On the other hand, the difference between the asymptotic boundary conditions of Φ_2 tends to $3c_0$, which is not a physically realistic behavior. For this reason we discard Φ_2 and consider only Φ_1, which we shall denote by Φ (omitting subscript 1) in the following. Once Φ is determined, we directly obtain the corresponding u and η from Eq. (12), which represents the the exact thermoviscous shock solution. Inserting the first of Eqs. (23) into Eq. (12) we find that the solution satisfies the following asymptotic boundary conditions

$$u \to \begin{cases} \theta_1 + u_1 & \text{if } \xi \to -\infty \\ u_1 & \text{if } \xi \to +\infty \end{cases}, \qquad \eta \to \begin{cases} v\theta_1 + \eta_1 & \text{if } \xi \to -\infty \\ \eta_1 & \text{if } \xi \to +\infty \end{cases}, \tag{24}$$

Hence, the four parameters, v, θ_1, u_1, and η_1 completely determine these boundary conditions. These four parameters must satisfy the first of Eqs. (21). Hence, we interpret this equation as the "jump condition" for the smooth thermoviscous shock. Due to the logarithms in (22), two singular solutions appear in Fig. 1 with singularities at $\xi = 0$. These singularities may indicate the possibility of the existence of collapsing solutions of the model (2).

For the purpose of numerical simulations we finally need to derive a formula for $\psi(x, t)$. By multiplying Eq. (13) by $d\xi/d\Phi$ and integrating with respect to Φ, we obtain the following expression

$$\Psi = -\int^\Phi \hat{\Phi}\frac{d\xi}{d\Phi}\Big|_{\Phi = \hat{\Phi}} d\hat{\Phi}. \tag{25}$$
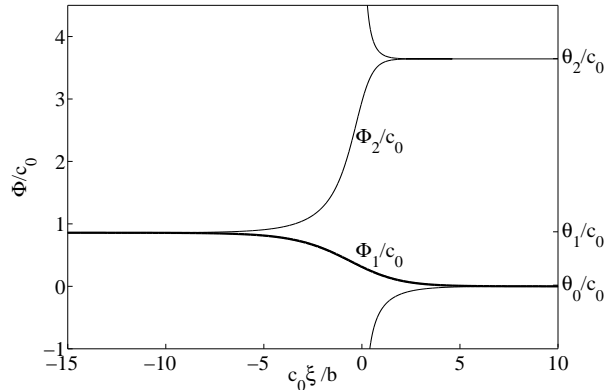
Figure 1: Plot of Φ versus ξ obtained from Eq. (22) using $\gamma = 1.4$, $v = 1.5c_0$, $u_1 = 0$, $\eta_1 = 0$, $\theta_0 = 0$ and $\xi_0 = 0$. The solution represents two smooth steps Φ_1 and Φ_2, of which only Φ_1 (indicated in bold line) corresponds to a physically realistic thermoviscous shock. In addition there are two singular solutions for $\xi > 0$.

The derivative $d\xi/d\Phi$ is determined from Eq. (22) and inserted into Eq. (25). After carrying out the integration and inserting Eq. (25) into Eq. (11) we obtain

$$\psi(x,t) = \frac{vb}{\delta}\left(\Phi + \frac{\beta - D}{2D}\left[\Phi + \theta_1 \ln(|\Phi - \theta_1|)\right]\right.$$

$$\left. - \frac{\beta + D}{2D}\left[\Phi + \theta_2 \ln\left(|\Phi - \theta_2|\right)\right]\right) - u_1 x + \eta_1 t, \quad (26)$$

which is the exact solution for the velocity potential. In the above expression we have set the arbitrary constant of integration to zero as it plays no role in the following analysis.

4   Rarefaction wave

In the theory for hyperbolic problems the presence of rarefaction waves is well-described by e.g. LeVeque in reference [18], who treats the case with no damping $b = 0$. Here we shall use an alternative approach to the study of rarefraction waves by introducing a similarity transformation in which the dependent variables are functions of x/t multiplied by t. This leads to solutions where the fluid velocity and the acoustic pressure are constants along rays through $(x,t) = (0,0)$. If we set $b = 0$ in Eq. (2), then the equation reduces to a hyperbolic problem. By following a line of thought, in which the underlying assumptions are similar to those of the established theory, we shall here derive the lossless rarefaction wave solution for the equation (2) with $b = 0$. Once this solution is obtained we shall compare it to the thermoviscous rarefaction wave obtained in the case of $b > 0$ by means of numerical simulations.

We introduce the following assumption

$$\psi(x,t) = tF(x/t)$$
$$= tF(z)\,,$$
$$\quad (27)$$

where $z \equiv x/t$. By differentiation with respect to x and t, respectively,

6

we obtain

$$u(x,t) = -F' \equiv U(z) \qquad \text{and} \qquad \eta(x,t) = F - zF' \equiv H(z)\,, \qquad (28)$$

where prime denotes differentiation with respect to z, $u = -\psi_x$, and $\eta = \psi_t$. Hence, we observe that u and η depend on z alone and not explicitly on x and t. The rarefaction wave itself has the following form

$$u(x,t) = \begin{cases} u_2 & \text{if } x/t \leq z_2, \\ U(x/t) & \text{if } z_2 \leq x/t \leq z_1, \\ u_1 & \text{if } x/t \geq z_1, \end{cases} \qquad (29a)$$

$$\eta(x,t) = \begin{cases} \eta_2 & \text{if } x/t \leq z_2, \\ H(x/t) & \text{if } z_2 \leq x/t \leq z_1, \\ \eta_1 & \text{if } x/t \geq z_1, \end{cases} \qquad (29b)$$

$$\psi(x,t) = \begin{cases} -u_2 x + \eta_2 t & \text{if } x/t \leq z_2, \\ tF(x/t) & \text{if } z_2 \leq x/t \leq z_1, \\ -u_1 x + \eta_1 t & \text{if } x/t \geq z_1. \end{cases} \qquad (29c)$$

where z_1, z_2, u_1, u_2, η_1, and η_2 represent points on U and H in the following manner

$$U(z_1) = u_1, \qquad H(z_1) = \eta_1, \qquad (30a)$$
$$U(z_2) = u_2, \qquad H(z_2) = \eta_2. \qquad (30b)$$

To determine F we start out by inserting Eq. (27) into Eq. (2) with $b = 0$, which yields the following equation

$$\frac{\gamma + 1}{2}F'^2 + (\gamma + 1)zF' - (\gamma - 1)F = -z^2 + c_0^2. \qquad (31)$$

Note that Eq. (31) does not depend explicitly on x and t but only on z, thus our problem is reduced to the problem of solving an ODE. This will not be the case if $b > 0$, since, in that case the corresponding equation depends explicitly on both z and t (or z and x). In order to solve the ODE we assume that the solution is of the following form

$$F = a_2 z^2 + a_1 z + a_0. \qquad (32)$$

Inserting Eq. (32) into Eq. (31) leads to

$$F = -\frac{1}{\gamma + 1}z^2 + a_1 z + \frac{(\gamma + 1)a_1^2 - 2c_0^2}{2(\gamma - 1)}\,, \qquad (33)$$

where a_1 is still an arbitrary constant. In order for this solution to satisfy Eqs. (30a) we find, by inserting Eq. (33) into Eqs. (28), that

$$z_1 = u_1 + \frac{S}{2} \qquad (34)$$

and

7

$$a_1 = \frac{-(\gamma - 1)u_1 + S}{\gamma + 1}, \tag{35}$$

where

$$S \equiv \sqrt{4(\gamma - 1)\eta_1 - 2(\gamma - 1)u_1^2 + 4c_0^2}. \tag{36}$$

Inserting Eq. (35) into Eq. (33) yields

$$F = -\frac{1}{\gamma + 1}z^2 + \frac{-(\gamma - 1)u_1 + S}{\gamma + 1}z + \frac{[-(\gamma - 1)u_1 + S]^2}{2(\gamma - 1)(\gamma + 1)} - \frac{c_0^2}{\gamma - 1}. \tag{37}$$

Furthermore, in order for Eq. (37) to also satisfy Eq. (30b) we find that

$$z_2 = \frac{1}{2}[u_2(\gamma + 1) - u_1(\gamma - 1) + S], \tag{38}$$

and u_1, u_2, η_1, and η_2 must satisfy the following condition

$$\frac{\gamma + 1}{4}(u_1^2 + u_2^2) - u_1^2 + \frac{1 - \gamma}{2}u_1 u_2 - \frac{S}{2}(u_1 - u_2) + \eta_1 - \eta_2 = 0. \tag{39}$$

Finally, the rarefaction wave is obtained by: (a) choosing u_1, u_2, η_1, and η_2 in such a way that Eq. (39) is satisfied, (b) inserting Eq. (37) into Eq. (28) and inserting the result into Eq. (29), and (c) inserting Eqs. (34) and (38) into Eq. (29).

Above we have derived an exact lossless rarefaction wave solution for the case of $b = 0$. In order to compare that solution to a thermoviscous rarefaction wave encountered in the case of $b > 0$ we shall make use of numerical simulations. In order to generate a thermoviscous rarefaction wave we introduce a smooth step for use as initial condition in our simulations. We describe this step in the following way

$$u(x) = \frac{1}{2}\left[u_1 + u_2 - (u_1 - u_2)\tanh\frac{x}{l}\right], \tag{40a}$$

$$\eta(x) = \frac{1}{2}\left[\eta_1 + \eta_2 - (\eta_1 - \eta_2)\tanh\frac{x}{l}\right], \tag{40b}$$

where l is the width of the step. Integrating Eq. (40a) with respect to x we obtain

$$\psi(x) = -\frac{1}{2}\left[(u_1 + u_2)x - (u_1 - u_2)l \ln\left(\cosh\frac{x}{l}\right)\right], \tag{40c}$$

which is required for numerical simulations. At $t = 0$ the lossless rarefaction wave (29a) and (29b) represents a jump discontinuity located at $x = 0$. Similar jumps are obtained by letting $l \to 0$ in Eqs. (40a) and (40b). We generate the thermoviscous rarefaction wave by choosing u_1, u_2, η_1, and η_2 such that Eq. (39) is satisfied and using Eqs. (40) as initial condition in the computation of a numerical solution of Eq. (2). Fig. 2 shows a comparison between a thermoviscous rarefaction wave obtained in this manner and the exact lossless rarefaction wave solution given by Eq. (29). From the figure we see that the thermoviscous solution is smooth in the neighborhood of $x = z_1 t$ and $x = z_2 t$. At these points the lossless rarefaction wave has jumps in the first derivatives of u and η. Away from these points the two solutions agree.
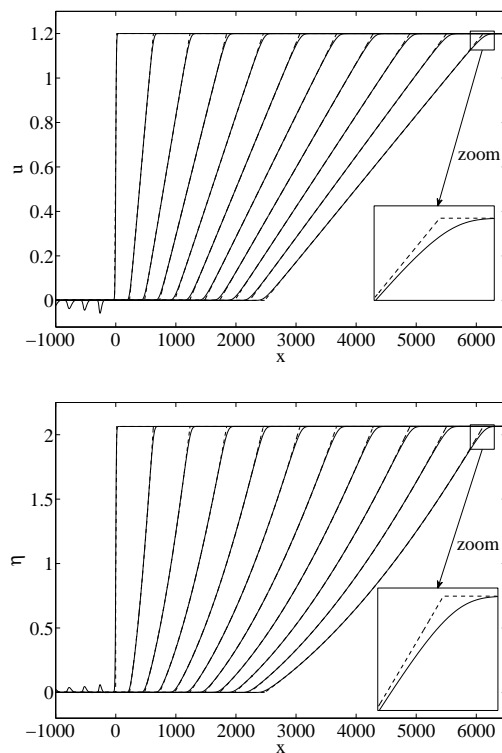
Figure 2: Comparison between a lossless (dashed line) and a thermoviscous (solid line) rarefaction wave. The lossless solution is obtained from Eq. (29) and the thermoviscous one is obtained by solving numerically Eq. (2). The parameters $\gamma = 1.4$ and $u_1 = 0$, $\eta_1 = 0$, $u_2 = 1.2$, and $\eta_2 = 2.064$ were chosen such that Eq. (39) is satisfied. The inserts show a magnification of the upper corner of the solution. Similar behaviour at the lower corner may be observed.

5 Stability properties

We first investigate the linear stability properties of an elementary solution $\psi(x,t)$, which is linear in x and t, such that the first order derivatives, u and η, take constant values and all higher order derivatives are zero. Once the linear stability properties of this solution are determined we shall verify and investigate the analytical findings by means of numerical simulations. Finally, we shall demonstrate that stability properties of the shock and rarefaction wave solutions discussed above may be deduced from the stability of the elementary solution.

The solution we consider is the following

$$\psi(x,t) = -Kx + Lt \tag{41}$$

where K and L are arbitrary constants. Eq. (41) is an exact solution of the nonlinear wave equation (2). In order to investigate the linear stability properties of the solution we introduce a perturbation, $\chi(x,t)$, in the following way

$$\psi(x,t) = -Kx + Lt + \varepsilon\chi(x,t), \tag{42}$$

where $\varepsilon \ll 1$. Inserting Eq. (42) into Eq. (2) and keeping terms up to first order in ε yields the following linear equation for the perturbation

$$\chi_{tt} - b\chi_{xxt} + 2K\chi_{xt} + \left(\frac{\gamma+1}{2}K^2 - (\gamma-1)L - c_0^2\right)\chi_{xx} = 0. \tag{43}$$

Inserting the single Fourier mode $e^{i(kx-\omega t)}$, where k is the wave number and ω is the angular frequency, into Eq. (43), we obtain the following dispersion relation

$$\omega^2 + (ibk^2 - 2Kk)\omega + \left(\frac{\gamma+1}{2}K^2 - (\gamma-1)L - c_0^2\right)k^2 = 0. \tag{44}$$

The solution (41) is asymptotically stable if all solutions of Eq. (43) approach zero as $t \to \infty$. This is the case when the imaginary part of both roots in Eq. (44), ω_1 and ω_2, are negative. It can be shown that the only requirement in order for the imaginary part of both roots to be negative is

$$s \equiv \frac{\gamma+1}{2}K^2 - (\gamma-1)L - c_0^2 < 0. \tag{45}$$

This requirement does not, remarkably, depend on the wave number, k, of the perturbation. Furthermore, it is noteworthy that Eq. (42) does not depend on the themoviscous dissipation parameter, b. In fact the equivalent analysis of Eq. (2) with $b = 0$ leads also to the stability criterion (45). If the criterion is not met the solution (41) is unstable.

In order to verify and investigate numerically the stability criterion (45) we use Eq. (42) as initial condition ($t = 0$) in two numerical simulations of Eq. (2). We choose K and L such that in one simulation the solution is linearly stable ($s < 0$) and in the other one it is linearly unstable ($s > 0$). The results of the two numerical simulations are shown in Fig. 3. From the simulations we see that the initial perturbation either decays or grows in time, in agreement with the stability criterion (45).
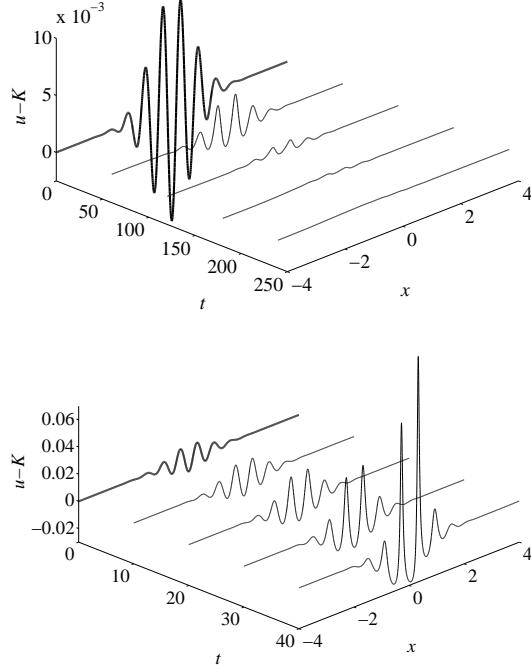
Figure 3: The initial conditions (bold line) in the two numerical simulations are obtained from Eq. (42). For the perturbation, $\varepsilon\chi(x,0)$, we use a stationary wave packet. The following parameters were used $L = 1.8$ and $B/A = 0.4$. Upper and lower simulation $K = 1.19$ and $K = 1.21$.
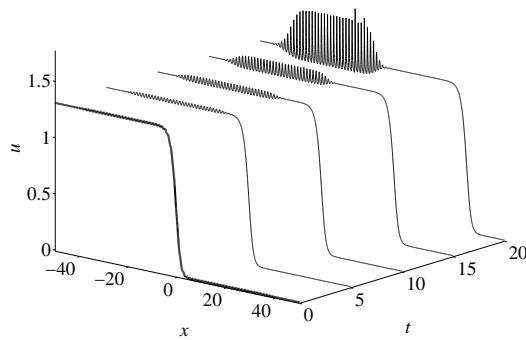

Figure 4: The initial condition (bold line) in the numerical simulation is obtained from the exact thermoviscous shock solution given by Eq. (26). A small perturbation is added to the exact solution. The following parameters were used: $v = 1.75$, $\lambda = 0$, $\sigma = 0$, $B/A = 0.4$. For this choice of parameters the left asymptote of the shock causes instability of the solution.

In the two previous sections we discussed the thermoviscous shock and rarefaction wave solutions of Eq. (2). In order for each of these solutions to be stable it is a necessary condition that their asymptotes as $\xi \to \pm\infty$ both correspond to $s \leq 0$. This means substituting the asymptotic values of u and η for K and L in Eq. (45). Fig. 4 shows a numerical simulation of a thermoviscous shock whose left asymptote causes instability of the solution. We have also checked that the original momentum balance equation (Navier-Stokes equations) and conservation of mass do not possess this type of instability. Thus, the above instability is an artifact of the model in Eq. (2).

6 Compound waves

In this section we investigate solutions of Eq. (2) that are compounded by two waves. Each of the two waves can be a shock or a rarefaction wave, as introduced in the previous sections. In particular we investigate three examples of compound waves:

i) In the first example we study the evolution in time of an initial condition, which represents a shock tube problem. Initially $u = 0$ everywhere on the spatial domain in the tube and η jumps at the centre of the spatial domain, i.e. we consider a Riemann problem. The result of a numerical simulation of Eq. (2) with such an initial condition is shown in Fig. 5. From the simulation we see that two waves emerge from the initial condition. A rarefaction wave that propagates to the left and a shock that propagates to the right.

ii) In our second example we investigate two shocks that propagate at different speeds in the same direction. The shocks collide once the faster one catch up with the slower one. Each of the two shocks that make up the initial condition is an exact solution given by Eq. (26) with its asymptotic boundary conditions satisfying the shock jump condition (21). From the numerical simulation shown in Fig. 6 we see that two new shocks emerge from the collision. The two shocks propagate to the left and right, respectively, away from the point of collision. Note that the weaker shock is reflected backwards from the collision zone.

iii) Our third example is similar to the second one. However, in this example the two shocks in the initial condition propagate towards each other and make a head-on collision at a later moment in time. From Fig. 7 we see that the collision results in two shocks that propagate away from each other. The contour plot shows that these shocks travel at a higher speed compared to the speed of the shocks before the collision.

In the following we shall analyze solutions that are compounded by two waves, such as the ones described in the three examples above. We assume that shocks which emerge in the compound solutions are exact solutions of the form (26) and that their asymptotic boundary conditions satisfy the shock jump condition (21). Similarly, we assume that the asymptotic boundary conditions of the thermoviscous rarefaction waves that emerge satisfy the boundary conditions of the lossless rarefaction wave. These boundary conditions are given by Eq. (39).

Let us assume that the compound solution is continuous and satisfy the following set of arbitrary boundary conditions
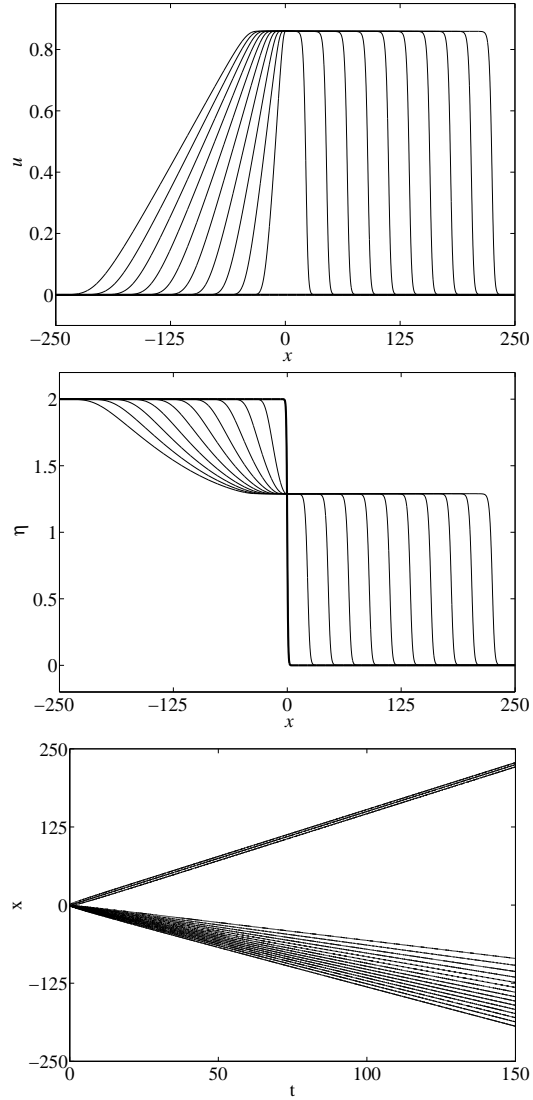
Figure 5: Numerical simulation of Eq. (2). The initial condition (bold line in the two topmost plots) represents a shock tube problem. At $t = 0$ there is a jump in η at $x = 0$ (represented by a smooth step function) and $u(x, 0) = 0$. The fluid nonlinearity parameter was set to $B/A = 0.4$. Lowermost: contour lines given by $\eta = Z_i$, where Z_i are constants.
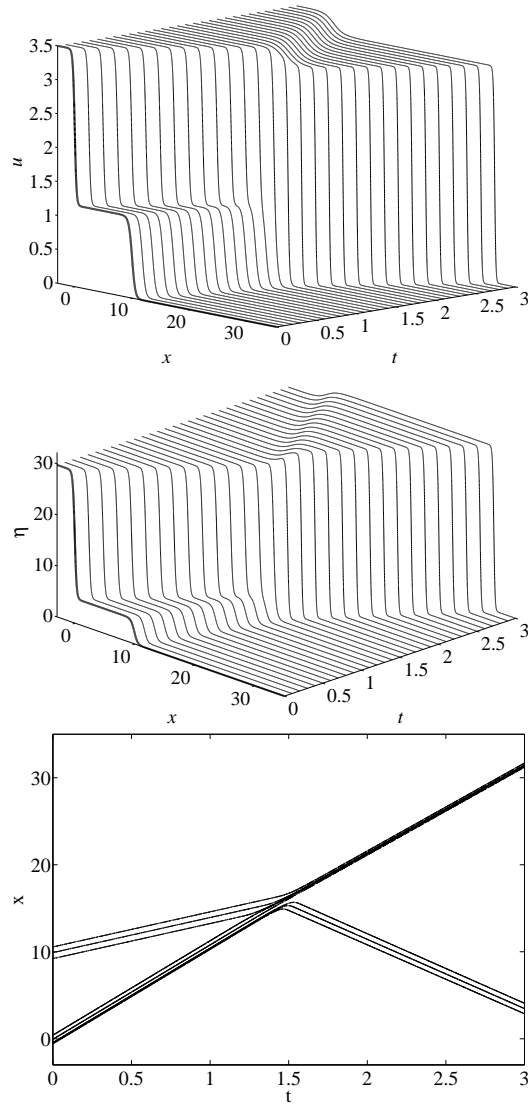
Figure 6: Numerical simulation of Eq. (2). The initial condition represents two shocks that propagate at different speeds in the same direction. Initial condition: Left shock: $v = 10.848$ and $\theta = 2.3$. Right shock: $v = 4.0313$ and $\theta = 1.2$. The fluid nonlinearity parameter was set to $B/A = 5$. Lowermost: contour lines given by $u = Z_i$, where Z_i are constants. After the collison the velocity of the merged right running shock is $v = 10.096$ and the left running reflected shock travels with the velocity $v = -7.9681$
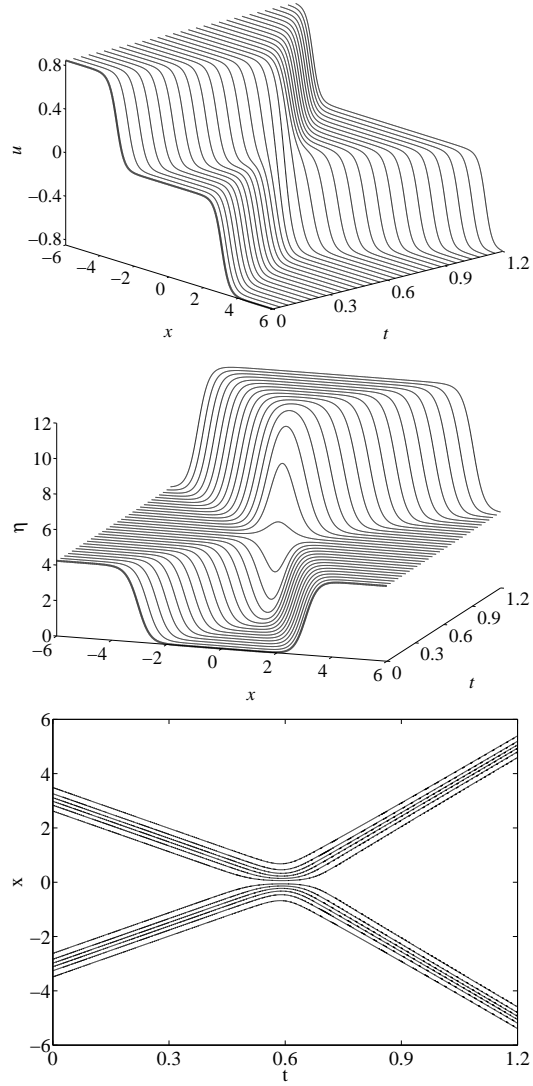
Figure 7: Numerical simulation of Eq. (2). The initial condition represents two identical shocks traveling towards each other. $v = \pm 5$ and $\theta = 0.848$. The fluid nonlinearity parameter was set to $B/A = 10$. Lowermost: contour lines given by $u = Z_i$, where Z_i are constants. After the collison the shock propagation velocities are $v = \pm 8.3962$.
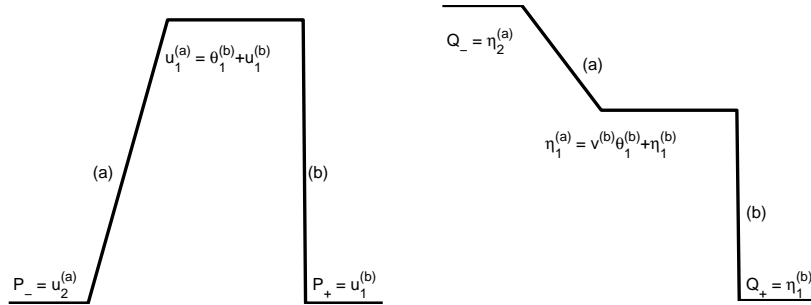
15

Figure 8: Sketch of the procedure for calculating the outcome of the Riemann problem presented in Fig. 5. The rarefraction wave propagating to the left is denoted by (a) and the right runnnig shock wave is denoted by (b). Initial state values $P_- = u_2^{(a)} = 0$, $P_+ = u_1^{(b)} = 0$, $Q_- = \eta_2^{(a)} = 2$, $Q_+ = \eta_1^{(b)} = 0$. Calculated values at time $t = 150$ are $u_1^{(a)} = \theta_1^{(b)} + u_1^{(b)} = 0.86377$ and $\eta_1^{(a)} = v^{(b)}\theta_1^{(b)} + \eta_1^{(b)} = 1.29008$ and the velocity of the shock wave is $v^{(b)} = 1.50085$. The calculated data fits precisely with the simulation in Fig. 5.

$$u \to \begin{cases} P_-, & x \to -\infty \\ P_+, & x \to +\infty \end{cases} , \quad \eta \to \begin{cases} Q_-, & x \to -\infty \\ Q_+, & x \to +\infty \end{cases} . \qquad (46)$$

The above limits will typically be known in an experiment, that is the fluid velocities and the pressure are determined at the boundaries.

i) For the case presented in Fig. (5) we can determine the outcome as follows. Let superscript (a) denote variables pertaining to the rarefraction wave and let superscript (b) denote variables for the right going shock wave, see Fig. 8. For the rarefraction wave the list of unknown variables is: $u_1^{(a)}$, $u_2^{(a)}$, $\eta_1^{(a)}$ and $\eta_2^{(a)}$. For the shock wave the list of unknown variables is: $u_1^{(b)}$, $\eta_1^{(b)}$, $v^{(b)}$ and $\theta_1^{(b)}$. This is a total of 8 variables, which need to be determined. The boundary conditions in Eq. (46) provides 4 equations: $P_- = u_2^{(a)}$, $P_+ = u_1^{(b)}$, $Q_- = \eta_2^{(a)}$ and $Q_+ = \eta_1^{(b)}$. Furthermore, we need to demand that the left running rarefraction wave and the right running shock wave are connected continuously in both the fluid velocity variable and the pressure variable. This condition provides the two additional equations: $u_1^{(a)} = \theta_1^{(b)} + u_1^{(b)}$ and $\eta_1^{(a)} = v^{(b)}\theta_1^{(b)} + \eta_1^{(b)}$ (see Eq. (24)). The final two relations are Eq. (21) with $\theta_1^{(b)} = -[\beta(u_1^{(b)}, v^{(b)}) + D(u_1^{(b)}, v^{(b)}, \eta_1^{(b)})]/(2\alpha)$ and Eq.(39) with $(u_1, \eta_1, u_2, \eta_2)$ replaced by $(u_1^{(a)}, \eta_1^{(a)}, u_2^{(a)}, \eta_2^{(a)})$. In the expression given by Eq. (21) both $(u_1^{(b)})^2$ and $(v^{(b)})^2$ enters and hence the algebraic equations possesses multiple solutions. However, from heuristic arguments we can rule out those which are not physical relevant. The Eq. (39) is strictly derived for rarefraction waves with no damping, that is $b=0$. However, the algebraic equations are indeed valid for the case $b \neq 0$ as the jump hight is unaffected by the damping term.

ii and iii) For the head on colliding shocks, illustrated by the simulation result in Fig. (7), we can predict the wave pattern after the collision by invoking the same type of argumentation as above for the Riemann problem. Again the boundary values of the compound waves are given by the limits in Eq. (46). We shall label the right running wave (left wave initially) by superscript (a) and the left running wave (right wave initially) is labeled by a superscript (b), see Fig. 9. The boundary conditions in Eq. (46) provides the 4 equalities: $P_- = \theta_1^{(a)} + u_1^{(a)}$, $P_+ = u_1^{(b)}$,
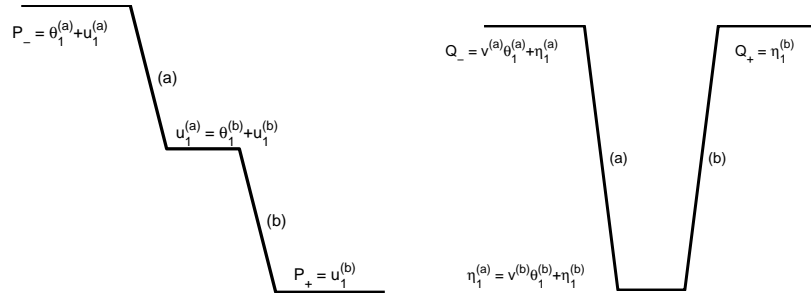
Figure 9: Sketch of the procedure for calculating the outcome of the head-on collison presented in Fig. 7. The initial state is shown with the right running shock denoted by (a) and the left running shock denoted by (b). Initial state values $P_- = \theta_1^{(a)} + u_1^{(a)} = 0.848$, $P_+ = u_1^{(b)} = -0.848$, $Q_- = v^{(a)}\theta_1^{(a)} + \eta_1^{(a)} = 4.24$ and $Q_+ = \eta_1^{(b)} = 4.24$. The continuity condition of the interconnection between the shock waves are $u_1^{(a)} = \theta_1^{(b)} + u_1^{(b)} = 0$ and $\eta_1^{(a)} = v^{(b)}\theta_1^{(b)} + \eta_1^{(b)} = 0$. The initial shock wave velocities are $v^{(a)} = 5$ and $v^{(b)} = -5$. After the collison at time $t = 1.2$ the continuity condition of the interconnection between the shock waves are $u_1^{(a)} = \theta_1^{(b)} + u_1^{(b)} = 0$ and $\eta_1^{(a)} = v^{(b)}\theta_1^{(b)} + \eta_1^{(b)} = 11.36$. The calculated velocities are $v^{(a)} = 8.3962$ and $v^{(b)} = -8.3962$. The calculated data fits precisely with the simulation in Fig. 7.

$Q_- = v^{(a)}\theta_1^{(a)} + \eta_1^{(a)}$ and $Q_+ = \eta_1^{(b)}$. Continuity of the connecting interface between the two waves leads to the additional two equations $u_1^{(a)} = \theta_1^{(b)} + u_1^{(b)}$ and $\eta_1^{(a)} = v^{(b)}\theta_1^{(b)} + \eta_1^{(b)}$. The final two equations for determining the 8 unknowns are Eq. (21) in the forms $\theta_1^{(a)} = -[\beta(u_1^{(a)}, v^{(a)}) + D(u_1^{(a)}, v^{(a)}, \eta_1^{(a)})]/(2\alpha)$ and $\theta_1^{(b)} = -[\beta(u_1^{(b)}, v^{(b)}) + D(u_1^{(b)}, v^{(b)}, \eta_1^{(b)})]/(2\alpha)$. Again these later equations have multiple solutions which provide both the initial compound wave configuration as well as the wave pattern after the collision. The physical relevant solutions can easily be identified. For the overtake of a slow shock wave by a fast shock wave in Fig. (6) the argument for predicting the outcome after the two waves have interacted is identical to the case for the above head-on collision and hence omitted here.

7   Summary

We have determined generalized travelling shock wave solutions for a model of thermoviscous fluids presented in reference [6]. The generalized travelling wave ansatz for the velocity potential consists of a function of the travelling wave coordinate $\xi = x - vt$ plus a linear combination of the space and time variables. The latter makes it possible to analytically determine the wave pattern after the interaction of two compound shock waves. Examples of interacting compound waves have been illustrated by numerical simulations. Compound wave interaction can result in formation of rarefraction waves. Hence we studied rarefraction waves and found analytical expressions by a similarity transformation for the the case of no damping, that is neglecting viscosity and heat transfer. For rarefraction waves we have shown that the jump height is not influenced by the damping term.

References

[1] P. M. Jordan, "An analytical study of Kuznetsov's equation: diffusive solitions, shock formation, and solution bifurcation," *Phys. Lett. A*, vol. 326, pp. 77–84, 2004.

[2] V. P. Kuznetsov, "Equations of nonlinear acoustics," *Sov. Phys. Acoust.*, vol. 16, pp. 467–470, 1971.

[3] P. M. Jordan and A. Puri, "A note on traveling wave solutions for a class of nonlinear viscoelastic media," *Physics Letters A*, vol. 335, pp. 150–156, 2005.

[4] P. M. Jordan and A. Puri, "Addendum to: A note on traveling wave solutions for a class of nonlinear viscoelastic media," *Physics Letters A*, vol. 361, pp. 529–533, 2007.

[5] M. Chen, M. Torres, and T. Walsh, "Existence of traveling wave solutions of a high-order nonlinear acoustic wave equation," *Physics Letters A*, vol. 373, pp. 1037–1043, 2009.

[6] L. H. Söderholm, "A higher order acoustic equation for the slightly viscous case," *Acustica*, vol. 87, pp. 29–33, 2001.

[7] A. R. Rasmussen, M. P. Sorensen, Y. B. Gaididei, and P. L. Christiansen, "Analytical and numerical modeling of front propagation and interaction of fronts in nonlinear thermoviscous fluids including dissipation," *arXiv 0806.0105v1*, vol. [physics.flu-dyn], pp. 1–10, 2008.

[8] M. F. Hamilton and C. L. Morfey, "Model equations," in *Nonlinear Acoustics* (M. F. Hamilton and D. T. Blackstock, eds.), ch. 3, pp. 41–64, San Diego: Academic Press, 1998.

[9] H. Ockendon and J. R. Ockendon, "Nonlinearity in fluid resonances," *Meccanica*, vol. 36, pp. 297–321, 2001.

[10] D. T. Blackstock, "Some model equations of nonlinear acoustics," in *Handbook of acoustics* (M. J. Crocker, ed.), ch. 16, pp. 181–186, New York: Wiley-Interscience, 1998.

[11] K. Naugolnykh and L. Ostrovsky, *Nonlinear Wave Processes in Acoustics*. Cambridge: Cambridge University Press, 1998.

[12] J. H. Ginsberg, "Perturbation methods," in *Nonlinear Acoustics* (M. F. Hamilton and D. T. Blackstock, eds.), ch. 10, pp. 279–308, San Diego: Academic Press, 1998.

[13] I. Christov, C. I. Christov, and P. M. Jordan, "Modeling weakly nonlinear acoustic wave propagation," *Q. J. Mechanics. Appl. Math.*, vol. 60, no. 4, pp. 473–495, 2007.

[14] I. Christov, P. M. Jordan, and C. I. Christov, "Nonlinear acoustic propagation in homentropic perfect gasses: a numerical study," *Phys. Lett. A*, vol. 353, pp. 273–280, 2006.

[15] I. Christov, C. I. Christov, and P. M. Jordan, "Cumulative nonlinear effects in acoustic wave propagation," *Comput. Model. Engng. Sci.*, vol. 17, pp. 47–54, 2007.

[16] S. Makarov and M. Ochmann, "Nonlinear and thermoviscous phenomena in acoustics, part I," *Acustica*, vol. 82, pp. 579–606, 1996.

[17] R. T. Beyer, "The parameter B/A," in *Nonlinear Acoustics* (M. F. Hamilton and D. T. Blackstock, eds.), ch. 2, pp. 25–39, San Diego: Academic Press, 1998.

[18] R. J. LeVeque, *Finite volume methods for hyperbolic problems*. Cambridge: Cambridge University Press, 2002.

Appendix D

Example of COMSOL MULTIPHYSICS® code

The below COMSOL MULTIPHYSICS code computes the numerical solutions shown in Figs. 3.5–3.7. The problem is solved as a stationary problem on a 2D (space, time) geometry, using adaptive mesh refinement and streamline diffusion. This strategy basically follows the shock tube problem described in the COMSOL MULTIPHYSICS documentation.

```
clear all; close all;

ngen = 4;  % number of mesh refinements (increase)
t1 = 8;    % time
x1 = 5*t1; % space

for eq = [1 2] % 1: Higher order equation, 2: Euler's equations
    clear fem;
    fem.geom    = rect2(x1,t1,'Pos',[-2*x1/5 0]); % geometry
    fem.mesh    = meshinit(fem,'hauto',5); % initial mesh
    fem.form    = 'general';
    fem.const   = {'gamma',1.4,'delta',1,'BA',0.4,'K',0.7};
    fem.sdim    = {'x','time'};
    fem.equ.f   = {{'F1';'F2'}};
    fem.equ.ga  = {{{0 0} {0 0}}};
    fem.bnd.ind = [2 3 1 3];
    switch eq
        case 1 % Lossless higher order acoustic equation
            fem.dim = {'eta' 'u'};
            fem.equ.expr = {'F1','etatime - (3-gamma)*u*utime
            + ux + (gamma-1)*(etax*u+eta*ux) -
            (gamma+1)/2*ux*u^2', 'F2','utime+etax'};
            fem.equ.weak = {{'delta*h*(etatime_test -
            (3-gamma)*u*utime_test + ux_test +
```

117

```
                (gamma-1)*(etax_test*u+eta*ux_test)
                - (gamma+1)/2*ux_test*u^2)*F1';
                'delta*h*(utime_test+etax_test)*F2'}};
            fem.bnd.r = {0,{'eta-(((1+0.8*exp(-x^2))^BA-1)
                /BA+K^2/2)';'u-K'},{'eta-(((1+0.8*exp(-10^2))^BA-1)
                /BA+K^2/2)';'u-K'}};
            fem.equ.init =
                {{'((1+0.8*exp(-10^2))^BA-1)/BA+K^2/2' 'K'}};
        case 2 % Euler's equations
            fem.dim = {'rho' 'ru'};
            fem.equ.expr = {'F1','rhotime + rux',
                'F2','rutime + (2*ru*rux/rho-ru^2*rhox/rho^2)
                + rhox*rho^(gamma-1)'};
            fem.equ.weak = {{'delta*h*(rhotime_test +
                rux_test)*F1'; 'delta*h*(rutime_test +
                (2*ru*rux_test/rho-ru^2*rhox_test/rho^2)
                + rhox_test*rho^(gamma-1))*F2'}};
            fem.bnd.r = {0,{'rho-(1+0.8*exp(-x^2))'
                ;'ru-(1+0.8*exp(-x^2))*0.7'},
                {'rho-(1+0.8*exp(-25^2))';
                'ru-((1+0.8*exp(-25^2))*0.7)'}};
            fem.equ.init = {{'1+0.8*exp(-25^2)'
                '(1+0.8*exp(-25^2))*0.7'}};
    end
    fem.shape = 2;
    fem.xmesh = meshextend(fem);
    [fem fem.stop] = adaption(fem,'ngen',ngen,'out',
    {'fem','stop'},'maxt',2147483647,'uscale','none',
    'complexfun','on','maxiter',250);
    fem.xmesh = meshextend(fem);
    flsave(['eq' num2str(eq)],fem)
end


x = linspace(-10,20,1000);
t = t1;
[X,T] = meshgrid(x,t);
p = [X(:)';T(:)'];
flload eq2
plot(x,postinterp(fem,'ru/rho',p),'b')
hold on
flload eq1
plot(x,postinterp(fem,'u',p),'r')
```